Advances in Flexible Metallic Transparent Electrodes

Viet Huong Nguyen, Dorina Papanastasiou, Joao Resende, Laetitia Bardet, Thomas Sannicolo, Carmen Jiménez, David Muñoz-Rojas, Ngoc Duy Nguyen, Daniel Bellet

Advances in flexible metallic transparent electrodes

Viet Huong Nguyen,[1,*] Dorina T. Papanastasiou,[2] Joao Resende,[3] Laetitia Bardet,[2] Thomas Sannicolo,[4] Carmen Jiménez,[2] David Muñoz-Rojas,[2] Ngoc Duy Nguyen,[5] Daniel Bellet[2]

[1]*Faculty of Materials Science and Engineering, Phenikaa University, Hanoi 12116, Viet Nam*

[2]*Univ. Grenoble Alpes, CNRS, Grenoble INP, LMGP, F-38016, Grenoble, France*

[3]*AlmaScience Colab, Madan Parque, 2829-516 Caparica, Portugal*

[4]*Department of Materials Science and Engineering, Massachusetts Institute of Technology, Cambridge, Massachusetts 02139, United States*

[5]*Département de Physique, CESAM/Q-MAT, SPIN, Université de Liège, B-4000 Liège, Belgium*

Abstract:

Transparent electrodes (TEs) are pivotal components in many modern devices such as solar cells, light-emitting diodes, touch screens, wearable electronic devices, smart windows, or transparent heaters. Recently, the high demand for flexibility and low cost in TEs requires a new class of transparent conductive materials (TCMs) as substitutes for conventional indium tin oxide (ITO), which is so far the most used TCM but exhibits brittleness and high cost. Among the different emerging alternative materials to ITO, metallic nanomaterials have received much interest due to their remarkable optical-electrical properties, low cost, ease of manufacturing, flexibility, and widespread applicability. These involve metal grids, thin oxide/metal/oxide multilayers, metal nanowire percolating networks, or nanocomposites based on metallic nanostructures. In this review, a comparison between TCMs based on metallic nanomaterials and other TCM technologies is discussed. Next, the different types of metal-based TCMs developed so far and the fabrication technologies used are presented. Then, the challenges that these TCMs face towards integration in functional devices are discussed. Finally, the various fields in which metal-based TCMs have been successfully applied as well as emerging and potential applications are summarized.

Keywords: metallic transparent electrodes, flexibility, stretchability, metal nanowires, stability

1. Introduction

Transparent electrodes (TEs) constitute a specific class of materials possessing both optical transparency and electrical conductivity. TEs are essential components of many modern devices, such as solar cells, organic light-emitting diodes (OLEDs), liquid-crystal displays (LCDs), transparent heaters (THs), smart windows, etc.[1–4] The field of TEs has traditionally been dominated by transparent conductive oxides (TCOs). As early as the 1950s, the introduction of wide band-gap semiconductors, such as SnO_2 and In_2O_3 with high optical transparency (> 80 %), and the possibility to enhance their conductivity via impurity doping opened up numerous practical applications.[5,6] As a result, a whole industrial ecosystem and know-how associated with TCOs do exist, at both the laboratory and industry levels. After over sixty years of extensive study, Indium Tin Oxide (ITO) films of excellent optical and electronic properties are now the most commonly used TE materials and can be obtained from mature vacuum-based sputtering technologies.[7] However, ITO faces certain issues related to its ceramic nature and indium scarcity, which makes it not suitable for certain applications including flexible devices. In this context, the enormous progress made in the search of new materials of greater performances and additional properties including better flexibility, stability, abundance of raw materials, and lower processing cost, has been challenging the ITO's dominant position.[8] TE candidates other than TCOs include three main classes of materials, also known as emerging transparent conductive materials: (i) carbon nanomaterials, such as carbon nanotubes (CNTs)[9–12] or graphene,[13–15] (ii) conductive polymers, such as poly(3,4ethylenedioxythiophene): poly(styrene sulfonate) (PEDOT:PSS)[16–20] and (iii) metallic nanostructures, such as metallic thin films, metal nanowire or fiber networks, or metal grids.[21] These nanomaterials have been extensively studied and have already demonstrated their high potential to solve the critical issues of ITO.

Of these various alternatives, metal-based TEs appear the most promising candidates due to i) their intrinsically high electrical conductivity, ii) potential to achieve high optical transparency by using nanostructures and iii) large possibility to have additional properties such as flexibility, stretchability, tunable bandgap alignment, haziness when being combined with other materials. Metallic TEs were studied and fabricated as early as 1877 by evaporation and sputtering.[22] It is interesting to note that although ITO is currently the most popular TE, the first reported applications of TEs were metallic ultrathin films, such as Ag, Au, or Pt, on selenium photoelectric cells in the 1880s.[23] At the initial stage, metal- and oxide-based TEs found a great interest in various applications such as LCDs,[24] transparent heaters on aircraft windows (for de-icing and de-fogging systems), imaging devices, ferroelectric memories, and also solar energy conversion.[25] The fundamental property that makes metallic nanomaterials interesting as TEs is that the high free-electron density of metals (> 10^{22} cm^{-3}) is maintained at the nanoscale. With an electrical conductivity of 6.3×10^7 S/m, Ag is indeed the best electrical conducting material at room temperature, and therefore Ag-based materials have a good potential for acting as efficient TEs. While many studies have been devoted to electrodes based on Ag nanostructures, [1,26–28] lately other metals are investigated as well: Cu [29–31] and Ni-Cu [32,33] for instance. Another advantage of metals is their ductility (which is further enhanced when shaped at the nanoscale),unlike TCOs. On the other side, the drawback associated with the large free-electron density is the high reflectivity of metals, thus uniform metallic layers generally exhibit low optical transmittance.

Several efforts have been devoted to improving the transparency of metallic-based TEs. For instance, ultrathin metal films or non-continuous metal nanostructures such as periodic metal

grids or random metal nanowire networks can be of great interest as efficient TEs. Although ITO has been used in many different applications, in practice, different applications do not require the same TE specifications. A typical example is the case of TEs in solar cells and flat-panel displays. Both require materials of low electrical sheet resistance (R_{sh} < 10–20 Ω/sq) and high optical transparency (> 90% at 550 nm). However, while the integration of TEs within flat-panel displays requires a very low haziness (defined as the ratio between diffuse and total transmittance of light) to avoid blurred vision, photovoltaic devices do benefit from maximizing the haziness of TEs. Indeed, hazy TEs increase solar cell efficiency by maximizing the light pathway along with the absorber material, resulting in enhanced absorption and short-circuit current density, as has been demonstrated for the case of Dye-Sensitized Solar Cells.[34] Therefore, efforts have been devoted to increasing the haziness of transparent electrodes without losing too much neither transparency nor conduction.[35,36] Such a compromise, unavoidable for some applications, poses a challenge for the efficient integration of those TEs in working devices. In addition to the two basic properties, i.e. transparency and conductivity, extensive researches have been also recently devoted to improving the mechanical properties of TEs. The recently developed flexible and stretchable electronics for health monitoring, biological studies,[37] energy harvesting devices, as well as soft robotics strongly require transparent thin-film transistors,[38] transparent soft actuators/sensors.[39] This motivates the fields of transparent conductive materials towards flexible and stretchable metal-based transparent materials.

In this paper, we summarize state-of-the-art researches in metallic TEs including thin metallic films, metal grids, metal nanowires, and some other emerging nanostructured networks such as templates, metal nanotrough network, metal fiber or metal nanowire-based nanocomposites. For each type of metallic TEs, we review their main properties, advantages, disadvantages, and fabrication feasibility and compare with those of TCOs or other TEs. We then discuss the different challenges to tackle in terms of efficient integration, long-term stability so that these alternatives can gain in maturity. Finally, we review the recent advances in using metallic TEs for a variety of applications, including some main markets as well as niches. Eventually this work will particularly focus on the comparison between the different metallic solutions and on the next strategies that appear pertinent for the future.

2. Metallic TEs in comparison with other TCMs: a general overview

For use as TEs, thin solid films have first of all to fulfil two fundamental requirements, i.e. electrical conductivity and optical transparency, which indeed have been the focus of the research in most of the published works so far related to TE materials. Nevertheless, transparency and conductivity are antagonistic physical properties, and it is therefore not easy to obtain high values of these two parameters simultaneously. For the optimization of TE materials, as well as the direct comparison between different types of TEs, the definition of a Figure of Merit (FoM) that links the optical and electrical properties is of great importance. There have been different attempts to establish such a coefficient. The simple version by Fraser and Cook in 1972 (FoM = T/R_{sh} with T and R_{sh} refer to the optical transmittance and sheet resistance, respectively) seems the first FoM used for TEs.[40] The issue with such as definition is that the maximum FoM occurs at a film thickness corresponding to an optical transmittance of only 37%, which is too low and useless in TE applications.

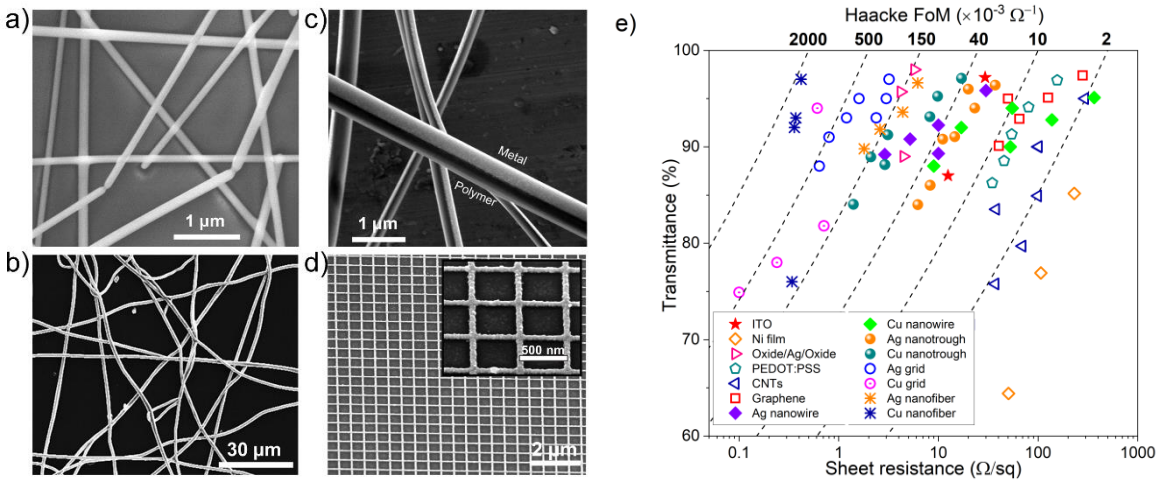

Figure 1: SEM micrographs of: a) Ag nanowire (AgNW) network with an average diameter of 60 nm. Reprinted with permission.[41] Copyright 2018, American Chemical Society. b) Cu nanofiber network on PDMS deposited by electrospinning. Reproduced with permission.[42] Copyright 2016, Wiley-VCH. c) PVP polymer nanofibers coated with a thin layer of gold for the fabrication of a gold nanotrough network. Reproduced with permission.[43] Copyright 2013, Springer Nature. d) a metal grid with a periodicity of 500 nm and a wire width of 55 nm. Reprinted with permission.[44] Copyright 2012, American Chemical Society. (e) Optical transmittance at λ = 550 nm (without substrate contribution) versus sheet resistance diagram for various transparent electrodes. Data are extracted from literature: graphene,[45] carbon nanotubes (CNTs) networks,[46] AgNW networks,[47,48] ITO,[43,49,50] metal nanotrough,[43,51,52] metal grids[53–56] and oxide/Ag/oxide multilayer structures.[57–59] The dashed lines fit with iso-values of the Haacke figure of merit (FoM): 10, 20, 40, 80, 160, 320 (10^{-3} Ω^{-1}). For data extracted from ref[57,59], the transmittance values without substrate contribution were estimated with assumption that the bare glass substrate has a total transmittance of 92%.

In 1976, Haacke introduced an exponent for the transmittance, i.e. $FoM=T^x/R_{sq}$, and proposed that $x = 10$ offers the most convenient choice since the new FoM was maximized for films with transmittance higher than 90%. Recently, several new models for FoM have been proposed to evaluate TE materials.[60,61] For instance, De and Coleman have remarked that the transmittance and the sheet resistance of a thin conducting film can be related as follows:[60]

$$T = \left(1 + \frac{Z_0}{2R_{sh}} \frac{\sigma_{Op}}{\sigma_{DC}}\right)^{-2} \quad (1)$$

Where Z_0 is the impedance of free space (= 377 Ω), σ_{DC} and σ_{op} are the DC and the optical conductivity. From Eq (1), they suggested that the ratio σ_{DC}/σ_{op} can be used as a new FoM because high values of this ratio result in the desired properties (high T, low R_{sh}). But it should be noted that the optical conductivity in this approach is related to the Lambert-Beer absorption coefficient α, by $\sigma_{op} = \alpha/188.5$ ($m^{-1}\Omega^{-1}$). Consequently, it is not completely appropriate to apply for nanostructured TEs such as metal nanowire networks or grids because the optical transmittance in these discontinuous materials do not obey the Lambert-Beer law but depends on the coverage of the nanostructures on the substrate surface. The latter is quite independent of the structure thickness. Despite new models of FoM proposed, Haacke's FoM seems by far the most used expression for TE material optimization and comparison due to its simplicity in numerical calculations, and because in most applications transparency and conductivity are the main parameters to be optimized. For instance, a prominent advantage of using Haacke's FoM is that, in practice, the evaluation of sheet resistance does not require the film thickness measurement, which is more complicated in the cases of polymers (being soft materials) or 1D nanomaterial networks than in the case of continuous thin films. Figure 1a-d show Scanning Electron Microscopy (SEM) pictures of typical examples of metal nanowire network, metal nanofiber network,[42] metal nanotrough network,[43] and metal grid.[44] While being transparent (with transparency of about 90%) thanks to a large number of empty spaces between metallic pathways, such metallic nanostructures can exhibit sheet electrical resistance as low as a few

Ohms per square. For the sake of comparison, Figure 1e reports typical values of the optical transmittance versus sheet resistance for various transparent electrodes, including those based on ITO,[7,49] Ni,[62] oxide/metal/oxide,[63–66] PEDOT-PSS,[67] carbon nanotubes (CNTs) networks,[68–70,46,9] graphene,[45,7] metal nanowire networks,[71,48,50,72,73] metal nanotrough,[43] metal grids[54,56,74] and metal nanofibers.[42,75] The selected data extracted from the literature are representative of rather optimized experimental conditions. The dashed lines correspond to the relation between T and R_{sh} according to Haacke's formula for different iso-values of the FoM, i.e. 2, 10, 40, 150, 500, 2000 ($\times 10^{-3}\ \Omega^{-1}$). It is worth mentioning that special attention should be paid when reporting the transmittance of different TE materials in the visible range. For homogeneous and continuous layers such as TCOs or conductive polymers, it would be convenient to report transmittance values averaged in the visible range due to the presence of interference fringes. In contrast, the transmittance in the visible range can be reported at a unique wavelength (for instance at 550 nm) for MNW networks [48] or metal grids, for which the optical transparency is often observed as a linear decreasing function of the areal mass density (*amd*) or the surface coverage.[76,77] Often in literature, the optical transparency is estimated after substrate contribution removal for the sake of a fair comparison. We chose to do likewise in this review

As illustrated in Figure 1e, there are already several emerging TEs exhibiting performances as high as, or even better than that of ITO. This is the case for metal nanofibers, metal nanotroughs, metal nanowire networks (including Ag and Cu), metal grids, and oxide-metal-oxide structures. On the contrary, despite predicted high theoretical performances, carbon-based materials (graphene and CNT networks) show rather low optical and electrical performances compared to ITO's. For instance, while individual CNTs can be excellent electrical conductors, the highest electrical conductivity value of CNT networks is usually less than 4% of the intrinsic conductivity of an individual CNT. That is usually attributed to the reported high contact resistance between single CNTs.[1,12] This junction resistance issue remains in the case of metallic nanostructures. However, the latter's magnitude is much less detrimental compared to carbon-based TE materials due to the isotropic feature of electrical conductivity in metals.

Beyond the key material properties aforementioned, there are indeed several other critical parameters that need to be taken into consideration, depending on the requirements attached to a specific application. For instance, the additional desired properties relevant for TEs in solar cells include high haziness, and work-function compatibility with the adjacent functional layers to optimize charge collection, but not necessarily post-fabrication high thermal stability due to low-temperature working conditions of the devices. In contrast, transparent heaters require excellent thermal stability since, in their working mode, in-operando temperatures can reach up to 400 – 500 °C.[4] Hence, depending on the envisaged application, the requirements for TEs can be significantly different. In addition to transparency and conductivity, other criteria include mechanical properties (flexibility, stretchability), morphological stabilities, material compatibility with adjacent active layers (surface roughness, bandgap alignment), or even technological compatibility for the TEs fabrication technique with other processing steps of the final devices.

The remarkable advantage of using metal-based TEs lies in their ability to meet several criteria simultaneously. One of the initial driving forces of the growth of metal-based TEs is their better flexibility compared to the traditional ceramic materials such as Indium Tin Oxide (ITO) or Fluorine doped Tin Oxide (FTO), and therefore, extended possibilities for flexible

devices.[78] Besides, high transparency in the near-infrared (NIR) region, for some metallic nanostructured TEs such as metal nanowire networks, is of great interest in some applications. For instance, in multi-junction solar cells, metal nanowire networks maintain high levels of transparency even in the NIR while that of TCOs quickly drops due to the strong plasmonic absorption in the same region of wavelengths.[79] Low emissivity window coatings made of silver nanowires (AgNWs) are also valuable as they allow the passage of solar NIR wavelengths which could be used to warm the indoor spaces.[80] It is also worth mentioning that, in most practical applications, TE materials are often combined with other functional adjacent layers. What makes metal-based TEs gain much attraction is the ease in combining metallic materials with other layers such as oxide coatings or graphene to make high-performance TEs, or to adjust the compatibility of the TE layer with the nearby active layers in devices.

The most critical disadvantage of using metal-based TEs is probably their stability. The issues related to material stability could originate from the mechanical, electrical, thermal, and chemical constraints. Metal-based TEs are mostly used in various nanometric forms such as nanowires, nanofibers, or ultrathin films, resulting in high morphological instability under electrical or thermal stress. For instance, a typical morphological failure of metal nanowire networks is the evolution of the wire shape into disconnected spheres, which is usually called spheroidization, when temperatures much below the melting temperature of the metal bulk counterparts are applied to the material. Unlike oxide-based TEs, the failure of the metallic TE materials is often thermally accelerated under the working environment due to, for instance, sulfidation or oxidation. Understanding the degradation mechanism of TE materials for each specific targeted application is essential to the discovery of an appropriate strategy to improve the material stability for their successful integration. Also, the roughness of TEs or their adhesion with the substrate and other layers can be detrimental to the device performance in certain applications such as solar cells or OLEDs. For instance, AgNW networks have excellent mechanical flexibility, conductivity and can be solution-processed. However, their surface roughness associated with AgNWs-covered substrates could result in large leakage current or even electrical shortage in flexible organic solar cells.[81,82]

In the following sections, we will review in more detail the main properties, advantages, and disadvantages of the different metal-based nanomaterials which have been investigated for TE applications. They will be classified into 4 main categories according to their structures: continuous, ordered, random structures, and nanocomposites based on metal nanowires.

3. Metallic nanomaterials for TEs

3.1. Continuous films

Pure metals such as Ag, Au, or Cu, are known to be very conductive, of which Ag is the most electrically conductive element, i.e. 6.30×10^7 S/m at 20 °C. The resistivities of metallic materials increase when they are downscaled below a critical length, mainly due to the electron scattering at the interfaces and grain boundaries. In general, thin metal films deposited by physical vapor deposition (PVD) techniques such as evaporation or sputtering are prone to grow in the island-like mode. Thus, there exists a critical film thickness beyond which the deposited film is continuous and achieves a reasonable conductivity for TE applications. For instance, Au and Ag films grown on glass substrates show the island-like growth mode with continuous films appearing at a critical thickness of about 8 nm.[83,84] Bi *et al.* have demonstrated that a 7 nm Au film grown by thermal evaporation could achieve smooth surface morphology with a root-mean-square roughness of only 0.35 nm, and sheet resistance of 23.75 Ω/sq. However, the

average optical transmittance of only 70% in the visible range appears too low for TE applications. Another critical issue of using ultrathin metallic films is their morphological instability, particularly at high temperatures or applied electrical currents. To obtain smooth ultrathin metallic films, there have been several strategies to hinder the island-like growth mode, including pre-evaporating a seed metallic layer to enhance the wettability of the deposited metal layer with the seed one or via co-sputtering of different metals.[85–88] Despite many efforts devoted to improving the physical and morphological properties of ultrathin and continuous metallic films, modest optical transmittance remains a challenging factor for their widespread adoption as TE applications.

To circumvent the aforementioned problems, thin metal-oxide multilayer structures consisting of an ultrathin metal film inserted between transparent oxide films, also called Oxide/Metal/Oxide (OMO) structures, are promising. Because of a wide range of choices among wide bandgap oxide materials, the OMO structures have a high potential to feature improved transparency and conductivity,[58] great compatibility with different substrates in terms of adhesion and charge injection/collection, as well as good anti-corrosion performance.[89] Table 1 summarizes the major performances of various types of thin OMO structures. There have also been some reviews dedicated to this multilayer structure such as the works done by Guillén *et al.* (2011) or Bi *et al.* (2019).[90,91] Here, we reported some recent data extracted from selected works. Although several metals have been investigated: Cu, Ag, Au, Al, and Pt, it is remarked that Ag is the most commonly used metal in such OMO structure due to its good chemical stability and high conductivity and that the related optoelectrical performances could already compete with the one of ITO. In most of the cases shown in Table 1, the sheet resistance of the OMO composite TEs is below 10 Ω/sq, which is even better than that of commercial ITO films. The bottom oxide layer can play the role of an efficient seed layer for metal thin film growth, which enhances its smoothness and continuity at a very low thickness.[92] Additionally, it is possible to adapt the work function of the composite electrodes with the adjacent functional layers via a relevant choice of the oxides, or even via doping effect such as Al-doped ZnO (AZO).[93] For instance, hole transport layers such as NiO,[94] WO_3[95,96], and MoO_3,[97,98] and electron transport layers such as ZnO[99] and TiO_2[100] have been used in the OMO TEs in organic, dye-sensitized solar cells and polymer light-emitting diodes.

Table 1: Summary of optical transmittance (T) and sheet resistance (R_{sh}) for various types of Oxide/Metal/Oxide structures, data extracted from some recently selected references. The transmittance values reported here are represented with the substrate contribution. The thicknesses of different layers and the substrate type are also given.

Structure	t (nm)	Substrate	T (%)	R_{sh} (Ω/sq)	Ref
NiO/Ag/NiO	35/11/35	PET	82 (400-700 nm)	7.6	[94]
TiO_2/Ag/TiO_2	42/10/42	Glass	89 (450-600 nm)	4.48	[59]
Nb_2O_5/Ag/Nb_2O_5	30/9.5/30	PEN	86 @ 550 nm	7.2	[101]
ZnO/Ag/ZnO	10/8/40	PET	89.7 (380-770 nm)	7.8	[102]
AZO/Ag/AZO	30/10/30	Glass	80.5 (400-800 nm)	6.6	[103]
IZO/Ag/IZO	40/12/40	Glass	87.7 (380-750 nm)	5.65	[104]
TiO_2/Ag/AZO	30/8/40	Willow glass	86.7 (375-700 nm)	6.3	[92]
$InZnSnO_x$/Ag/$InZnSnO_x$	30/14/30	PET	86 @ 550 nm	4.99	[105]
TiO_2/Ag/AZO	25/12/40	Glass	91.6 (400-700 nm)	5.75	[58]
MoO_x/Au/MoO_x	40/10/40	Glass	87 (400-700 nm)	10	[106]
SnO_x/Au/SnO_x	35/5.2/35	Glass	~82 (400-800 nm)	52	[107]
ZnO/Au/ZnO	50/3/47	Glass	77.6 (400-800 nm)	20	[108]

AZO/Au/AZO	58/10/58	Mica	81.7 (400-800 nm)	5	[109]
IZO/Au/IZO	40/12/40	Glass	~ 80 @ 550 nm	5.49	[110]
TiO_2/Cu/TiO_2	30/6/30	PEN	81 @ 630 nm	19	[111]
ZnO/Cu/ZnO	30/6/30	PEN	75.1 (400-700 nm)	8.3	[112]
ZnSnO/AgPdCu/ZnSnO	20/14/15	PET	73.5 (400-800 nm)	3.43	[113]
ZnO/Cu doped Ag/Al_2O_3	24/6.5/56	PET	88.4 (400-700 nm)	18.6	[66]

Another remarkable advantage of the OMO multilayer structures is the ability to overcome the drawback of low transmission of the bare metal layers by appropriately tuning the thickness of the oxide layers to obtain an anti-reflective effect. This is widely and traditionally used in photovoltaic devices for the front TE.[114–116] Maniyara *et al*. have theoretically and experimentally demonstrated the possibility to obtain OMO TEs on fused silica substrate with transmission higher than 98% (without substrate contribution), and low electrical sheet resistance (5.75 Ω/sq).[58] This was possible by optimizing the thicknesses of the top and the bottom oxide layers, i.e. Al-doped ZnO (AZO) and TiO_2 respectively, applied to a 12 nm-thick Ag film. Recently, Ji *et al*. have optimized the OMO multilayer structure on a flexible substrate (PET) and even obtained a transmittance (88.4%) higher than that of the bare substrate (88.1%).[66] The optimization principle is summarized as follows: i) choose a low-loss and highly conductive metallic film (in most cases, use Ag), ii) use high refractive index materials for the bottom oxide, iii) the thickness of this layer should be adapted along with its refractive index to obtain a phase angle of π/2 at the metal/bottom oxide interface, iv) optimize the refractive index and the thickness of the top oxide layer within a small range to achieve the optimal broadband transmittance.[66] Figure 2a-b show a scheme of an asymmetric OMO transparent electrode with design parameters and reflection waves at various interfaces, and the simulated averaged transmittance of such structure versus the refractive index and the thickness of the top oxide when the bottom oxide and the metallic layer are selected as 24 nm ZnO and 6.5 nm Cu doped Ag, respectively. The optimized 56 nm Al_2O_3/6.5 nm Cu-Ag alloy/ 24 nm ZnO transparent electrode has a sheet resistance of 18.6 Ω/sq and an absolute transmittance of 88.4%, even higher than that of the PET substrate (88.1%), as shown in Figure 2c-d. This is indeed a very interesting approach in tuning the transmittance of metal-based TEs since there are a wide range of oxides of different optical properties that can be used for the capping layers in the OMO structures.

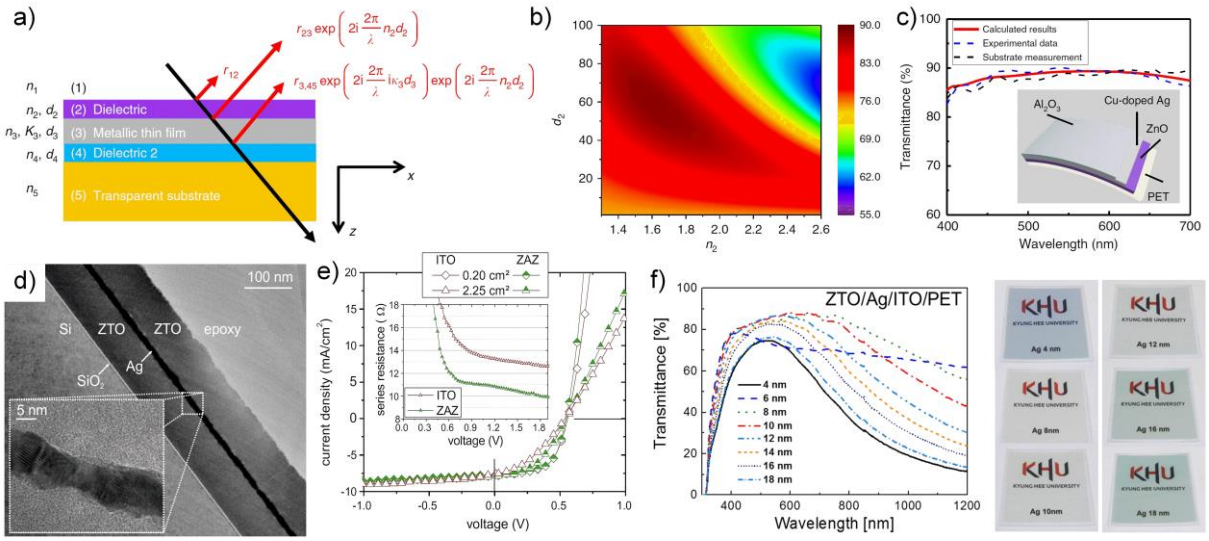

Figure 2: a) Scheme of an asymmetric OMO transparent electrode with design parameters and reflection waves at various interfaces, b) Simulated averaged transmittance (%) of the OMO electrode dependent on the refractive index and the thickness of the top oxide when the bottom oxide and the metallic layer are selected as 24 nm ZnO and 6.5 nm Cu doped Ag, respectively, c) calculated and measured absolute transmittance from 400 to 700 nm of the optimized 56 nm Al_2O_3/6.5 nm Cu-Ag alloy/24 nm ZnO transparent electrode. The transmittance (~88.4%) of the optimized design is even higher than that of the bare PET substrate with an averaged transmittance of ~88.1%. Reproduced with permission.[66] Copyright 2020, Springer Nature. d) Cross-sectional TEM image of ZTO/Ag/ZTO multilayer transparent electrodes, and e) J–V characteristics of semi-transparent organic solar cells with ITO and ZTO/Ag/ZTO top electrode for two different active areas. Reproduced with permission.[63] Copyright 2011, Elsevier. f) Transmittance and images of asymmetric ZnSnO(ZTO)/Ag/ITO multilayer films as a function of Ag interlayer thickness from 4 to 18 nm. Reproduced with permission.[117] Copyright 2018, Elsevier.

To the best of our knowledge, the OMO structure so far generates transparent electrodes with the highest optoelectronic performances in the category of continuous metallic thin films. A uniform, continuous, and smooth surface morphology is an essential requirement to successfully integrate TEs into devices such as solar cells, OLEDs, or screens. Figure 2d-e show a cross-section TEM image of ZTO/Ag/ZTO multilayer transparent electrodes and J-V characteristics of semi-transparent organic solar cells with ITO and ZTO/Ag/ZTO top electrode, respectively.[63] The authors, Winkler *et al* have demonstrated that a triple-layered electrode exhibits a very smooth surface, which would facilitate the charge collection. As a result, cells with ZTO/Ag/ZTO top contact show higher current densities under forwarding bias owing to a lower series resistance compared to cells with ITO (see Figure 2e).[63] OMO structures also exhibit excellent performance as flexible transparent electrodes in OLEDs. For instance, Lee *et al.* demonstrated the possibility of asymmetric multilayers as flexible electrodes for flexible organic light-emitting diodes.[117] Figure 2f shows the optical transmittance spectra and images of the asymmetric ZTO/Ag/ITO/PET multilayer films for different Ag thicknesses. It is evident that the pictures of the samples with 8 and 10 nm Ag interlayers showed high transparency (86.35% for a sample having an Ag interlayer thickness of 8 nm). The OMO TEs have been then used for phosphorescent OLEDs, demonstrating a similar performance as samples fabricated with ITO on glass.[117] The mentioned examples demonstrate that the OMO multilayer electrode is promising and can be used efficiently in flexible devices.

From the technological point of view, the OMO transparent electrodes can be fabricated at low temperature,[59] and therefore on polymeric substrates, which would make their fabrication using roll-to-roll technology become possible. Recently in 2018, Seok *et al.* have successfully fabricated transparent flexible ZnSnO/AgPdCu/ZnSnO multi-stacked electrodes using mass-production-scale roll-to-roll sputtering at room temperature on a 1500-mm-large commercial PET substrate.[113] The obtained TEs showed a low sheet resistance (3.43 Ω/sq),

high optical transmittance (81%), and have been then used for high-performance flexible thin-film heaters and heat-shielding films. It should be noted that the oxide layers can already be fabricated using advanced but low-cost chemical approaches such as atmospheric pressure spatial atomic layer deposition (AP-SALD).[118–121] However, the promising features of the OMO transparent electrodes are mainly inherited from the maturity of sputtering technology, which is essential to obtain an ultrathin but highly conductive metal layer. Therefore, the challenges towards further cost reduction lie in developing new technology for ultrathin metallic film deposition that should be able to operate at low temperatures, in the open air, and with a high-throughput.

3.2. Ordered metallic structures

As aforementioned in Figure 1, state-of-the-art metal grids made of periodic structures of metal lines can exhibit very high Haacke's FoM (about 10 times higher than ITO) with sheet resistance below 10 Ω/sq and optical transmittance higher than 90%. This is far better than vacuum-deposited ITO films.[122,123] The key factor towards such remarkable improvement in optoelectrical performances compared to ultrathin metal films originates from the possibility to separately optimize the optical transmittance and the electrical conductivity. Indeed, in continuous metal film-based TEs, the optical transparency is hindered by the light-electron interaction, which quickly becomes detrimental for films thicker than few nanometers. In metal grids, the transmittance (without substrate contribution) can ~~is~~ be approximately given by the percentage of the space between metal lines and can be easily tuned via the grid geometric parameters such as the line width (*w*), and the pitch (also called line spacing, *p*), as schematically displayed in Figure 3. Because of the particular design of patterned metal grids, the possible plasmonic absorption and scattering can be easily tuned through their characteristic geometric parameters. For instance, the plasmonic absorption enhancement in the active layers for the solar cells is possible with varying the width and the period of the metal grid.[124].

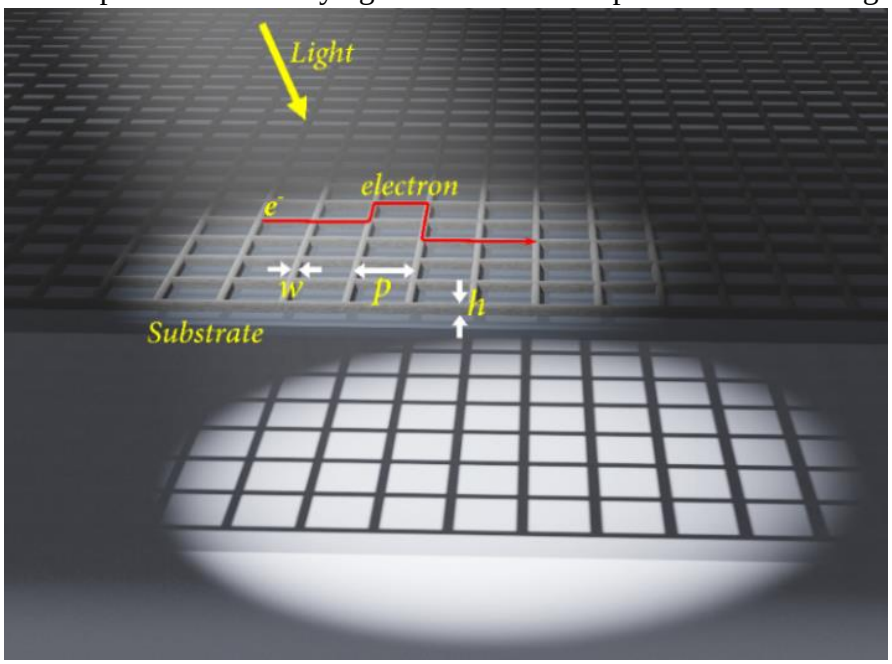

Figure 3: scheme of a metal grid transparent electrode deposited on a transparent substrate under illumination. The line width (w), the pitch (p), and the height (h) of the metal grid lines are depicted. The transmittance in such metal grids is given by the percentage of the space between metal lines, while the grid ensures the electron conduction, depending on the grid density and thickness.

On the other hand, the grid conductivity is related not only to the coverage factor of the metal lines, i.e. *w* and *p*, but also to the height of the metal line (*h*). Therefore, the transparency-conductivity trade-off of metal grids can be directly controlled by their geometric parameters. From the materials' point of view, metal grid-based transparent electrodes have been successfully fabricated from various types of metals including Ag,[56,74] Cu,[55,125] Au[122] or Ni,[126,127] but Ag and Cu are the most widely used thanks to their cost-effectiveness. Then, the optimization of metal grids in terms of electrical properties requires producing grids with a high aspect ratio, i.e. the ratio between the thickness and the width of the metal-grid lines. Thus, the fabrication process is a crucial parameter. Several processes have been investigated by many research groups to produce metal grid-based TEs on either rigid or flexible substrates such as lithography,[56,125,128] imprinting,[129,130] laser patterning/sintering,[131–137] or printing techniques.[74,122,123,138,139] Lee *et al.* recently published a review dedicated to metal mesh-based TEs for organic optoelectronic device applications.[78] In the present work, we mainly focus on the state-of-the-art metal grids of high optoelectrical performances similar to or higher than that of ITO. Schneider *et al.* have combined the nanoscale resolution and the 3D capabilities of electrohydrodynamic (EHD) NanoDrip printing to pattern high aspect ratio Ag and Au metal grid transparent electrodes.[122] As schematically shown in Figure 4a, in EHD NanoDrip printing the viscous ink containing metal nanoparticles is pulled out of a fine nozzle (of about 1 µm outer diameter) and continuously injected toward the substrate to pattern the metal nanogrids with line widths from 80 to 500 nm. Figure 4b-c show printed square Ag and truncated hexagonal Au grids obtained by thermal EHD NanoDrip printing followed by a thermal annealing process to remove the insulating surfactant around the nanoparticles and induce the sintering process as well.[122] EHD NanoDrip printing allows obtaining metal grid-based TEs optimized for low sheet resistances (8 Ω/sq at a relative transmittance of 94%) and a high aspect ratio of 3. Recently, Zhang *et al.* have demonstrated the fabrication of Ag grids via EHD jet printing with even higher aspect ratios, up to 20.[123] The obtained Ag grids exhibit excellent optoelectrical performances, i.e. an average sheet resistance of 3 Ω/sq and relative transparency of 96%. In this work, a nozzle with a large inner diameter of 150 µm was used, resulting in a line width of about 8 µm, thus the pitch diameter was extended to several hundred micrometers to obtain a reasonable optical transmittance. It is worth noting that high line thickness is favorable to achieve a good conductivity while it does not significantly decrease the optical transparency. However, it leads to an increased surface roughness, which is usually not desired for TE integration into certain devices, such as solar cells or OLEDs. Kang *et al.*[140] have demonstrated the fabrication of different metal grid TEs by nanoimprint lithography (NIL)[141] with the metal line width below 100 nm. The authors have employed a soft PDMS stamp fabricated from a nanoimprinted resist template to transfer metal grid on a PEDOT:PSS-coated substrate by slight pressure and heat. However, this process requires the deposition of thin metallic layers on the PDMS stamp by techniques such as electron-beam evaporation, which might eventually increase the fabrication cost. Song *et al.* have successfully fabricated Ag nanomesh TEs with high transmittance of 88% and low sheet resistance of 15 Ω/sq on a flexible substrate using NIL and transfer printing without an intermediate polymer.[142] The flexible inverted organic solar cells (IOSCs) with these TEs exhibited a power conversion efficiency (PCE) of ~ 7.15% at one sun, which is similar to ITO-based devices, as well as superior long-term stability under ambient conditions.

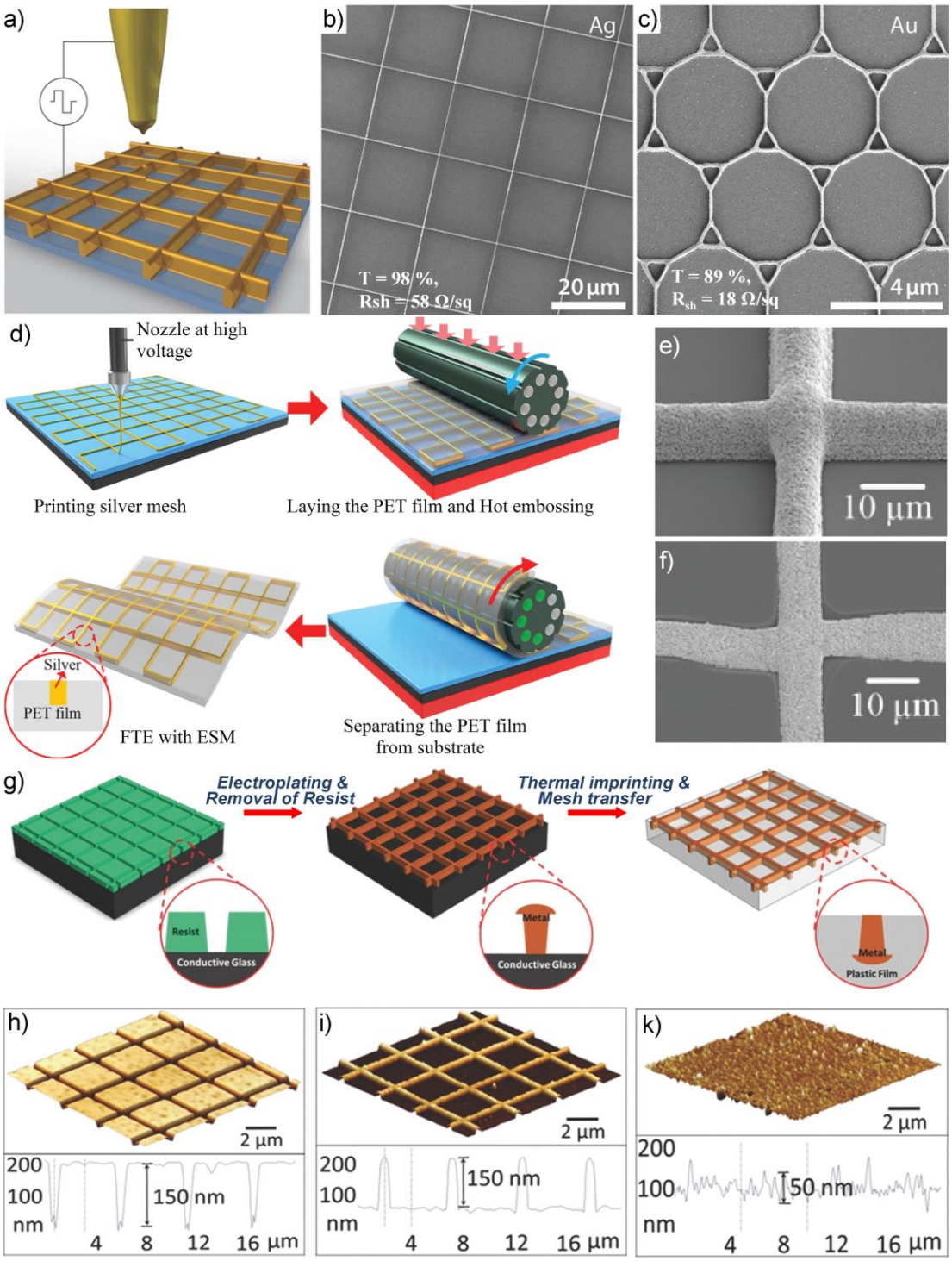

Figure 4: a) Illustration of metal grid fabrication with electrohydrodynamic NanoDrip printing, b) Printed square Ag grid with a pitch of 20 µm and an aspect ratio of 2.5, c) Truncated hexagonal Au grid with fine line-width of 80 nm, and line AR of 2.3. The values for Ag and Au samples were obtained after thermal annealing at 200 °C and 400 °C. Reproduced with permission.[122] Copyright 2015, Wiley-VCH. d) A schematic of the fabrication process of flexible embedded Ag grid by electric-field-driven microscale 3D printing and hybrid hot embossing, and e-f) SEM images of the embossed- and embedded silver grids with 3 printed layers, respectively. Reproduced with permission.[143] Copyright 2021, Wiley-VCH. g) Schematic illustrations templated electrodeposition and imprint transfer (TEIT) process: mesh patterns formed in a resist layer by lithography, electrodeposition of metal inside the resist trenches, then removal of resisting to obtain standing bare metal mesh on the conductive substrate, finally heating and pressing the metal mesh into a plastic film then peeling off the plastic film with the metal mesh transferred in a fully embedded form, and h-k) morphological characterization by AFM of embedded metal grids at different fabrication stages: PMMA nanomesh patterns by electron beam lithography, electroplated Cu nanomesh on the FTO glass substrate after removal of PMMA resist and Cu nanomesh transferred and fully embedded in a cyclic olefin copolymer (COC) film. Reproduced with permission.[56] Copyright 2016, Wiley-VCH

Yu *et al.* have developed a roll-to-roll thermal-imprinting process combined with a doctor blade method to fabricate embedded Ag grids with engraving roughness of about 20 nm.[144] This technique results in Ag grid transparent electrodes with 80.35% transmittance and 6.85 Ω/sq sheet resistance. Moreover, it does not require any vacuum processing but it actually uses the water-based nano-silver paste as in a traditional printing method, which is fully compatible with the industrial roll-to-roll process. Recently, Zhu *et al.* have fabricated embedded Ag grid via the combination of electric-field-driven microscale 3D printing technique and a hybrid hot-embossing process. Figure 4d shows a schematic illustration of this process, resulting in flexible Ag grid-based TEs with transmittance of 85.79%, sheet resistance of 0.75 Ω/sq, and remarkable mechanical stability under diverse cyclic tests.[143] Figure 4e-f show SEM images of the embossed- and embedded Ag grids with 3 printed layers, respectively. The embedded one has a low surface roughness below 20 nm, which is helpful for successful integration in a large range of devices.[143] Another interesting solution to navigate the drawback of high surface roughness commonly observed in metal grid-based TEs is to fabricate metal grids fully embedded and mechanically anchored in a flexible substrate, as proposed by Khan *et al.*[56] Figure 4g illustrates different steps of the templated electrodeposition and imprint transfer (TEIT) process to fabricate such embedded metal grids, resulting in flexible transparent electrodes of excellent optoelectrical performances ($T > 90\%$, $R_{sh} < 1$ Ω/sq) and remarkable surface smoothess, as indicated by AFM imaging presented in Figure 4h-k.[56] The same group have recently applied the embedded Ni grid as a TE for bifacial dye-sensitized solar cells and obtained promising photovoltaic performances, i.e. J_{sc} of 9.25 mA.cm^{-2}, V_{oc} of 0.74 V, FF of 65.4% and PCE of 4.53% with back illumination.[127]

It is also worth mentioning that a regular metal grid can be fabricated according to other geometrical symmetries than square ones: lines,[145] triangular,[146] brick-walls,[147] hexagonal-based[148,149], nanohole array[150] or even coffee ring array[151] patterns using various technologies. For instance Neyts *et al.*[149] found that hexagonal grids should be slightly more efficient than a square grid for OLED applications. The model developed for such analysis constitutes a simple and versatile tool to estimate and then optimize the optical and electrical properties for efficient integration of metal grid-based TEs into devices. Transparent Pt-mesh electrodes with an asymmetric pentagonal tiling were also lately reported.[77] They exhibited good performances when being used as flexible transparent heaters.

In summary, metal grid TEs have gained prominence as excellent alternatives of ITO for optoelectronic applications because of their enhanced mechanical, electrical, and optical properties. Using lithography-based techniques such as photolithography or nanoimprint lithography allows high precision control of grid patterning, but at the expense of affordability. The templated electrodeposition and imprint transfer (TEIT) process appears as a promising technique to obtain high-performance metal grid-based TEs with a remarkable smoothness mainly due to the embedded nature of the grid in a polymer. However, the TEIT process often involves complicated multiple transfer and peel-off procedures, which could lead to problems of cost-effectiveness, reproducibility, and homogeneity at mass manufacture. The direct printing techniques are of great interest due to the large-scale applicability and simplicity of their fabrication steps. Certain printing techniques are even able to fabricate metal grids of excellent optoelectrical performances and with line width below 100 nm, for instance, the case of electrohydrodynamic NanoDrip printing.[122] The requirements for material properties and the associated fabrication techniques depend on the targeted application and will be discussed in detail in part 4 and part 5.

3.3. Random metallic structures

3.3.1. Metal nanowire (MNW) networks

MNW networks have received remarkable research interest since the 2010s.[3,152,153] Such TEs consist of randomly oriented and interconnected MNWs deposited on a substrate, which can be either glass, polymeric, textile or paper.[154] The nanowire diameter is usually in a range of 10–200 nm, the length is typically in the range of 5–100 μm and the aspect ratio greater than 10.[155] The most widely investigated sort of MNW has so far been Ag nanowires (AgNW) due to their good chemical stability and their relatively simple solution synthesis, mainly by the well-known polyol process.[26,156] A capping agent, for instance, poly(N-vinylpyrrolidone) (PVP), is typically included in the process to control the shape of AgNWs. Recent studies report the replacement of polyvinylpyrrolidone (PVP) capping agent and the passivation with other molecules such as the 11-mercaptoundecanoic acid (MUA) to increase the chemical stability[157] or other surfactant-free approaches.[158] Other prominent types of MNWs for TEs have also been investigated such as Cu nanowires (CuNWs),[30,29,159–162,31] cupronickel nanowires[33,163], and Cu-graphene core-shell nanowires[164,165]. Although Cu-based nanowires have great potential due to their significantly lower cost in raw material, their synthesis is less mastered and reproducible as compared to AgNWs. They are also much more prone to oxidation.[31] In contrast, Cu content in the earth's crust is considered to be 700 times higher than that of Ag, and also it is about 100 times cheaper than Ag.[153] Hence, cheap and abundant metals like Cu (when compared with Ag) should play a key role in the future as long as the issues related to their synthesis and stability will have been solved. Recent studies have reported very promising results towards the synthesis of highly purified CuNW without oxidation[166,167] and the encapsulation of CuNW with protective layers, as discussed later in this section. In any case, when comparing the amount of the critical metal in TEs: 750 – 1050 mg/m^2 of indium (In) in ITO film and 40 – 200 mg/m^2 of Ag in AgNWs network, one can remark a significantly lower consumption of Ag to achieve similar optoelectrical performances (R_{sh} =10 – 100 Ω/sq, T=90%) as the In-based TE.[3]

The solution-processing of MNWs and their compatibility with wet coating methods are of important advantages compared to other candidates for the fabrication of cost-effective, indium-free TEs.[168] Several methods have been investigated for the deposition of random AgNW networks. The Figure of Merit (FoM) of the resulting TE is a traditional way to compare the efficacy of these techniques. But other crucial aspects such as the versatility and the cost regarding the development of the process towards industrial scales and the integration of TEs into devices should be taken into account. For example, the spin-coating method is a quick, well-controlled technique that does not require a large solution volume and is often found in the literature.[169] However, it is restricted to laboratory, small-sized substrates and leads to non-isotropic deposition.[170,171] Spray coating is also one of the most reported methods and is promising for the scalable fabrication of highly uniform transparent electrodes.[172] Similarly, other methods, which are compatible with roll-to-roll industrial deposition as well, are the Mayer rod coating[173,174] and the slot-die coating.[175,176] Inkjet and electrohydrodynamic printing are also suitable for up-scalable deposition of MNW networks on a wide range of polymer substrates like polydimethylsiloxane (PDMS), for the elaboration of flexible and stretchable transparent electrodes.[177–180]

From another point of view, the development of the eco-friendly synthesis of MNWs using for example green reducing agents or water-based methods and low toxicity solvents is of great interest.[181,182] Waste management related to fabrication, and the recycling of critical metal

should also be taken into consideration, regarding the cost-effectiveness and the environmental impact. There are few studies on this issue until the present. In the step of chemical synthesis, Wang *et al*. recycled the Ag from the waste generated in diverse nanotemplate reactions and resynthesized AgNWs with common, very good physical and chemical properties.[183] Yoo *et al*. demonstrated a recycling procedure during the patterning of AgNWs on polymer substrates and the recycled nanowires achieved comparable performance with the pristine ones and even higher compared to commercial ITO.[184] Moreover, Han *et al*. demonstrated a "nanorecycling" approach using a laser-induced selective photothermochemical reduction, to restore oxidized Cu to a metallic state for repetitive reuse.[185] Finally, an interesting approach to rapidly diagnose the environmental risk of metal release from transparent electrodes of optoelectronic devices is recently reported by Omaña-Sanz *et al*.[186]

One of the main physical parameters of MNW networks is their density: below a critical density, n_c, there is no percolation (i.e. no pathways for conducting free charges between the two opposite electrodes at each side of the network).[187] This critical density is related to the "2D stick percolation theory" and has been investigated via Monte Carlo simulations and experimental approaches. For MNW networks associated with a network density slightly larger than n_c, geometrical quantized percolation can be observed experimentally when temperature or electrical bias is slightly increased so that some junctions start to be active and more nanowires are participating in the onset of percolation.[27] However, for the great majority of target applications, the density of MNW networks needs to be much higher than the critical density. The group of J. Coleman has published several seminal articles related to the influence of network density on the physical properties of MNW networks.[188–190] For instance, they showed that beyond the n_c,another transition exists (much less known and studied than the stick percolation) which separates the percolative regime from the bulk regime, the latter ~~one~~ being associated with denser networks.[190]

Thus, as opposed to ordered metallic structures, where percolation and conduction is ensured thanks to the imposed pattern, transparent electrodes based on disordered networks rely on effective percolation to be functional. While it could seem that having to reach percolation to have a conductive electrodes is a limitation for random metallic nanostructures, this is not the case. To begin with, random networks are much easier to obtain since they can be fabricated by different low cost methods, such as spray coating or rod coating from suspensions containing the initial metallic nanostructures (mostly nanowires), with no pattering needed. And as said above, most applications require resistance values for which the density of nanostructures is high enough to ensure percolation. Indeed, simulations show that random nanowire networks can provide lower R_{sh} for electrodes in which nanowires are deposited in an ordered fashion (vertically and horizontally). In addition, in a percolative network based on nanowires, the are many wires that, while not forming part of any percolation pathway between electrodes can effectively collect/inject charges from/to the active layer (i.e. absorber in a solar cell or active materials in a LED device). This is not the case for electrodes based on ordered structures, in which charge collection/injection depends only on the charge diffusion length being larger that the gaps in the electrode. Also, for applications where micron to mm size patterns may be needed (antennas or electromagnetic filter, for instance), these could be made by depositing the random networks through masks, as in a recent work by Papanastasiou *et al.* where the latter are easily fabricated thanks to 3D printing.[191] This being said, it is also worth noticing that efforts were made from the community lately concerning aligned one-dimensional object. A review was lately devoted to the current methods for preparing macroscopic composite films in

which the long axis of individual 1D-nanoobjects is more or less parallel to the x,y-plane of the substrate as well as to each other (alignment direction).[192] Related directly to metallic based TE, for instance the oriented deposition of AgNWs using grazing incidence spraying AgNW suspension on a substrate comprising parallel surface wrinkles produces highly oriented AgNW networks.[193] The resulting linear arrangement of AgNWs leads to a pronounced macroscopic optical anisotropy measured by conventional polarized UV–vis–NIR spectroscopy. By exploiting the balance between shear forces and substrate–nanowire interactions mediated by wrinkles offers a way to control the self-assembly of nanoparticles into more complex patterns that can help to tune the metallic based TE.[193] This area would deserve more attention by the community in the future.

The dimensions of MNWs also play a key role in the associated network properties. The average MNW diameter was proved to impact the optical transparency and haziness,[194–197] the electron scattering,[198,199] or the characteristic temperatures of the resulting networks. The latter concerns temperatures observed during a thermal post-treatment: either temperature that minimizes the AgNW network electrical resistance or the spheroidization temperature for which the electrical resistance is diverging.[48] On the other hand, the average MNW length, the wire curvature, and the angular distribution of the deposited nanowires were proved to drastically influence the network density (i.e. the number of MNW per unit area) associated with the onset of percolation.[200] It was also demonstrated that it is possible to reach a low haze factor when using ultra-long MNWs due to the limited number of NWs required to reach a high conduction level.[201–203] Nowadays there are more and more studies showing a rapid and one-step synthesis of ultra-long AgNWs.[204,174] Another important parameter linked with the length of the nanowires is the toxicity issues; the group of J.-P. Simonato has reported a safer by design approach to promoting the use of short AgNWs because they are less toxic towards murine macrophages.[205]

Increasing the MNW network density results in a linear increase of the haziness of the electrode, as shown by Figure 5a. This is in agreement with other similar studies.[206,207] The denser the network the lower the optical transparency and the lower the electrical resistance, as shown by Figure 5a as well. It is therefore required to look for a trade-off when trying to maximize the Haacke's FoM.[48,189] One of the highest values recently reported is for AgNW networks deposited by Mayer rod coating, presenting 94% transmittance and 5 Ω/sq sheet resistance, which gives a FoM of 107.7×10^{-3} Ω^{-1}. However, the traditional Haacke's FoM[208] or the DC-to-optical conductivity ratio,[49] are related only to the electrical and optical performance of the MNW networks. Other critical parameters such as haziness (in solar cells or displays), flexibility (in wearable devices), or thermal stability (in transparent heaters) are not involved, but indeed of great importance in device integration. Many studies reported that in the case of as-deposited MNW networks, the nanowire-nanowire contact resistance is too large due to the lack of intimate contacts and the potential presence of organic residues. Therefore, post-deposition treatments such as thermal annealing,[209] mechanical pressing or rolling,[210] capillary-force-induced cold welding,[211–213] plasma-induced welding,[214] light irradiation sintering,[215] chemical treatments,[32] laser sintering[216,217] or self-limited nanosoldering[218] have been reported. Ding *et al*. recently summarized the different techniques used for welding the nanowires.[219] These methods can drastically reduce the network electrical resistance from 10^4 or 10^5 to about few or few tens of Ω/sq. Such a large reduction can for instance be attributed to the reduction of organic residues on the surface of the nanowires and/or the surface diffusion induced local sintering of the junctions.[209] Bellew[220] and Nian[221] were

able to measure the electrical resistance of NWs and individual NW-NW junctions before and after post-deposition treatments. These two investigations showed that for optimized networks, the junction's final resistance is relatively low, the same order of magnitude as the resistance of individual NWs, and therefore they do not play a critical role in the overall network's electrical resistance anymore. The post-deposition treatments are not limited to the electrical performance enhancement but can be beneficial for other properties as well, such as the surface roughness and the adhesion to the substrates or other active layers in devices. Other important aspects of the post-treatment methods that should be taken into account are, first of all, their impact on substrates that are sensitive to heat, solvents or radiation, especially polymers that are necessary for flexible electronic devices or solar cells. Liu *et al*. have shown that capillary force can effectively cause self-limited cold welding of the nanowire-nanowire junction and can be simply achieved by applying moisture on the AgNW film, without any technical support like the addition of materials or the use of specific facilities.[213] Indeed, small water drops can accumulate near the junctions and fill up the gaps between nanowires and as the water evaporates, a meniscus shaped capillary bridge would form between the nanowires, yielding an attractive force to join the separate nanowires into contact. Furthermore, the compatibility of post-treatment methods to the TE fabrication techniques is crucial, for scalable, commercialized processing. Kumar *et al.* have reported a treatment with three sequential steps (thermal embossing, infrared sintering and a nitrogen plasma treatment) that is compatible with roll-to-roll fabrication of organic photovoltaics (OPV). This process leads to a TE with a sheet resistance of 2.5 Ω/sq and 85% transmittance and reduced surface roughness.[222]

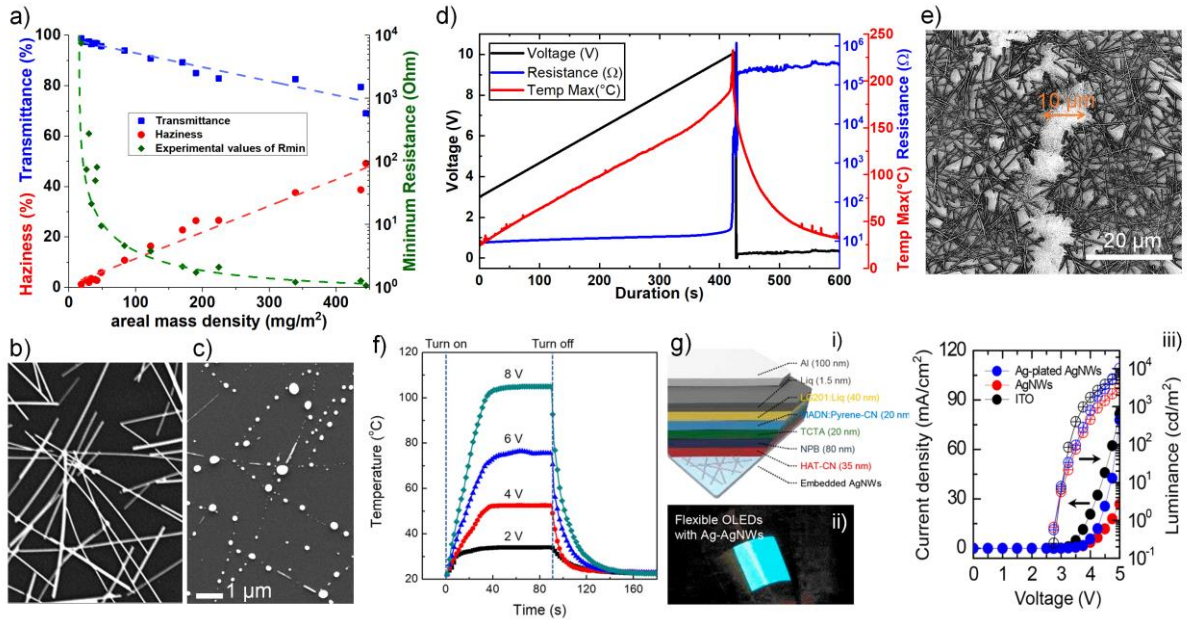

Figure 5: a) Influence of the AgNW network density on the electrical and optical properties (transparency and haze factor). A linear decrease (increase) in transmittance (haze factor) is observed. The symbols correspond to the experimental data while the dashed line is associated to the modelling as reported in Lagrange et al.[48] Reproduced with permission.[48] Copyright 2015, Royal Society of Chemistry. b) As-deposited AgNW network; c) Spheroidized AgNW network after thermal annealing exceeding 270 °C; d) Experimental observation of the degradation of AgNW network with an initial resistance of 8.9 Ω: time evolution of resistance and maximum temperature when applying a voltage ramp of 1 V/min, starting from 3V, until voltage breakdown observed around 10 V. Reproduced with permission.[223] Copyright 2020, Royal Society of Chemistry. e) SEM image of the AgNW network degradation or "crack" visible due to the differences in charging effect on the secondary electron detector. Reproduced with permission.[223] Copyright 2020, Royal Society of Chemistry. f) TH based on Ag NW network on PET with dimensions of 35×35 mm², with a sheet resistance of 7.2 Ω/sq at a transmittance of 90.2%: temperature profiles upon application of different input voltages. Reprinted with permission.[218]Copyright 2019, American Chemical Society. g) Flexible OLEDs with a Ag-AgNW anode: i) schematic device structure and ii) photographic image of the OLEDs, iii) Current density

and luminance characteristics as functions of applied voltage (J–V–L characteristics) of OLEDs based on ITO, as-coated AgNW, and Ag-AgNW anodes. Reprinted with permission.[224] Copyright 2018, Royal Society of Chemistry

MNW networks are prone to degradation when being subjected to either thermal and/or electrical stress or a load of environmental nature.[171,225–227] Thus, stability is one of the main limitations for the successful integration of MNW networks in devices.[228] Such issues have been studied by different approaches, from single nanowire and junctions between them (nanoscale) to the macroscopic failure of the whole network.[223,229–232] Figure 5c reports a typical example where AgNWs do not exhibit a well cylindrical shape anymore, as shown in Figure 5b for as-deposited AgNW network, but for which spheroidization has occurred, due to the Plateau-Rayleigh instability at high thermal stress. The spheroidization of the network leads to breakage in percolation paths and eventually to network failure if the load is not stopped.[209] In addition, the degradation of the AgNW networks under electrical stress has been studied thanks to *in situ* experiments and dynamic simulations.[170,223] Sannicolo *et al*. and Charvin *et al*. demonstrated that the failure dynamics of AgNW networks at high voltages occurs by the formation of resistive hotspots visualized by infra-red (IR) imaging of the surface temperature of the network under electrical stress.[170,223] In Figure 5d presents the evolution of electrical resistance and the temperature of a AgNW network during a voltage ramp; at the voltage failure, the resistance increases sharply. At the same time, propagation of hotspots in a line nearly parallel to the vertical electrodes is observed by IR imaging. After the breakdown of the sample, SEM images reveal that there is a localized degradation of the nanowires, only in the regions where the hotspots have propagated. Such response has been reported also recently by Zhu *et al*.[233] Another cause of degradation is the visible light that has been studied by Wang *et al*.[234] Similarly to the effect of thermal annealing that apart from the junctions optimization it can also lead to the degradation of the MNW networks at high temperatures, light irradiation induces the migration of Ag to enhance the nanowire contacts while also leading to the generation and growth of particles and diameter loss in the nanowire. Light irradiation accelerates the sulfidation and oxidation of the AgNWs as well, resulting in the appearance of degradation products on the nanowire surface. Such degradation mechanisms can indeed be lowered or avoided thanks to efficient coating. For example, Ahn *et al*. reported the use of a graphene shell deposited at the top of the CuNWs, which blocks the atomic diffusion at the surface of the CuNWs, and therefore prevents the structure from morphological instability.[164] Similar results have been reported by Celle *et al*.[31] for a very thin alumina coating that can successfully prevent the oxidation of CuNWs. Several studies have shown stability enhancement of AgNW networks by coating them with thin metal or graphene oxide layers such as zinc oxide (ZnO)[41,235,236], aluminum oxide (Al_2O_3)[237–239], aluminum-doped zinc oxide (AZO), or graphene oxide (GO). Such nanocomposites are thoroughly discussed in section 3.4 of the present review.

Electrically conductive materials that are both transparent and flexible or even stretchable have been one of the major challenges toward achieving various flexible electronic devices such as foldable displays, flexible solar cells, smart windows, wearable devices, robotic/electronic skin, implantable devices, supercapacitors, sensors, and dielectric elastomer actuators.[240–249] One of the most difficult challenges in the development of stretchable electronics is the simultaneous achievement of both excellent mechanical robustness and electronic performance[250–252]. AgNW and other MNW networks embedded in polymer substrates like PEN, PET, PMMA, PDMS, show excellent flexibility with a negligible increase in the sheet resistance and very good response under stretching strain, a property that has been already

demonstrated in several studies.[253–255] The ability of these electrodes to withstand external mechanical stresses is far above the traditional TCOs and it is a major advantage compared to them.[256]

The flexibility of MNW networks is important even when the fabrication of devices uses roll-to-roll techniques, for example in the case of organic photovoltaics, independently if the final product is flexible or not.[210] Park *et al.* used numerical calculations correlated with experimental observations to further support the percolation behavior that is responsible for the density-dependent reliability of the AgNW networks during bending fatigue; the reliability of the AgNW network was degraded as the density of the network decreased.[257] Concerning the elaboration of stretchable, transparent electrodes, PDMS is the most used elastomer, as it is a biocompatible and low-cost material and there are several, simple techniques to fabricate AgNW-PDMS embedded composites.[258–263] Pre-straining the substrates or curving the MNWs before deposition has been proven an interesting strategy to reduce the damage of the nanowires during stretching.[264,265] Seo *et al.* used a nondrying glycerogel that allowed the deposition of wavy Ag nanowires using the pre-strain method up to 400% pre-strain, without causing kinks and interfacial cracks often found with nanowires layered onto PDMS. With a pre-strain of 100%, the resulting nanowire-gel conductor exhibited optical transparency (85%) and electrical conductivity (17.1 Ω/sq) even after 5000 stretching cycles.[266] In addition, selective nanowelding of the AgNWs with high electrostatic potential at the junctions can lead to high-performance stretchable electrodes.[267] A different approach for stable, stretchable devices is a solution-based, low-cost patterning of AgNW networks embedded on flexible and stretchable polymers like PDMS.[268] Furthermore, the elaboration of 3D AgNW conductors in polymeric scaffolds, as reported by Weng *et al.*, leads to novel deformation characteristics suitable for soft, skin electronics.[269] Finally, the adhesion of MNWs to various types of elastic substrates is a crucial parameter affecting the mechanical properties. Thus, measuring the stability after repeating tape tests is a useful technique for such studies.[41] MNW networks embedded on polymers or other organic molecular layers combine the high electrical and optical properties of the MNW network with the desirable mechanical properties of polymers and appear also very promising.[270,271] Another approach is the magnetically assisted electrodeposition of thin films, such as Ni, on top of the AgNWs.[272]

Fabrication of devices using MNW networks has been attempted by many groups. For instance, AgNW networks were successfully integrated for the first time by Celle *et al.* in transparent heaters (TH),[273] the latter being very useful for many applications (defogging-defrosting transparent windows, thermochromics, and medical applications).[274] Following this seminal work, especially the last 5 years, there is a highly increasing interest in the use of MNW networks as transparent heaters.[275] An example of TH is presented in Figure 5f: the TH shows a stable heating response under different low-voltages.[218] AgNW networks were also used as an alternative electrode to ITO in polymer-dispersed liquid crystal smart windows by Khaligh *et al.* and results showed that AgNW networks exhibit superior electro-optical characteristics than ITO and for a lower cost.[276] A flexible touch screen panel with a 400 mm wide AgNW network fabricated by R2R[175] is promising towards industrial upscaling, as well as CuNW networks spray deposited in a large area for resistive touch screens.[161] Lin *et al.* reported recently the AgNW/PDMS patterned transparent electrodes for highly transparent electroluminescent displays, showing reliable emission intensity during bending and stretching cycles.[277] Kang *et al.* fabricated OLEDs with Ag-electroplated AgNW anodes (schema and photo in Figure 5g-i and ii), which exhibited increased luminance than pristine AgNWs and

comparable performance with commercial ITO ones, as presented in Figure 5g-iii.[224] Furthermore, Veeramuthu *et al*. blended AgNW-coated PDMS with thermochromic ink to fabricate a stretchable thermochromic transparent heater for defrosting windows.[245] Stretchable electrochromic devices using AgNW based composites have also been reported.[262,278] MNW networks have been investigated to be used as well as TE in solar cells[279–283] or as sensors.[244,263,284,285] Cu-Ni nanowires have been also used successfully as anodes for OPV.[32] A recent example from the domain of biomedical applications is the all-plant-material-based biodegradable capacitive tactile pressure sensor with AgNW based transparent, flexible electrodes.[286] Many other examples of successful integration of MNW networks in devices can be found in the following references.[253–255,275,287]

Among some examples of devices based on nanocomposite/hybrids with improved MNW networks properties and enhanced stability: the electrodeposition of silver on AgNW networks results in the welding of the nanowires junctions, leading to reduced junction resistance and lower surface roughness, which is beneficial for thin-film solar cells.[282] Also, nickel-enhanced AgNW networks have been fabricated for large size TH of 30×200 mm^2 size with high heating temperature up to 284 °C[288]. In addition, the encapsulation of Cu nanowires with transparent oxides or graphene can result in the fabrication of more stable transparent electrodes. Kim *et al*. reported the fabrication of the Al-doped ZnO/Cu@Ni-NW network as a window electrode for perovskite solar cells.[163] Hybrid graphene/CuNW electrodes with high electronic performance stability ($\Delta R/R_0 < 0.2$ within 180 days) have been applied to triboelectric nanogenerators and quantum dot LED (QLED).[289] Fang *et al*. have recently presented a solution-processed free-standing PEDOT:PSS/AgNWs/PEDOT:PSS hybrid electrode using a capillary force-assisted lift-off process. Such electrodes exhibit good mechanical robustness, electrical conductivity, high transmittance, gas/ion permeability, and show better signal acquisition ability than commercial gel electrodes when used as epidermal electrodes for electrocardiology (ECG) and electromyogram (EMG) signal recordings.[290] Finally, applications of AgNW-enhanced base materials are very useful in facilitating energy-efficient building design, particularly for phase change materials and electrochromic windows, meaning that the field of MNW in the building industry is very promising for future research.[156] UVA exposure degradation problem is also important to take into consideration especially for such outdoor applications and as stated recently by Lin *et al*. the difference between material-level and device-level degradation should be further explored.[291] Further details related to the integration of MNW networks into devices and their applicative domains will be discussed in sections 4 and 5, respectively.

3.3.2. Metal nanofiber networks

The percolation theory for a 2D system composed of 1D sticks of length l predicts that the critical percolation threshold, N_c, dramatically decreases as l increases because $N_c l^2$ is a constant, as proved by Li et Zhang.[292] Therefore, the maximization of the aspect ratio of 1D materials allows to enhance the conductivity of a network while maintaining or degrading as little as possible its optical transparency. The average length of typical (monocrystalline) nanowires is from several micrometers to tens of micrometers, resulting in a relatively high percolation network density (mg/m^2). This is not favorable to obtain high optical transparency and a good stretchability, which is indeed highly required in next-generation transparent and stretchable electronics. Using metal (polycrystalline) nanofiber (MNF) networks is a promising solution since the length of NFs can be in the order of a centimeter, which means that the percolation critical density of nanofiber networks can be theoretically $10^6 – 10^8$ times lower than that of metal nanowire networks. Electrospinning is one of the most popular techniques that enables

the economical fabrication of continuous ultralong NFs for various applications. It has been initially used to fabricate polymer NFs,[293] but then quickly also explored for oxides,[294,295] carbon-based[296], and recently MNFs. The electrospinning technique employs a strong electrical field, in the order of [5-50 kV], to draw very fine, typically micro- or nanofibers, from a polymer solution, as schematically illustrated in Figure 6a. The size of the injection nozzle can vary from micrometers to millimeters. Currently, there are several electrospinning-based systems developed for oriented, twisted, or even multi-component fibers, such as coaxial electrospinning or multi-needle systems which are very interesting in fabricating hollow or core-shell nanofiber networks.[297] The NFs can be used to fabricate transparent electrodes from two different approaches: i) bottom-up, where electrospun NF networks are used as a template, then the NFs are metalized via, for instance, electroless deposition, and finally, the conductive NF network is transferred to another transparent substrate; ii) top-down, where electrospun NF networks are deposited on a metal thin film and serve as a mask for metal etching.[43,298,299] In most of the published work on MNF-based transparent electrodes, the former approaches are dominant due to their low-cost, vacuum-free, and economical consumption of raw materials. However, they suffer from a high or uncontrollable surface roughness.

Cui *et al.* were one of the first groups exploring low-cost scalable electrospinning processes for high-performance transparent electrodes based on MNF networks.[300] They have demonstrated that electrospun copper nanofibers (CuNFs) with ultrahigh aspect ratios of up to 10^5 could result in transparent electrodes with T = 90 % and R_{sh} = 50 Ω/sq. Then when integrated in organic solar cells fabricated as TE, a power efficiency of 3.0%, comparable to devices made with ITO electrodes, was achieved. But Cu-based nanomaterials are prone to corrosion and oxidation when integrate into devices. For instance, the acidic PEDOT:PSS in organic solar cells could degrade electrospun CuNF-based TEs.[300] Jang *et al.* have demonstrated the rapid production via direct electrospinning of stretchable transparent heaters based on electrospun Ag nanofibers (AgNFs) (T = 90%, R_{sh} = 1.3 Ω/sq), as shown in Figure 6b.[301] Such electrospinning process allows the use of commercially available Ag nanoparticles-based ink to fabricate NFs within few seconds, which is indeed remarkable in terms of rapidity and simplicity of the process. However, if taking into account the economical aspect of consuming raw materials, the CuNF-based TEs are indeed more attractive. An *et al.*[42] and Jo *et al.*[302] have combined electrospinning with electroplating techniques to fabricate CuNF-based TEs. Different fabrication steps are illustrated in Figure 6c, along with an SEM image that corresponds to obtained nanomaterials after each step.[302] The TEs obtained with this multistep fabrication technique exhibits very high optoelectrical performances (T > 95%, R_{sh} < 0.5 Ω/sq), thanks to the ability of the electroplating process to efficiently fill the space around the crossed NFs, thus dramatically decreasing junction resistance. Jo *et al.*[302] have also demonstrated the application of CuNF-based TEs as an efficient stretchable transparent heater, as shown in Figure 6d, for a sample with T = 96%, R_{sh} = 0.37 Ω/sq.

Despite the enhanced performances, the use of sputtered Pt could eventually increase the cost of the whole process. A low-cost approach based on electrospinning and electroless deposition has been developed by Hsu *et al.*[303] for both CuNF and AgNF TEs (T = 90%, R_{sh} = 10 Ω/sq). Electrospun polyvinyl butyral (PVB) NFs were used as a template for the subsequent electroless deposition of Cu. The key factor in such a process lies in the selectivity of electroless metal deposition on the templated NFs instead of the substrate. For that, the electrospun templated NFs were fabricated from $SnCl_2$-dissolved PVB solution, then when the NFs are immersed in $Cu(NO_3)_2$ aqueous solution, Sn^{2+} reduces Cu^{2+} and forms a Cu seed layer

on the surface, which acts as the catalytic nucleation site for Cu electroless deposition.[303] Nevertheless, the obtained MNF networks exhibit surface roughness up to several hundreds of nanometers, particularly at the junctions between nanofibers, which is enough to cause electrical shorting in devices.[300] Using a similar approach, Kim *et al.* could obtain flat CuNF-based TEs (Figure 6e).[304] These CuNF-based TEs are fabricated as follows: (i) electrospinning of Palladium embedded NFs, (ii) calcination to eliminate the organic compounds, and (iii) Cu electroless deposition.

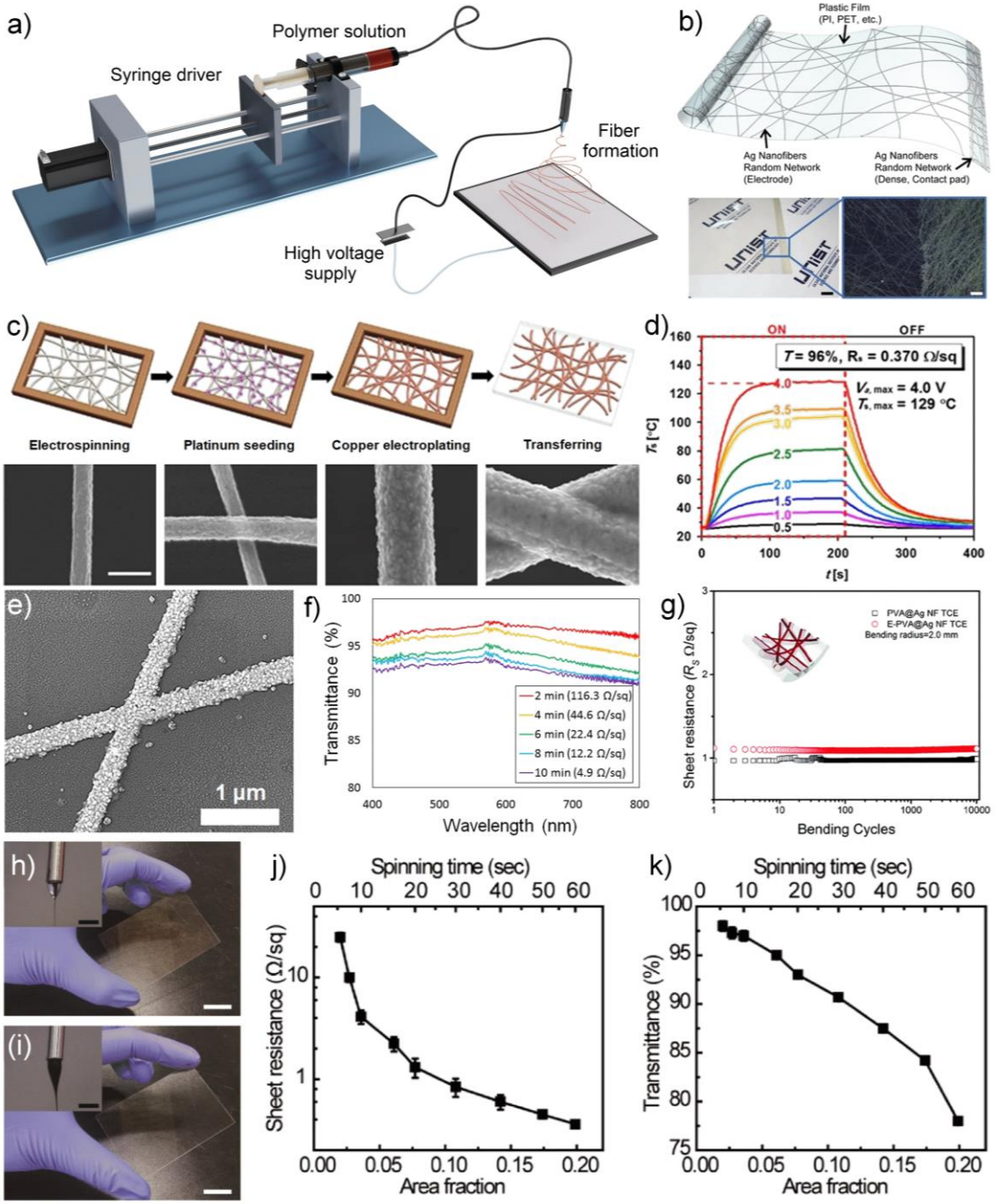

Figure 6: a) Scheme of a typical electrospinning system. b) (top) scheme of the stretchable and transparent heater composed of an AgNF network fabricated with electrospinning, and (bottom) a photograph (left, scale bar: 5 mm) and magnified optical micrograph (right, scale bar: 20 μm) of the border between the electrode and the contact pad. Reproduced with permission.[301] Copyright 2017, Springer Nature. c-d) schematic of different fabrication steps based on electrospinning and electroplating for CuNF-based TEs and corresponding SEM image for each step: pristine PAN, platinum-seeded, Cu-electroplated, and transferred NFs. The scale bar is 1 μm; and temperature profiles of the CuNF-based transparent heater with T = 96%, R_{sh} = 0.37 Ω/sq at different applied voltages. Reproduced with permission.[302] Copyright 2017, Springer Nature e-f) SEM image of CuNFs deposited for 6 min using the following process: electrospinning of palladium-embedded NFs, calcination to eliminate

the polymer component of the NF and Cu electroless deposition; and transmittance of CuNF-based TEs fabricated using different electroless deposition times. Reproduced with permission.[304] Copyright 2018, Springer Nature. g) Sheet resistance of PVA@AgNF- and E-PVA@AgNF-based TEs with compressive stress at a bending radius of 2 mm. Reproduced with permission.[305] Copyright 2017, Royal Society of Chemistry. h-i) A bare CuNF-based TE and a black CuNF-based TE fabricated by normal electrospinning and coaxial electrospinning, respectively. j) Sheet resistance as a function of area fraction and electrospinning time. k) Optical transmittance as a function of area fraction and electrospinning time. Reproduced with permission.[306] Copyright 2019, Elsevier.

This process results in CuNF-based TEs with transparency higher than 90% in the visible range, and sheet resistance of 4.9 Ω/sq (Figure 6f). In particular, the surface roughness of the obtained TEs is reduced to below 100 nm with flat and junction-free NF networks. Further reduction of surface roughness could be achieved using an embedded structure in a polymer substrate (as described in section 3.2 for metal grids). Singh *et al.* have demonstrated the enhanced mechanical stability of PVA@AgNF- and E-PVA@AgNF-based TEs when being subjected to compressive stress at a bending radius of 2 mm, as shown in Figure 6g.[305] This research group then applied embedded PEDOT:PSS/AgNF TEs for solid-state supercapacitors, which exhibit high areal capacitance (0.91 mF/cm^2) with high bending stability.[307]

For certain applications such as transparent heaters, material failure due to atomic diffusion of metal atoms in nanomaterials is a major concern that affects the lifetime of devices. A common way to navigate this issue is to create a core/shell structure in which the shell plays the role of a diffusion barrier. Such complex core/shell structures can be easily fabricated in a coaxial electrospinning process. Ji *et al.* have reported the fabrication of continuous CuNFs conformally coated with a shell layer of carbon black in a single coaxial electrospinning process.[306] The core solution was prepared from Cu nanoparticles dispersed in Terpineol solvent while the shell one was prepared from PVP-dissolved methanol. PVP was then thermally decomposed at 300 °C to form the black carbon shell. Figure 6h and Figure 6i illustrate a bare CuNF-based TE and a black CuNF-based TE fabricated by normal electrospinning and coaxial electrospinning, respectively. The Taylor cones at the end of injection nozzles can be observed in inset images, showing the black shell solution for coaxial electrospinning. Figure 6j-k show the sheet resistance and the total transmittance of the CuNFs based TEs as the area fraction of the NFs increases, respectively. The optimized electrospinning time for transparent CuNF-TCEs was determined to be 30 s, showing outstanding properties, namely R_{sh} = 0.8 Ω/sq, T = 91%, and haze factor = 3.1%.[306]

A new concept in the fabrication of AgNF transparent electrodes that allows the selective deposition of metal onto polymeric electrospun NF networks has been recently reported by Hatton *et al.*[308]. The selective deposition of Ag over the PVP-based NFs is based on the small condensation coefficient for Ag vapour on organofluorine compounds such as HFE-7500,[309] which are deposited on the substrate prior to the fibers. The AgNF-based TEs fabricated via this technique have average transparency of 90.8% and sheet resistance of 6.3 Ω/sq, which is comparable to the performance of standard ITO films. Nevertheless, this approach still employs a vacuum-based metal deposition technique that might eventually increase the fabrication cost when being scaled up or integrated into roll-to-roll processing.

In summary, MNF network TEs can be fabricated from different techniques including bottom-up and top-down approaches. However, the use of electrospinning seems the most popular and powerful approach, providing TEs with outstanding FoM (T > 95%, R_{sh} < 0.5 Ω/sq) and with high mechanical stability. Such excellent transparency-conductivity trade-off could be achieved due to: i) the low threshold percolation density of ultralong NFs, ii) excellent electrical contact between NFs when combining electrospinning with electroplating for instance. In some cases, junction-free flat MNF networks with relatively low surface roughness (< 100

nm) have been demonstrated. Finally, as with other nanostructured metallic TE materials, using an embedded structure in a polymer substrate could even further reduce the surface roughness.

3.3.3. Metal meshes based on cracked templates

In nanofabrication, the most common top-down approach involves lithographic patterning techniques – a mature field widely used in microelectronics. As discussed in the previous parts, some top-down nanofabrication techniques such as photolithography, nanoimprint lithography, or electron beam lithography have been developed for periodic metal grids-based TEs. The obtained materials exhibit excellent optoelectrical properties (for being used as transparent electrodes) with precise control of patterning at the expense of affordability. Recently, low-cost and simple top-down techniques have been proposed to prepare metal grid electrodes using a self-cracking template. Interestingly, the cracking phenomenon in thin films is normally unwanted but now becomes an interesting approach for metal-based TEs. The mechanism of crack formation that occurs during thermal treatments or the drying process has been discussed in several papers.[310–313] The most used fabrication process of transparent electrodes based on self-cracking template involve three main steps: cracked template, metal deposition, and lift-off of the template, as schematically illustrated in Figure 7a-c.[314] Krzysztof *et al.* seem the first group to apply the self-cracking template to prepare Ag grid transparent electrode.[315] For the template film, the microcrystalline TiO_2-containing solution was first spin-coated on either glass or PET, followed by a low-temperature thermal treatment (< 50 °C) to create the cracking effect. The optimization of the averaged pitch (varying from 4 to 100 µm) and metal wire width (varying from 1 to 2 µm) via spin coating speed and cracking temperature results in an Ag wire network transparent electrode with 60 nm in thickness, 4.2 Ω/sq sheet resistance, and 82% transmittance.[315]

Later on, Kulkarni & Thelakkat and co-workers have reported a transparent conductive Ag metal network (R_{sh} = 10 Ω/sq, T = 86% @ 550 nm) templated by a cracked polymer thin film, which was produced by drying an acrylic-based colloidal dispersion.[314] An Ag film of 55 nm thick was then deposited by vacuum evaporation on top of the template. After lift-off, it yielded the creation of well interconnected Ag mesostructures of 2 µm wide, as shown in Figure 7d. The optical transparency of the resulting electrode was 86% at a wavelength of 550 nm while the sheet resistance was 10 Ω/sq.[314] It is worth noticing that the self-cracking template technique combined with physical vapor deposition of metal layer results in seamless-junction metal mesh, which is indeed a remarkable advantage when compared with single-crystal metal nanowire networks. As illustrated in Figure 7e, the surface roughness within the metal lines are just few nanometers while the stack of several AgNWs could generate a non-negligible surface roughness.[316] Such TE based on cracked templated was then successfully integrated into inverted P3HT–PCBM solar cell and the associated performances were found similar to that of the solar cell using conventional ITO electrodes.[314]

Rao and Kulkarni have also demonstrated the application of the Au wire network fabricated from the cracked template method in a high-temperature transparent heater, which can achieve 600 °C within a few tens of seconds, as shown in Figure 7f.[316] Such Au networks even get self-annealed and display excellent optoelectrical properties (R_{sh} = 3.2 Ω/sq, T = 92%). Most of the works on cracked template-based TEs have employed vacuum evaporation to deposit metal films, but this finally increases the fabrication cost and is no longer suitable for mass production. Electroplating is a low-cost vacuum-free technique that can be used in some cases with the presence of conductive substrate. Muzzillo *et al.* have fabricated the GaAs solar cells' front metal grids from cracked film lithography (CFL) and electroplating techniques and

demonstrated that prebaking at low temperature (< 140 °C) allows decreasing crack footprint down to below 1 µm, thus improving grid transmittance.[317] An energy-conversion efficiency of 24.7% was obtained with such a CFL approach, which is rather close to the performance obtained with standard photolithography technology, as shown in Figure 7g.

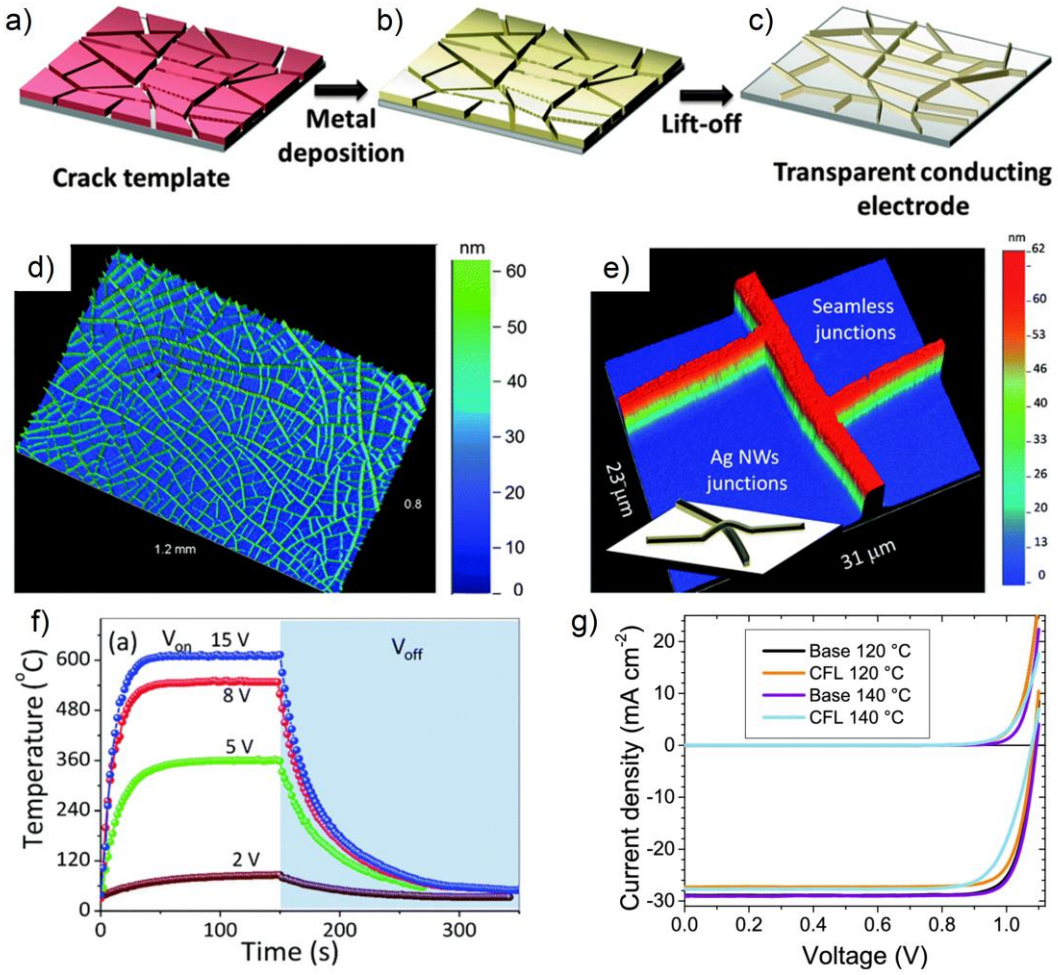

Figure 7: Schematic illustration of different fabrication steps of transparent electrodes based on self-cracking template: a) cracked template, b) metal deposition by vacuum evaporation, c) lift-off of the template, (d) the optical profiler image in a 3D view of the obtained Ag wire network. Reproduced with permission.[314] Copyright 2014, Royal Society of Chemistry. (e) A closer view of a seamless junction Au wire network fabricated from the self-cracking template and vacuum evaporation, the image was captured from an optical profilometry. The inset image illustrates a typical junction between single crystal Ag nanowires for comparison purposes, (f) temperature profiles of the Au wire network/quartz as a function of time at different applied voltages recorded using an IR camera. Reproduced with permission.[316] Copyright 2014, Royal Society of Chemistry. (g) Light and dark JV characteristics of GaAs solar cells with front grids patterned by cracked film method and standard lithography, resulting in devices of high energy-conversion efficiencies: 26.4% and 24.7%, respectively. Reprinted with permission.[317] Copyright 2020, American Chemical Society.

Another economical method is to combine solution processible metal nanoparticle ink, cracked template, and laser sintering, as demonstrated by Yeo & Ko *et al*.[318] Remarkably, they have demonstrated the possibility of using low-temperature fast scanning of CW laser to efficiently sinter Cu nanoparticles without damaging the polymeric substrate and oxidation of Cu lines, which is generally impossible for conventional thermal annealing steps.[318] Both laser sintering and electroplating techniques are low-cost, industrial scale-compatible, however, each presents its limitations. The former requires a substrate and bottom layers that are transparent at the laser wavelength, if not they can be damaged. In contrast, the latter requires a conductive substrate, thus, needs some extra transfer steps. Finally, as already discussed in the part of

periodic metal grids, the surface roughness is always an issue for a successful TE integration into devices. In the case of TEs based on a cracked template, the surface roughness is not so crucial and usually below 100 nm. Leng *et al.* have demonstrated that hybrid (Au/Ag) metal grid electrodes embedded in polyimide with a highly smooth surface could be fabricated via self-cracking template, thermal evaporation, and peeling transfer step.[319] From the point of view of raw material consumption, the use of physical vapor deposition and lift-off technique to fabricate metal random grids is not economical compared to, for instance, the electroplating technique. In this context, it is required to develop new technologies that allow selectively depositing metal on specific areas of a substrate. For instance, area-selective atomic layer deposition using inhibitors could be of great interest.[320]

3.3.4. Dealloyed ultrathin metallic films

As discussed in section 3.1, pure metallic layers could be used as TEs if they are made ultrathin (<10 nm). Another approach based on thin metallic layers consists of using alloys. Homogeneous thin metallic alloys would exhibit the same main features, and then possibly similar drawbacks, as pure metallic thin layers. However, the dealloying process allows the creation of a non-continuous layer which could potentially increase the optical transparency level. Dealloying refers to a selective dissolution (either chemical or electrochemical) of the less noble elements of an alloy via controlled corrosion.[321,322] The common method occurs in the liquid phase, i.e. dipping an alloy thin film predeposited on a substrate in a corrosive solution to be dealloyed. The delaminated metallic membrane floating on the surface is then transferred to another transparent substrate. However, the dealloying in the liquid phase exhibits several drawbacks such as agglomeration of the membrane, or poor electrical conductivity due to the presence of microcracks in the nanomesh.[323]

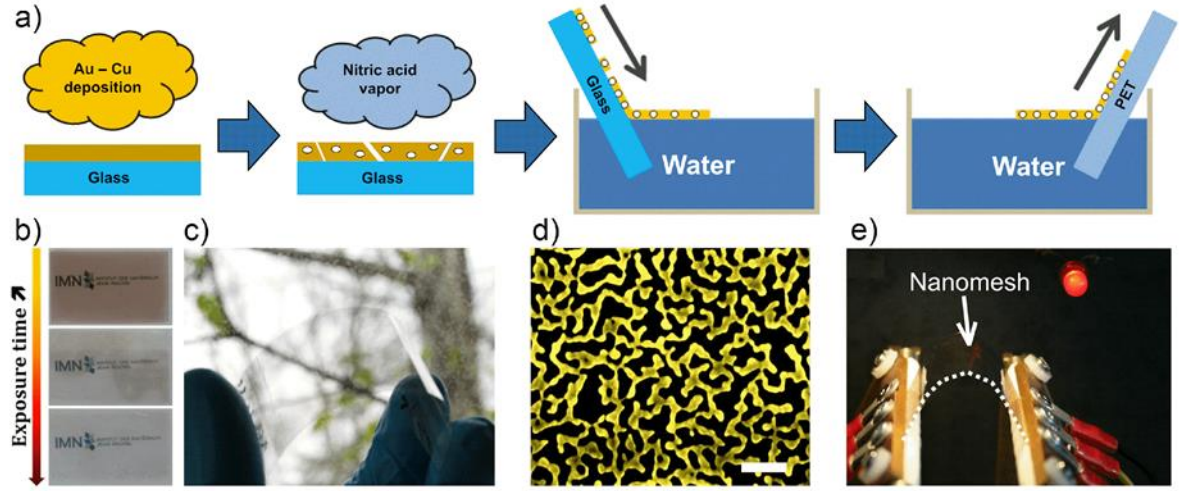

Figure 8: a) Scheme showing different steps to fabricate Au nanomesh electrodes: co-sputtering of Au-Cu ultrathin film, which is then exposed to nitric acid vapor before being transferred to PET substrate, b-c) photographs showing the evolution of an Au-Cu film versus exposure time to nitric acid vapors and a gold nanomesh on a PET substrate, d) colored SEM image of a 10 nm-thick gold nanomesh prepared using Au-Cu film with an initial Au content of 17 at.%, scale bar: 200 nm, e) photograph of nanomesh electrode on flexible PET substrate under a strain of 1.2%, being used to switch on a red LED. Reproduced with permission.[324] Copyright 2019, Springer Nature.

Recently, Chauvin *et al.* have reported remarkable progress on the fabrication of transparent conductive metal nanomesh electrodes from dealloying ultrathin Au-Cu films.[324] The key success factor in their work lies in using acidic vapors instead of a liquid phase for the dealloying process of ultrathin Au-Cu alloy, which strongly reduces the delamination of the nanomesh. Figure 8a-c show respectively different fabrication steps of such a process, the evolution of an Au-Cu film versus exposure time to nitric acid vapors, and a gold nanomesh on

a PET substrate. The obtained transparent electrodes exhibit average transparency in the visible range of about 79% and sheet resistance of 44 Ω/sq, which so far represents the best optoelectrical performances for dealloyed thin films as transparent electrodes. Furthermore, the 10 nm-thick percolating Au dealloyed film prepared from a Au-Cu film with an initial Au content of 17 at.% is illustrated in Figure 8d, which brings about promising and interesting technological options to use less noble metal in TE fabrications. It was also demonstrated by Chauvin *et al.*[324] that under a mechanical stability test with 10000 bending cycles (bending radius of 6 mm), the resistance of the Au nanomesh increases by 7%, compared to 54% and 2200% for the cases of Au-Cu reference and ITO films, respectively.[324] After metal/metal alloys, this method has also been applied to metal/carbon nanocomposites. For instance, Bouts *et al.* have performed selective etching on Cu/C nanocomposites thin films, resulting in TE with a sheet resistance of 140 Ω/sq and optical transparency lower than 70% at 550 nm.[325] So far, although such dealloying approach to fabricate transparent electrodes has several advantages such as low-temperature processing, tunable transparency and conductivity via adjusting the initial metal content in the alloy, it has been yet poorly explored in the literature. Further studies to optimize the fabrication process, optoelectrical properties and verify the material stability in different working conditions such as high temperatures are still required for dealloyed ultrathin metallic films to gain maturity in TE applications.

3.3.5. Metal nanotrough networks

Other particular nanostructures, namely nanotrough, have been also suggested for TE applications. Transparent electrodes based on metal nanotrough networks have been fabricated and optimized for the first time by Cui's group in 2013.[43] The 4-steps fabrication process of this unique concave nanostructure is summarized in Figure 9a: electrospinning of polymer nanofiber (NF) template, thermal or electron-beam evaporation of metal nanotrough on the template, transfer onto the desired substrate, and finally chemical etching of the polymeric template. Several remarkable advantages of this technology can be mentioned: high optoelectrical performances (junction resistance-free, high transmittance because of nanotrough structure), simplicity of fabrication process. Indeed, it is based on electrospinning, which is a low-cost, low-temperature, and fast technique, while the standard metal depositions employ vacuum-based mature technologies of a high degree of automation and process control. Additionally, the optical and electrical properties of the metal nanotrough networks are also outstanding. For instance, Cui *et al.* have obtained 2 Ω/sq at T = 90%, 10 Ω/sq at T = 95% and 17 Ω/sq at T = 97% for Cu nanotrough networks. Slightly lower performances could also be obtained for Au or Ag nanotrough networks, as shown in Figure 9b.[43] The authors also indicated that flat transmittance spectra obtained for a wide range of wavelengths, from 300 nm to 2000 nm, are highly desirable in several applications such as near-infrared sensors, solar cells, etc. Figure 9c-d show a photograph of Au nanotrough networks on paper after mechanical deformation and an SEM micrograph of Au nanotrough networks on Al foil after folding, respectively. This indicates the mechanical flexibility of nanotrough networks, even though the sheet resistance of the Au nanotrough network on paper increased 80%.

After the first work on metal nanotrough network, An and Park *et al.* have also developed TEs based on metallic glasses (CuZr) from electrospinning and co-sputtering process.[51,52] The optoelectrical performance (for instance, the sheet resistance of 3.8 Ω/sq at a transmittance of 90%) and SEM image of CuZr nanotrough networks are shown in Figure 9e-f. In addition to outstanding optoelectronic properties and mechanical robustness, the authors have demonstrated that CuZr nanotrough networks exhibited high chemical stability against harsh

environments (negligible degradation in performance for 10 days in 85% RH and 85 °C).[52] The application of the nanotrough networks in wearable transparent heaters was also illustrated in Figure 9g. To reduce surface roughness, metal nanotrough embedded polymeric substrates have been developed.[326,327] Flexible touch screen panel of ultrasmooth (surface topography < 1 nm) was fabricated using such metal nanotrough embedded films.[326]

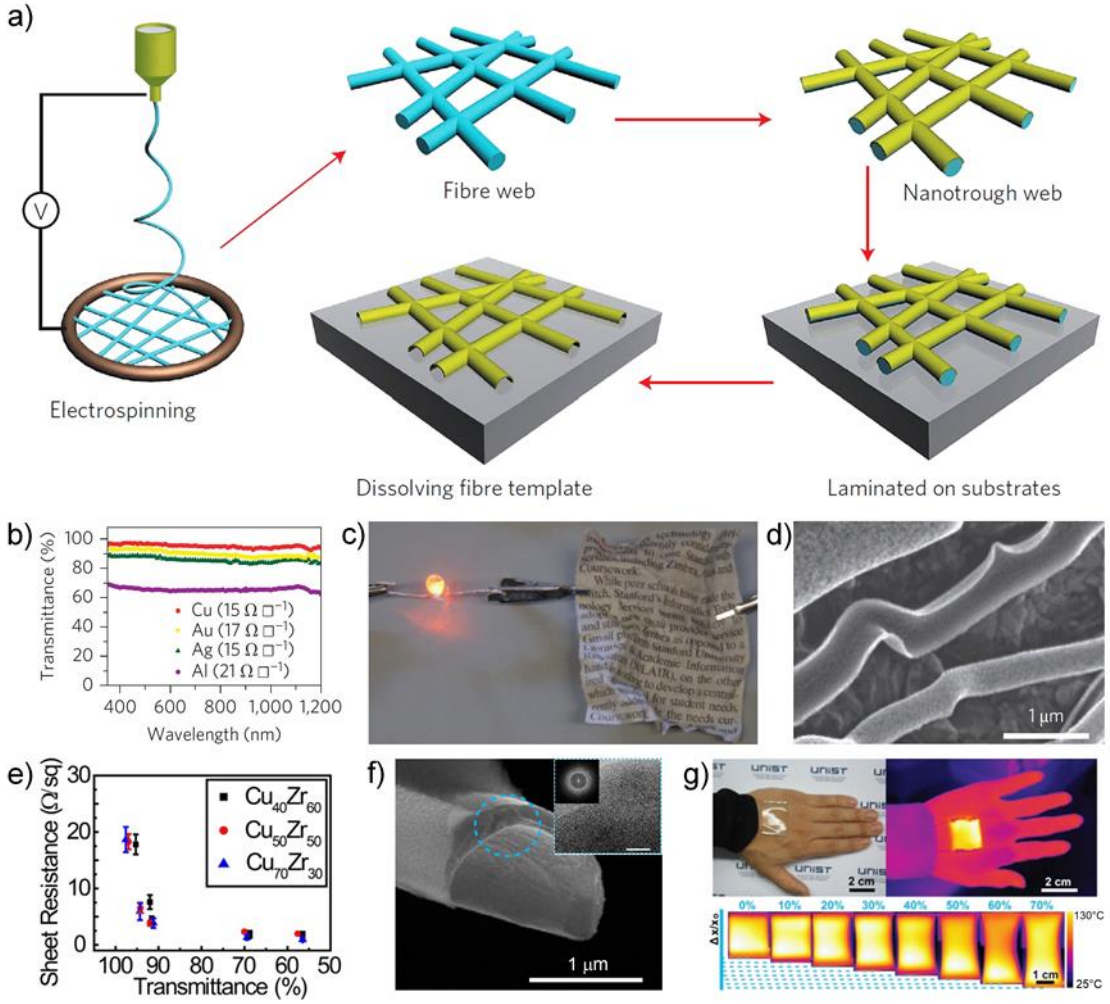

Figure 9: a) Fabrication and transfer process for metal nanotrough networks: electrospinning of polymer nanofiber templates, deposition of metal layer, transfer of coated nanofibers to a desired solid substrate, and finally dissolution of polymer-fiber templates. Reproduced with permission.[43] Copyright 2013, Springer Nature. b) transmittance of metal nanotrough networks made of different metals, showing excellent optical-electrical performances of Cu/Au nanotrough networks. Reproduced with permission. Copyright 2013, Springer Nature. c) photograph of Au nanotrough networks on paper after mechanical deformation, d) SEM micrograph of Au nanotrough networks on Al foil after folding. Reproduced with permission.[43] Copyright 2013, Springer Nature. e) Transmittance versus sheet resistance of the CuZr nanotrough network (prepared by electrospinning and co-sputtering process), f) SEM micrograph of a CuZr nanotrough, the inset TEM image with Fourier transformation diffraction pattern indicating the amorphous nature of the alloy, g) IR images of transparent heaters based on the CuZr nanotrough networks (prepared on PDMS substrates) under various tensile strains. Reprinted with permission.[52] Copyright 2016, American Chemical Society.

Guo, Ren *et al.* have also developed Au nanotrough network-based TEs of excellent fatigue performance (repeatedly stretched to strains up to 120% for 100000 cycles). To the authors' best knowledge, there are surprisingly few papers on metal nanotrough network-based TEs. So far, despite excellent optoelectrical performances, they haven't been widely used for TE applications. This could be explained via some of the drawbacks related to their fabrication process: i) involvement of vacuum-based metal deposition technique that increases the

processing cost, ii) selective deposition of metal on polymeric nanofibers is technically impossible, that, once again makes the fabrication process less economical.

3.4. Nanocomposites based on metal nanowires (MNWs)

In the particular case of metal nanowires, the development of nanocomposites that combine these nanostructures with different classes of materials can be a route to overcome some intrinsic issues of this type of TEs. Though MNW percolating networks present outstanding optical, electrical and mechanical properties, their application in devices is still limited due to issues related to stability, fatigue, surface roughness and adhesion to the substrate, hence the creation of composites with different matrix materials is highly explored.

3.4.1. MNWs and Oxide Thin films

Another strategy that has been widely used to enhance the stability of TE based on MNWs has been to combine them with an oxide material. The most common approach has involved the deposition of an oxide coating on top of the network, although some studies have also used a sandwich or multilayer configuration. In these cases, the MNWs lay between two layers of oxide, similarly as it has been done for metallic thin films (see section 3.1).[328–330]

Different oxides such as ZnO,[331–333] TiO_2[230,334] and Al_2O_3,[31,333] have been combined with Ag and Cu nanowire networks, showing in all cases a clear improvement in the stability of the networks. A key aspect for an efficient integration of such composites in industrial devices is that the deposition method used should be low-cost, high-throughput, and compatible with large-scale fabrication. However, the oxide coatings are usually deposited by methods like atomic layer deposition (ALD),[335] spin coating, or sputtering, which are vacuum-based techniques and usually present difficulties for upscaling. These facts could ultimately hinder the low cost and scalability of the AgNW-based transparent electrodes (TEs).

Therefore, alternative approaches are being studied lately, one of the most promising being the spatial atomic layer deposition (SALD) technique.[118] SALD is a recent variation of ALD in which the precursors are continuously injected in the reactor, as opposed to the lengthy sequential pulse-purge steps of ALD, in different locations of the reactor, while separated by regions of inert gas (for instance nitrogen or argon). By alternatively exposing the sample to the different regions, the typical ALD cycle is reproduced, but avoiding the purging steps. As a result, SALD can be up to two orders of magnitude faster than ALD, even when performed at atmospheric pressure. Both the faster deposition rates of SALD concerning ALD and the vacuum-free processing make the SALD more suited for up-scaling and mass production.[336] As the chemistry is the same and the process is based on surface-limited and self-terminated reactions, the main assets of ALD are maintained. As a result, SALD has already been largely applied to photovoltaic devices at the laboratory and industrial levels.[118] In a work by A. Khan *et al.*,[41] SALD was used to deposit thin layers of ZnO to improve the stability of AgNW networks. As expected, the ZnO coating improved the adhesion of the AgNW networks to the glass substrate, and a clear enhancement of the thermal and electrical stabilities were also observed. More interestingly, the authors studied the effect of the coating thickness on the stabilizing effect. Oxide films of 15 to 30 nm thick were deposited (Figure 10a-b) on top of the networks, and the results show that the thicker the coating layer the more enhanced the stability (Figure 10c). Based on the assumption that the coating stabilizes the AgNW by preventing atomic Ag diffusion, which is necessary for the morphological instability of the nanowires (eventually leading to spheroidization), the authors presented a model in which the failure

voltage of the network could be correlated to the thickness of the coating. However, a small and linear decrease of the optical transparency is shown when the coating thickness increases.

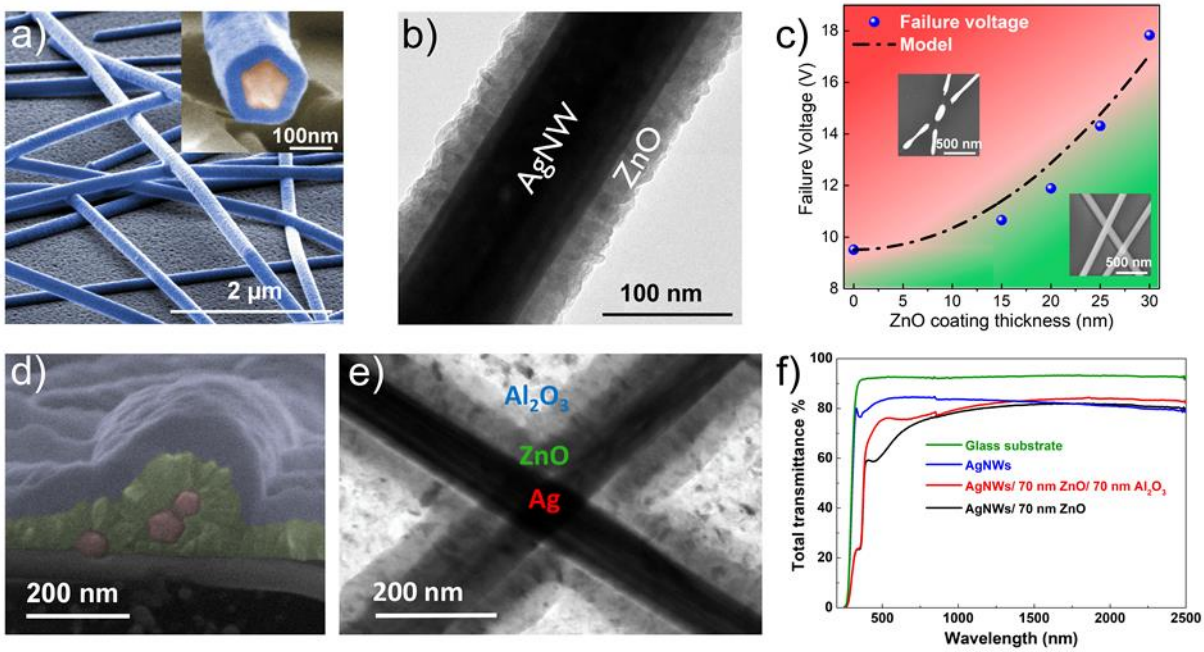

Figure 10. a) SEM image (false-colored) of AgNW networks coated with 30 nm ZnO (deposited with SALD) with a small back-scattered SEM image of a coated AgNW showing the usual 5-fold symmetry twinning of AgNWs surrounded by a uniform 30 nm thick ZnO layer, b) TEM image of a 30 nm thick ZnO-coated AgNW, c) failure voltage dependence versus ZnO coating thickness. Reprinted with permission.[41] Copyright 2018, American Chemical Society. d) SEM image (false-colored) of a cross-section of AgNW networks coated with 70 nm of ZnO and 70nm of Al_2O_3. e) TEM image of a thick ZnO and Al_2O_3 coating (deposited with SALD) around two different AgNWs. f) Total transmittance spectra of a bare AgNWs network and coated networks with ZnO and a combination of ZnO and Al_2O_3 coating of 70 nm each. Reproduced with permission.[239] Copyright 2019, Royal Society of Chemistry

To improve the figure of merit of such composites, the same group explored the deposition of a second Al_2O_3 coating, also by SALD (Figure 10d-e). The results show that the Al_2O_3 coating acts indeed as antireflective coating and the resulting composite shows an increase in transparency (Figure 10 f).[239] In an even more appealing combination to low-cost applications, cheaper CuNWs have also been efficiently protected by thin Al_2O_3 thin coatings deposited by SALD.[31] As shown, the nature and thickness of the oxide coating have a strong effect on the final properties of the composites and, therefore, must be tuned for the targeted application. For example, in the case of thermal heaters, the most important parameters are thermal stability and transparency.[4]

For integration in photovoltaic devices, it is of upmost importance to maximize the FoM of the composite electrode, by reaching sheet resistances ideally below 15 Ω/sq and transparency values above 80%. While single oxide coating MNW networks have been successfully used to obtain composite electrodes with the required FoM, a key aspect for integration in solar cells is the collection efficiency of the electrodes, in particular for the charges photo-generated far from the conductive nanowires. To enhance the collection efficiency of nanocomposite electrodes, AgNWs have been combined with TCOs, as ZnO:Al,[337,338] or ITO.[328] The contribution of the TCO to the conduction in the hybrid has been observed by Nguyen *et al*. by evaluating nanocomposites with a constant ZnO:Al thickness and varying areal mass density of the AgNW networks.[256] For composites with a network density close to the percolation threshold, a synergistic effect was observed between the two materials, resulting in a decrease of resistance when compared to either the ZnO:Al or

AgNW networks alone. A conduction model demonstrated that the conduction occurs between small clusters of percolating nanowires and through the conductive ZnO:Al coating.

Although it has been said that thermal stability and adhesion are less important parameters when intending to use composite electrodes in solar cells, attention must be paid to the device fabrication protocol to ensure that processing temperatures and mechanical stresses can be withstood by the composite electrode. Also, while stability studies of the composite electrodes alone are important to assess the robustness of the electrodes and potential applications, the chemical stability of the electrodes against the other components of the cell, and the overall device stability need to be evaluated. Lee *et al.* studied the chemical and mechanical stability of flexible hybrid perovskite solar cells fabricated with ZnO:Al /AgNWN/ ZnO:Al bottom electrodes. In this study, different types of electrodes were compared in which the top ZnO:Al layer was amorphous or crystalline. Their results showed that the amorphous top ZnO:Al layer provides both a better mechanical and chemical stability since, on the one hand, they show higher flexibility than the crystalline ZnO:Al layer and, on the other hand, the lack of grain boundaries prevents silver diffusion to the cell active layer, as observed by profile-XPS studies.[329] Jon *et al.* have also demonstrated that AgNW coated with a SnO_2:Sb layer are stable against the deposition of a hybrid perovskite active layer, which was not the case for the bare networks.[339]

For some research works, the coating may not provide the expected stabilization. For instance, Resende *et al.* have shown that composite electrodes of AgNW and TiO_2 deposited by SALD at low-temperature, fail at the same voltages as bare networks when subjected to a voltage ramp.[340] Nevertheless, a resistive switching mechanism was observed across the spheroidized region of the network left after the electrode initial failure. As a result, the composite electrodes were the first example of an in-plane transparent resistive switching device entirely fabricated with open-air, low-cost approaches, and showing on-off ratios of 10^6. For optimized network density, the switching voltage was as low as 0.16 V. The role of the oxide layer was the key factor to the switching, which only happens for composite electrodes having a narrow range of TiO_2 thicknesses. In addition, the study allowed to show that, differently from what was previously reported for other Ag-TiO_2 based switching devices, the switching takes place through a combined conduction mechanism involving tunnelling between Ag nanostructure edges, and the resulting Schottky emission across the TiO_2 coating.

As deduced from the above, the intrinsic properties of the oxide layers are of key importance to control the properties and potential integration of the composite electrodes in functional devices.

3.4.2. MNWs and Graphene-based materials

Graphene is another possible combination for metallic nanostructured materials. This allotrope carbon material is composed of a single layer of atoms in a two-dimensional honeycomb lattice, which results in a semimetal material due to its conduction bands configuration. Additionally, a single graphene sheet is highly transparent as it is extremely thin. Thus, the mixture of graphene and metallic nanostructures enables the development of enhanced transparent electrodes, both in optical, electrical conduction and stability properties.

A hybrid structure of a single layer graphene film and a silver nanowire network allows the fabrication of a highly transparent, low resistive and highly stable composite, as previously reported.[341] The deposition of graphene by chemical deposition methods, such as CVD, allows for a continuous single layer film through the network, leading to transmittance values as high as 88% at 550 nm wavelength. SEM and TEM images of graphene and silver nanowire

networks nanocomposites are presented in Figure 11a and b, respectively. The sheet resistance of this hybrid reduces from 22 Ω/sq after production to 13 Ω/sq after 4 months due to stabilization under ambient conditions. The combination of highly conductive nanowires to the graphene film allows to overcome one problem of this 2D material: the highly resistance grain-boundaries. The nanowire network can be used to create co-percolating conduction between the two materials, overcoming the high resistance grain boundaries issue, as the electrical transport can pass through the metal nanowires. This is schematically shown in Figure 11c-d.

In terms of mechanical stability, these hybrids exhibit high performances under mechanical pressure and bending, as well as substrate adhesion, when compared to separate graphene films and silver nanowire networks.[341] On the thermal and chemical stability, thanks to the gas-barrier property of the graphene layer, the latter constitutes a protective layer for the silver nanowires, reducing the oxidation of the nanostructured network. This leads to a superior long-term stability under ambient conditions, when compared to bare AgNW networks, enabling the integration within organic solar cell. So, photovoltaic devices with the graphene and AgNW network hybrid exhibited excellent performance, resulting in a power conversion efficiency of 3.3%, above organic cells produced with ITO.[342]

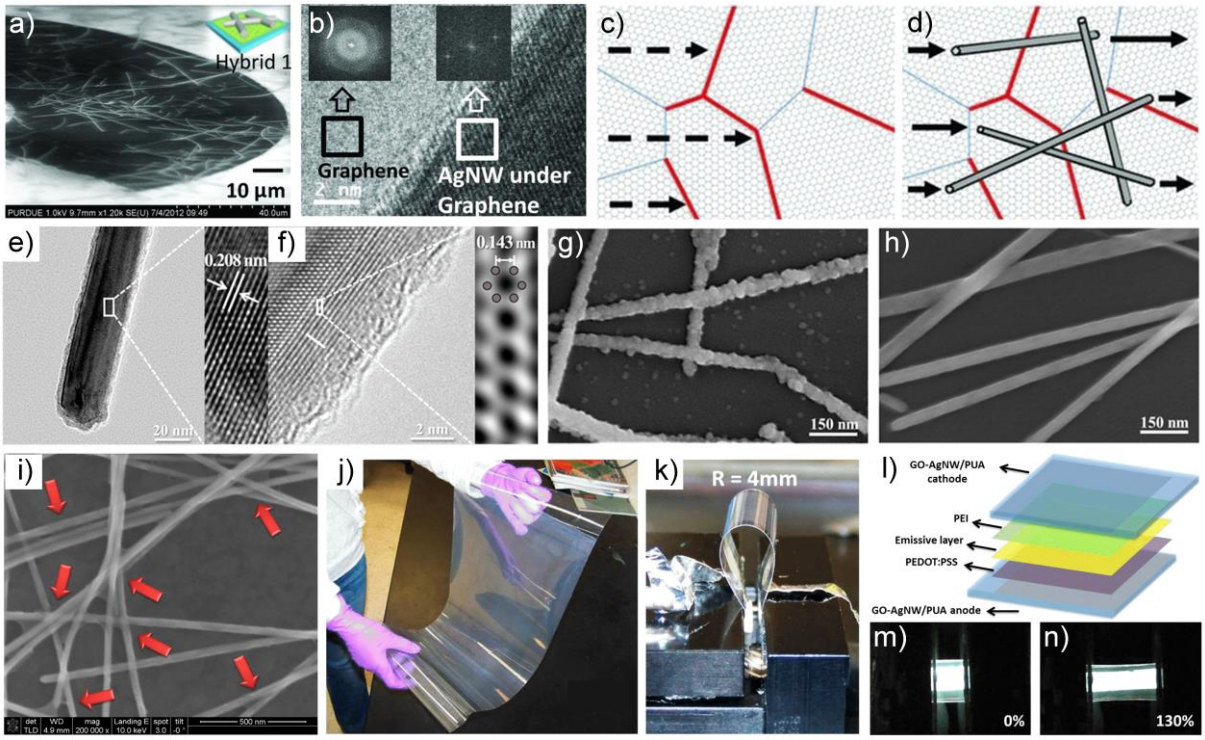

Figure 11 a) SEM image of AgNWs and graphene nanocomposite, b) TEM image of the interface between graphene and a single AgNW. Reproduced with permission.[341] Copyright 2013, Wiley-VCH. c) Scheme representing the electrical transport through the grain boundaries (GBs) in single layer graphene and d) the hybrid composite of graphene and AgNWs. Reproduced with permission.[341] Copyright 2013, Wiley-VCH. e-f) HRTEM image of CuNW-graphene core–shell nanostructure with a zoom to the CuNW part, and HRTEM image of the edge of the core–shell nanostructure, g-h) SEM images of CuNW and CuNW-graphene nanostructures, before and after stability test, respectively. Reprinted with permission.[164] Copyright 2015, American Chemical Society. i) SEM image of soldered junctions of AgNWs assisted by the presence of graphene oxide, j-k) photographs of a graphene oxide-AgNW on PET substrate, l) Schematic illustration of a stretchable polymer light-emitting diode (PLED) using GO-AgNW composite electrodes, and m-n) a PLED of original lighting area of 3mm×4mm, and stretched at a strain of 130%. Reprinted with permission.[343] Copyright 2015, American Chemical Society.

The use of copper instead of silver can be a path to reduce the cost of these nanocomposites. CuNWs and graphene core–shell nanostructure can indeed be produced using a low-temperature CVD method. Figure 11e-f present high-resolution TEM images of CuNW fully covered with 10-15 layers of graphene of which the thickness is about 5 nm.[164] This transparent

electrode exhibited very good optical and electrical properties, with a transmittance above 90% at 550 nm for a sheet resistance of 52 Ω/sq. Particularly, the coating layer could prevent the CuNWs from degradation after a thermal oxidation stability test, as can be seen in Figure 11g-h.[164] The transparent electrode was then integrated in bulk heterojunction polymer solar cells. The latter exhibits a power conversion efficiency (PCE) of 4.04%, well above the 1.9% PCE of the same solar cell using bare CuNW networks as transparent electrode.[164]

Other structures of sandwiches of graphene nanosheets and silver nanowires also improve the electrical transport properties of these nanocomposites. The electrical resistance associated with the nanowire network can be enhanced, both in the empty spaces between the metallic wires, as well as, in the direct contact between the AgNWs, since the top and bottom graphene nanosheets improve the contact connection.[344] This structure enables the creation of tailored films of AgNW with graphene nanosheets, since the concentration of both materials can be used to control the physical properties. A nanocomposite of AgNWs and graphene nanosheets shows a sheet resistance of 86 Ω/sq and a visible transmittance of 80%.[345]

Complementary to this carbon-based 2D-material, graphene oxide (GO) has also been investigated to enhance the properties of metallic networks. The use of GO sheets wrapped around of Ag- or CuNWs results in soldered junctions between wires and consequently a reduction of the overall resistance, as represented by SEM image of Figure 11i. The obtained structure on PET substrate shows excellent flexibility with an increase of resistance of only 2-3% after 12000 bending cycles with a radius of 4 mm (Figure 11j-k). This nanocomposite can be produced by simple solution methods, both for AgNWs[343,346] and CuNWs,[347] being then applied into stretchable polymer light-emitting diodes (PLED) (Figure 11l-n),[343] organic solar cell[346] and electrochromic devices[347] with outperforming properties when compared to bare nanostructured metallic electrodes.

The combination of AgNW network, oxide thin films and graphene-based materials can also be considered for the development of more complex nanocomposites. A hybrid of silver nanowires, zinc oxide and graphene was prepared by solution methods, using oxide nanoparticles and graphene flakes.[348] The optical and electrical properties of these nanocomposites reached values of 80% visible transmittance and 20.6 Ω/sq for AgNW combined with ZnO only, while the additional combination with graphene lead to a reduction of the sheet resistance to 17.6 Ω/sq, as well as, the transmittance to 73%. The obtained electrical improvement of these complex nanocomposites are based on the enhanced electrical transport, due to the improved connection between nanowires, while improving thermal and long-term ambient stability thanks to the combination of graphene and oxides around the metallic nanowires.[348]

3.4.3. MNWs and Polymers

As discussed in the sections 3.3.1 and 3.3.2, conductive nanowires and nanofibers can be incorporated into polymeric substrates to produce flexible and even stretchable TEs. Here we discuss TEs composed of MNWs and polymers, in which the latter can be conductive or non-conductive. One special material extensively studied with AgNWs is PEDOT:PSS. The large advantage of this material relies on its high conductivity, fundamental to create a transparent composite electrode. Since PEDOT:PSS is traditionally used for OLEDs and solar cells as hole blocking layer, the incorporation of AgNWs in its structure takes advantages from both elements of the nanocomposite. In the AgNW networks, the surface roughness is reduced by the creation of a smooth polymeric surface, while in the PEDOT:PSS, the electronic conduction is drastically improved by the presence of the nanowires.[349] The two materials can be

combined in solution to create an ink and then printed in a single-step process to obtain films with 86% transparency and 23 Ω/sq sheet resistance. The SEM micrograph and a transparent antenna of the nanocomposite are pictured in Figure 12a and b, respectively.[350,351] Additionally, mechanical properties are also enhanced due to the flexibility, stretchability, and higher adhesion to the substrate originated from the presence of the polymer. For the application in devices, the nanocomposite can be used as electrode and hole blocking layer at the same time, which can work for Cu(In,Ga)Se_2 (CIGS) solar cells, with PCE values up to 11.6%.[352]

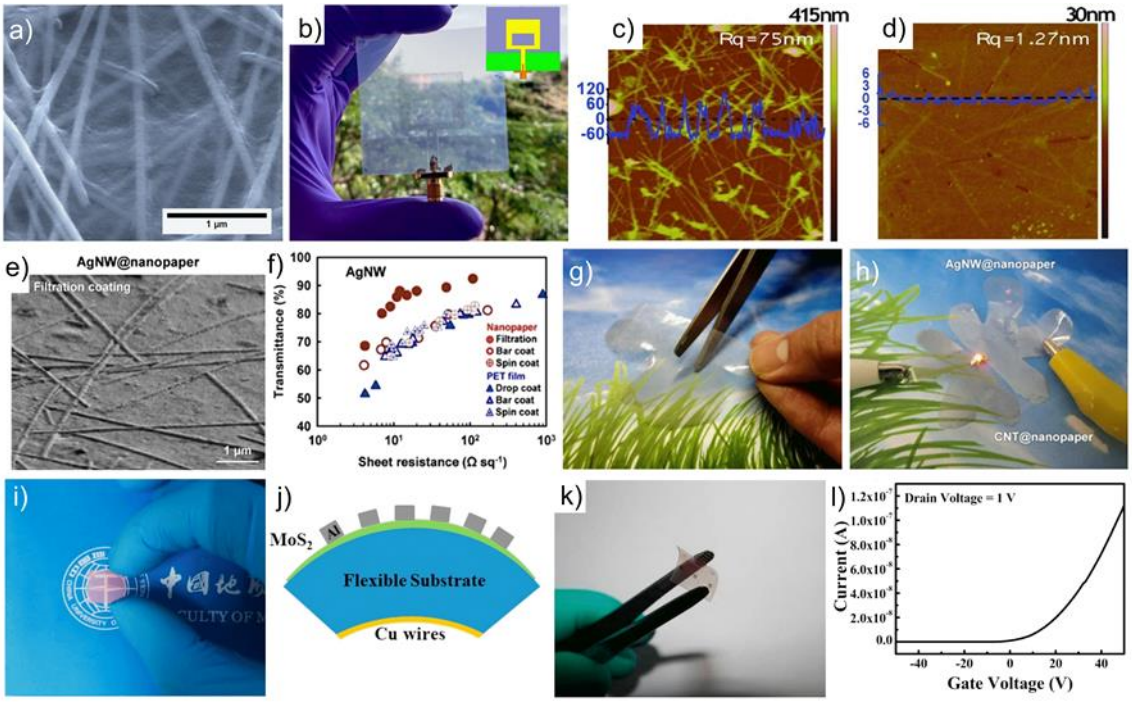

Figure 12: a) SEM micrograph and b) transparent antenna of the AgNW networks and PEDOT:PSS nanocomposite. Reproduced with permission.[350] Copyright 2020, American Chemical Society. c) AFM image of the bare AgNWs and d) AgNWs incorporated on PVA with a reduced surface roughness. Reproduced with permission.[353] Copyright 2010, Wiley-VCH. e-f) SEM images of AgNW@cellulose nanopaper prepared by filtration coating and comparison of transmittance at λ=550 nm as a function of sheet resistance for AgNW@cellulose nanopapers prepared by different techniques, g-h) Paper craft by using transparent conductive paper with AgNW and a light-up LED. Reproduced with permission.[354] Copyright 2014, Springer Nature. i) Nanopaper composed of CuNWs and cellulose under bending, j-k-l) scheme, photograph and I-V characteristics of a thin-film MoS_2 transistor as the cellulose works as dielectric layer and CuNWs as back electrodes. Reproduced with permission.[355] Copyright 2018, Elsevier.

The combination of three different materials can take further advantages to a nanocomposite as AgNW can be protected with TiO_2 followed by a PEDOT:PSS film. The oxide deposition by solution induces a capillary force to improve the contact junction between AgNWs, while the PEDOT:PSS can play a role of protecting layer to improve adhesion. This complex composite was then incorporated in an organic photovoltaic device, with similar efficiency to commercial ITO substrates.[356] Still, the long-term stability of PEDOT:PSS can be a detrimental problem, so other polymer can be used, as conductive PANI:PSS. The combination with AgNWs lead to the creation of an electrode with a sheet resistance of 25 Ω/sq and high transmittance of 83.5%.[357] While considering non-conductive polymers, PVA and PDMS are good candidates to obtain smooth surfaces for metal nanowire networks and improved mechanical, thermal and chemical stabilities. In the case of AgNW with a PVA film, the impact of the resistive nature of the polymer is visible for a sheet resistance of 63 Ω/sq with a high optical transmission of 87.5% and a smooth surface, as pictured by the AFM images in Figure 12c and d. Still, these properties are compatible with optoelectronic requirements for touch screen panels.[353] For the use of polydimethylsiloxane (PDMS), a composite with a low

sheet resistance of 9 Ω/sq and good tensile and flexible properties can be prepared, to be then incorporated in flexible light-emitting electrochemical cell.[358]

3.4.4. MNWs and Cellulose-based materials

A different approach to improve the properties of metallic nanostructures is to incorporate natural polymeric fibers such as cellulose. The use of this highly available and low-cost material enables the production of electrodes that can work as transparent electrodes and substrate at the same time. In the case of cellulose nanofibers (CNF), also called nanofibrillated cellulose (NFCs), membranes can be produce that are highly transparent and flexible, similar to more commonly used polymer substrates. A simple method to produce this nanocomposites is by filtration process of a solution with both metal nanowires and cellulose nanofibers, in order to obtain a connected conductive network implanted in the paper membrane. So, different studies present electrodes with a combination of CNF and AgNWs papers, showing high transparency close to 90%, sheet resistance of 12 Ω/sq,[354] good flexibility with 27% of strain, and a sheet resistance under strain below 60 Ω/sq.[359] Figure 12e-f respectively show SEM images of AgNWs prepared on cellulose nanopaper by filtration coating and optical transmittance at λ=550 nm of these samples in comparison with samples prepared by different techniques on both nanopaper and PET substrates.[354] In this case, the nanocomposite was applied as conductive material to light up an LED, as pictured in Figure 12g and h. These silver nanowires and nanocellulose fibers composited were already applied to flexible OPV, working as conductive and bendable substrate. A photovoltaic device using this electrode showed a high PCE of 7.47%, confirming the possibility to use these nanocomposites as sustainable, flexible and conductive substrates.[360] The control of the amount of each 1D-like material used in the composite can be used to tailor the optical and electrical properties, using alternative and low-cost deposition methods as screen-printing.[361] Additionally, these nanocomposites presented an excellent adhesion of the nanowires to the nanopaper and foldability, as the conductive properties of the network were maintained even after folding. All of these properties demonstrated the possibility to be used in foldable electronics.

The use of CuNWs with cellulose could enable another relevant and current aspect, as degradable electrodes can also be produced by combining this two low-cost materials. These structures using widely available copper and cellulose can be fundamental for disposable electronics that present a low impact on the environment after degradation. CuNWs and cellulose nanocomposite can be processed at room temperature, showing sheet resistance of 9.4 Ω/sq and visible transmittance around 80%, as represented in Figure 12i.[355] The increase of the CuNWs content can drastically improve the electrical conductivity, since 5.43×10^4 $S \cdot m^{-1}$ values are obtain for nanopaper with a high mass fraction of MNWs.[362] In this composite particular case, the structure can be applied for MoS_2 field effect transistors, as the cellulose works as dielectric layer and CuNWs as back electrodes (Figure 12j-k-l).[355]

Alternatively to cellulose fibers, other derivatives from cellulose can be also combined with metallic structures. AgNWs micromesh were embedded into a transparent substrate of ethyl cellulose, resulting in an electrode with a low sheet resistance of 25 Ω/sq, a high transmittance of 97%, and a low haze of 2.6%. Additionally, these composites present a good deformability and waterproofing characteristics.[363]

4. Challenges toward successful integration of metallic TEs into devices

In the previous sections, we have briefly summarized the recent advances in metallic TEs including metallic thin films, metal grids, metal nanowires, and some other emerging metallic nanostructures. Understanding the characteristics of these nanomaterials including the feasibility of their fabrication, the advantages and disadvantages is critical for the development of high-performance TEs. Beyond optical transparency and electrical conductivity, there are indeed several other critical parameters that need to be taken into consideration, depending on requirements for each specific case. Hence, to help users in selecting the most appropriate TE materials for their applications, we propose a set of criteria to evaluate different TE materials, as shown in Figure 13.

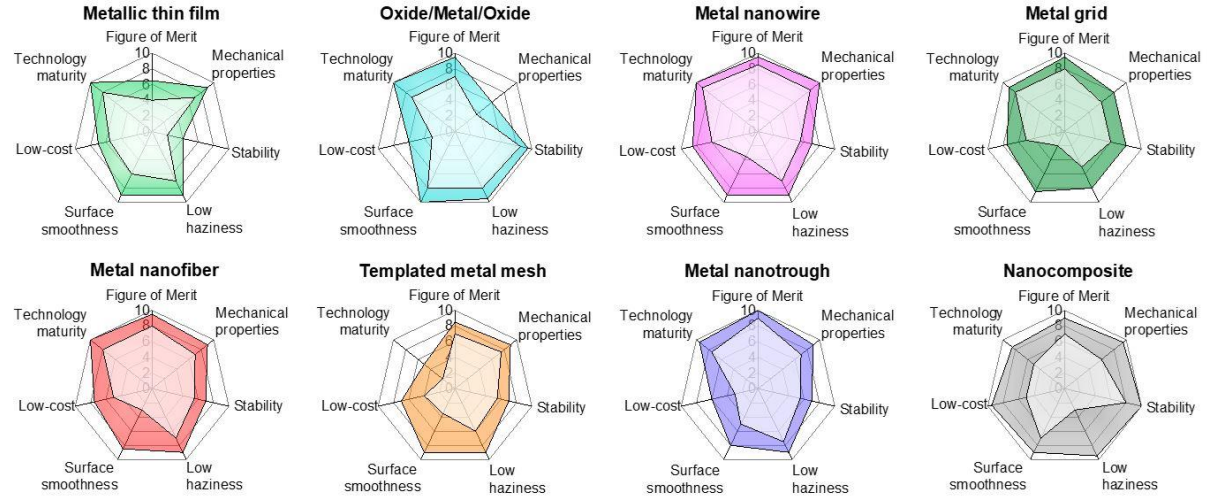

Figure 13: Comparison of TEs fabricated with different technologies. This figure shows the general trends with seven criteria (clockwise from the top): figure of merit (FoM), mechanical properties, stability, haziness, surface smoothness, cost-effectiveness, and technology maturity. Since the material selection is application-dependent, the marks are relatively given within the range [0-10] and only general indications. Scores of 10 and 0 correspond to excellent and extremely poor properties of the material at ~~that characteristic~~ each criterion, respectively. The light and dark colors in each chart represent the lower and upper limit, respectively, of each criterion for the TE technology analyzed.

This includes Haacke's FoM, mechanical properties, morphological stability, low haziness, surface smoothness, low-cost and technological readiness, as shown in Figure 13.

Haacke *Figure of Merit* evaluates two main and most important aspects of TE materials: optical transparency and electrical conductivity. This only considers the transparency in the visible range. Most of metallic TEs could provide high Haacke's FoM. However, it is worth mentioning that some applications such as solar cells, near-infrared region (NIR) sensors requires high transparency in the NIR, which excludes metallic thin films and oxide/metal/oxide films and some nanocomposites based on TCOs from the potential lists.

Mechanical properties cover both flexibility and stretchability. The flexibility refers to the ability to bend, twist the materials without losing their optoelectrical performances. The stretchability includes, in addition, the capability of maintaining the electrical conductivity under large strains (>> 1%). As flexibility is an intrinsic property of metallic materials, most of considering TEs have excellent mechanical properties, except from the oxide/metal/oxide thin films and some nanocomposites with presence of metal oxides. In contrast, stretchability is a more critical properties but now becomes highly required for novel soft electronic devices. This property of the TE materials is indeed related to the mechanical properties of the substrate as well. There have been many types of stretchable conductors developed and studied so far including i) CNTs or MNWs percolating networks embedded in an elastomeric matrix, and ii) conductive polymers-based stretchable TEs. However, those based on metal nanowires or

nanofibers are more favourable considering their low percolation threshold and relatively simple working mechanism.[364]

After the material performance, long-term *stability* is an essential factor for a viable technology. In the case of metallic TEs, stability includes morphological and chemical aspects. Indeed, the thermally- and electrically-induced atomic diffusion generally cause the morphological instability while the oxidation,[31] or sulfidation could lead to the failure of metallic nanostructures.[365] There have been extensive studies to improve the stability of TEs in devices. A popular approach towards enhanced stability of MNWs is to coat over the metallic TEs a protective layer, which can delay network degradation.[41,228] In this point of view, nanocomposites such as oxide/metal/oxide films, metal oxide-coated MNWs with ultraconformal coating technology such as ALD or core-shell nanofiber networks are very interesting options. However, in many cases, the high deposition temperature or the reactive chemicals used for the coating process should be taken into account to avoid damage of the TEs themselves or other adjacent layers of the final devices. Therefore, the coating technology should be appropriately selected to be compatible with the TEs and other functional layers of the final devices.

Haziness (or haze factor) measures indeed the ratio between the scattering (also called diffuse) transmittance with respect to the total transmittance. In the field of smart electrochromic windows or display devices that actually represent a major market share of TEs, materials of low haziness (typically below 3%) is highly required. Thin and continuous films such as ITO, AZO or oxide/metal/oxide structures have typically low haze factor (< 1%) since their primary size dimensions are significantly smaller than visible wavelengths.[58] In contrast, 1D conductive fillers-based TEs such as AgNW networks have usually shown a higher haziness. Experimental data show a linear increase in haze factor with network density, thus lower sheet resistance (Figure 5). As discussed in section 14, several recent studies have demonstrated that using ultralong AgNWs with smaller diameter could help to decrease the haze factor to below 3%, while maintaining total transmittance at higher 90%.[3,196,202,206] But the sheet resistance values of the networks shown in those studies are relatively high (> 20 Ω/sq). Additionally, toxicity issues related to making long AgNWs (> 20 µm) should be also taken into account.[205] Nanocomposites such as AgNWs embedded in ethyl cellulose substrates could also provide a low haze factor (2.6%, T = 97%) and still perform a relatively high conductivity (R=25 Ω/sq). The metal grids could also provide relatively low haze factor. Gao *et al.* have shown via theoretical calculations that the haze in metal grid or grating-like structures may be explained by Fraunhofer diffraction, and Mie scattering theory.[366] Bley *et al.* have demonstrated nanohole array-based metal grids reaching 84% transparency with a haze factor below 1%, but the geometric period in such structures are relatively large, i.e. µm range.[150] On the other hand, high haziness is preferentially expected in photovoltaic applications. Organic solar cells (OSCs) incorporating AgNW networks (haze factor of 5.6%) as transparent electrode exhibit power conversion efficiency of 4.47%, higher than that of OSCs with a conventional ITO electrode (3.63%, haze factor of ITO on glass is about 0.6%), as demonstrated by Wang *et al.*[367]. Han *et al.* have obtained a high haze factor of 36.5% by using a nanocomposite based on FTO layer and AgNWs, which could serve as electrode in perovskite solar cells and exhibits a better performance compared to the similar FTO-based devices.[368] Because of their possibility to turn haze factor from low to high values, nanocomposites show a large range of marks for *low haziness* criterion.

Surface smoothness is a critical condition for successful integration of TEs into a wide range of devices including display, solar cells, smart windows, etc. But it could be less critical in other devices, for instance transparent heaters. Obviously, continuous films such as OMO multilayers TEs have smoother surface compared to non-continuous metal nanostructures such as periodic metal grids or random metal nanowire networks. An interesting and efficient approach to fabricate smooth TEs is to fabricate metal nanostructures fully embedded and mechanically anchored in a flexible substrate such as PDMS, PET, and PEN (further details can be found in the previous sections 3.2, 3.3). Consequently, the marks given for surface smoothness extend in a relatively wide range, depending on the fabrication techniques and the nature of the used substrates.

The *cost-effectiveness* of both raw materials used and the fabrication process is finally a very important aspect. But this is often overlooked and only taken into account when the technology is mature enough to be brought to a larger scale. Among the metals investigated, while Ag-based TEs have been largely investigated lately, however Cu-based TEs could be also of clear interest, specifically thanks to their significantly lower price compared to other metals. Continuous TEs and metal nanotrough networks use vacuum-based technologies, thus are not the most cost-effective approaches. Printing technologies for metal grids, vacuum-free electrospinning for metal nanofibers or solution-based technologies for metal nanowires are commonly believed as more economical and easily scalable approaches. The problems related to the recyclability and the toxicity of the nanomaterials, as well as the environmental effects of the chemicals used in the fabrication processes are of great importance and should be thoroughly investigated. However, these are out of the scope of this review.

Finally, *technology maturity* estimates the readiness of the technology to be transferred into industrial level. For instance, the vacuum-based sputtering for fabrication of oxide/metal/oxide TEs, electrospinning for nanofibers or the spray coating for AgNWs are considered to be mature technologies, but the fabrication of metal mesh TEs via the cracked templates would require more optimization to achieve a higher reliability level.

In summary, each type of metallic TE has its unique advantages and disadvantages. But for the currently developing applications, one can easily select an appropriate TE technology that could fulfil a set of specific requirements. Particularly, the combination of different materials in the nanocomposite category to enhance a certain material property leaves the room for both users and researchers in material selection and improvements.

5. Applications

5.1. Introduction

The main applications for transparent electrodes (TEs) concern the domains of energy and electronics. The first one includes photovoltaics, efficient lighting (LEDs, OLEDs), smart windows, and low-emissivity coatings. The second relates, for instance, to touchscreens, flexible electronics, sensors, electromagnetic shielding, and flexible antennas. Another important application of metallic TEs is their use as transparent heaters (THs), which appears crucial for defogging or defrosting aircraft windscreens.[4,274] Soft robotics, health monitoring and biological studies that require flexible and stretchable TEs are also emerging applications for metallic TEs and have been recently attracted much attention.[38,37,39]

As described previously in this review, the traditional and well investigated TEs, and already much integrated into industrial devices, concern transparent conductive oxides (TCOs). For solar cells or TH devices, ITO, AZO, and FTO are the main used materials[2,369]. Metal-

based TEs started to be abundantly investigated much later compared to TCOs. For instance, the main works related to metal nanowire (MNW) networks started around 2005-2010[30,188,370] while those related to metal grids have appeared only since 2015. The search for TCO–free (and more often indium-free TE) investigations stems from several reasons[1]. TCOs are ceramics and by nature are not flexible nor stretchable, therefore they are usually not well adapted for flexible applications. Moreover, while ITO exhibits high electro-optical performances, indium appears to be a non-abundant material and could become critical. According to the European commission in 2020, indium is considered as one of the critical raw materials (CRMs) due to its extensive use in renewable energy technologies or high-tech applications.[371] Therefore metal-based TEs have been investigated with the prospect of their integration in flexible devices as well as of lowering the production cost.[1] For instance, MNW networks exhibit good electrical, optical properties, while being very flexible, and are compatible with the solution-based processes, and their fabrication is nowadays compatible with roll-to-roll technology[372,373]. Metal-based ordered grids, such as Ag or Cu grids, can be deposited on glass or polymeric substrates and can be associated with very large Haacke's FoM; they can match fairly well the requirements, e.g. for organic photovoltaics[374]. Oxide/metal/oxide have also been largely investigated these recent years since they can exhibit very low sheet resistance (0.1–0.3 Ω/sq), optical transmittance over 82% with uniform properties over a very large area (~1 m^2).[375] They can therefore be efficiently used as transparent automobile windshield heaters.[375] Cu- and Ag-based TEs are the most studied systems due to their high performance and reasonable cost. Li *et al.* recently reviewed the progress in research and development related to CuNWs in electronic applications, more precisely for optical devices, lithium-ion batteries as well as wearable devices.[153] The association between different materials such as metals and oxides provides stability enhancement and open novel material properties, representing as well new opportunities. As shown hereafter, this can be beneficial to address several applicative challenges.

Table 2 provides a general summary of the current situation related to various TE technologies, showing their main key features and examples of associated applicative domains. As discussed in section 4, one has to keep in mind that the indicators (positive with "+" and negative with "–") should be considered with care since this is drastically dependent upon considered application requirements as well as TE material and fabrication conditions. Table 2 clearly shows that metal-based TEs have been applied lately within a vast applicative domains range. The three main advantages of metallic TEs, in addition to their good electrical and optical properties, concern their low fabrication cost (compared to ITO), their enhanced mechanical properties, and their compatibility with upscaling depositing techniques such as all-solutions methods.

This section is focused on applications of metallic TE and is organized as follows. Part 5.2 presents the main aspects of the applications of metallic TEs within transparent heaters (THs). Parts 5.3 and 5.4 deal with the integration of metallic TEs into solar cells, touchscreens and displays, respectively. Part 5.5 deals with energy saving: this mainly concerns low-emissivity coatings and smart windows. In part 5.6, applications are associated with transparent flexible thin-film transistors (TFTs), electromagnetic interference shielding (EMIS) and high frequency antennas, and transparent flexible supercapacitors. Finally, part 5.7 briefly reports on recent efforts for integrating metal-based TE in biological and medical applications.

Table 2: Summary of the most common transparent electrodes (TE) technologies giving general indications and the main associated applicative domains. Indicators (positive with "+" and negative with "–") are given as general guides only since it strongly depends upon the used material and targeted applications. The main listed parameters are: sheet resistance (R_{sh}), optical transmittance (Tr), either for a wavelength of 550 nm and averaged with 400-700 nm range, the mechanical flexibility, the stability (encompassing electrical, thermal, or chemical stability), and compatibility with cost (associated to both material and deposition).

Transparent electrodes (TEs) domains	**TE technologies**	**Low R_{sh}**	**High T_r**	**Flexible**	**Stable**	**Low cost**	**Main applications**
Transparent conductive oxides (TCOs)	ITO	++	++	– –	++	– –	Electrochromics for smart windows[376]; Low emissivity coatings[377]
	Other TCOs (FTO, AZO)	++	++	– –	++	–	Solar cells; transparent heaters[4]; Touch screens; Low emissivity coatings[377]
Non-metallic TEs	Conducting polymers	+	++	++	– –	++	Transparent heaters[18,378]
	CVD graphene	–	++	++	++	– –	Solar Cells and Light Emitting Diodes[1]; Optoelectronic devices[2]
	Exfoliated graphene	– –	++	++	++	++	Supercapacitors[15]; Solar cells[13]; Light emitting diodes[13,14]; sensors[13]; Electromagnetic shielding[379]
	Carbone nanotubes	+	+	++	+	–	Sensors[10]; Touch Panels[11] and displays[1]; Solar Cell[10,11] and Light Emitting Diodes[10,11]
Metallic based TEs	Continuous metallic films Oxide/metal/oxide films	++	+	+	+	–	Transparent heater[375,380]; solar cells[99]; low-emissivity coatings[381,382]
	Ordered metallic structures: grids	++	+	++	+	+	Transparent heaters[383]; Low emissivity coatings[381,384]; Organic photovoltaics[374]; Smart windows[385]
	Random silver nanowire (AgNW) networks	++	++	++	–	+	Solar cells; Touch screens; Transparent heaters[386,387], Flexible organic electronics[152]; Antimicrobial activity[388]; Low-emissivity[389]; Smart windows[390]; Sensors for monitor human activities[391]
	Coated AgNW networks	++	++	++	++	+	Solar cells; Touch screens; Transparent heaters[41]; Low-emissivity[392]; Smart windows[245]
	CuNWs networks	++	+	++	– –	++	Electronics[153]; Transparent heaters[393]
	Metallic nanofibers	++	+	++	+	++	Transparent heaters[306]; Transparent and body-attachable multifunctional sensor[394]

5.2. Transparent heaters

One of the very first applications of transparent conductive materials was for transparent heaters (THs). They are essential components for a wide spectrum of devices with rather different specifications on temperature ranges, sizes, substrates and operation.[4,274] The outstanding properties of emerging metallic TEs, like the ones studied in the present review, are very promising for applications such as defrosting-defogging windshields, smart buildings, healthcare widgets, and several everyday-life gadgets.[395,386,396–400] As discussed thoroughly in section 4, recent studies have mainly focused on the stability enhancement for successful and versatile integration.[154] Despite extensive efforts, there is still room for improvement of the physical properties of TH, i.e. electrical and optical and long-term stability of THs in severe conditions.

The chemical stability is crucial for TH applications, since they can be exposed to a wide range of temperature and humidity conditions. Recent studies also demonstrate highly flexible and more stable TH achieved with the encapsulation of thin metal films or MNW networks by oxide layers and the use of metal-alloy or metal-mesh based composites.[31,154,380] Apart from the enhancement of stability, such composites and hybrids can improve the heating performances as well. For instance, Jang *et al.* reported a flexible defrosting Zn-doped SnO_x/Ag/Zn-doped SnO_x (ZTO/Ag/ZTO) multilayer thin film with fast heating rate (~160 °C/min). The sandwich nanostructure also shows high durability against humidity, i.e. constant transmittance and sheet resistance after 60 h in a humid environment (65 °C-90% RH in the air), which can be attributed to the incorporation of nitrogen into the material.[401] Tigan *et al*. demonstrated the protection of CuNW by oxide thin layers like ZnO and Al_2O_3 that lead to remarkable heating rates,[393] while the flexible Ni-grid based TH reported by Nam *et al*. demonstrated high corrosion resistance and mechanical stability, e.g. the relative variation of resistance $\Delta R/R_0 < 10\%$ after 9 days of immersion in seawater environment, and < 3% after 10000 bending cycles with a bending radius of 10 mm.[383] In the case of electrical stress, a chitosan–lactic acid coating on AgNW networks achieved 6.6 times increase of the lifetime compared to the pristine AgNW TH, under an applied current of 250 mA cm^{-2}.[402]

Size and heating response are important features for the integration in different type of devices from human body pads[403], like the one presented in Figure 13a,[404] to large-scale vehicle coatings[405]. For this purpose, Lee *et al.* evaluated the suitability and heating properties of Ag ultrathin films sandwiched by ZnO layers, for several sizes applications.[406] Furthermore, the uniform and stable heating performance under mechanical stress is a key point for the successful use of TH in modern devices. He *et al.* patterned a few nanometers thick Ag films on flexible substrates coated with ZnO seed layers. Such metal grids are the thinnest reported so far and demonstrated a very uniform heating performance under bending into a roll, as shown in Figure 13b.[407] As already mentioned in section 3.3.2, core-shell nanofiber (NF) structure using coaxial electrospinning is an efficient approach for high-temperature TEs. Indeed, material failure due to atomic diffusion of metal atoms in nanomaterial-based THs is a major concern that affects the lifetime of the device. Ji *et al.* have successfully demonstrated the use of such core-shell nanofibers in extremely high-temperature transparent heaters.[306] As shown in Figure 13c-d, black CuNF-based transparent heater with conformal carbon coating can reach 800 °C within 25 seconds while THs based on AgNFs degrade at about 670 °C. This was attributed to the higher activation energy in the electromigration of Cu compared to Ag.[306,408,409] The use of black coating also allows to reduce the reflection loss from 4% to 1% while maintaining the transmittance of the TEs.

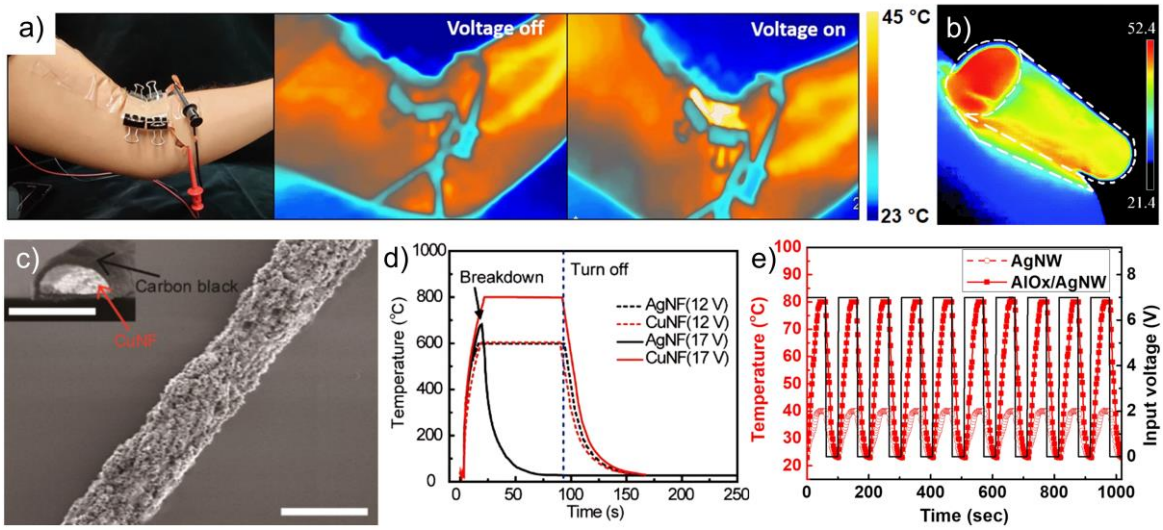

Figure 14: a) Photograph and IR images of the temperature distribution in a bioinspired thermotherapy patch to the cubital fossa area, based on AgNW TH. Reproduced with permission.[404] Copyright 2020, Springer Nature. b) IR image of a flexible TH based on patterned 8.4 nm thick Ag grid on ZnO-coated PE substrate, bent into a roll (6 cm×6 cm), under 5 V bias. Reproduced with permission.[407] Copyright 2021, Royal Society of Chemistry. c-d) SEM image of black CuNFs with a cross-sectional inset image of the CuNF (scale bar: 1 µm), and demonstration of extremely high-temperature heaters using SiO_2-coated AgNF and black CuNF networks. Reproduced with permission.[306] Copyright 2019, Elsevier. e) ON/OFF responses of AgNW-based heaters with and without AlO_x coating layer. Reproduced with permission.[238] Copyright 2020, Springer Nature.

In another example, Lee *et al.* coated the AgNWs with an AlO_x layer and achieved a fast response and uniform temperature distribution of the flexible TH, as shown in Figure 13e.[238] The improved properties of metallic TEs also open many opportunities as flexible THs in futuristic devices. As reported by Kim *et al.*, patterned CuNW embedded on polyurethane acrylate, can be used for the replication of the feeling of heat in virtual reality applications.[410] Furthermore, Park *et al.* conducted an interesting study about the control of the evaporation rate of water droplets on TH, previously not reported.[411] Kim *et al.* have combined fluoropolymer nanocoating and Cu grids for robust and hydrophobic transparent heaters, which appear helpful for icephobic and antifrost applications.[412] Another important aspect for the industrial integration of emerging TH is the assessement of the mechanical, chemical and optical properties of the substrates. Lee *et al.* demonstrated a TH based on self-assembled Ag network covered by waterproof, hydrophobic PTFE layer suitable for self-cleaning smart windows.[413] In addition, an increasing interest has emerged for THs deposited on flexible polyimide films that withstand higher temperatures than other common plastic substrates, and that are compatible with TH heating performances reaching even 400 °C.[414–416] Another recent approach is related to the combination of MNW networks with biocompatible polymers and flexible paper-based composites for enhanced mechanical stability.[417] A photo-curable polymer layer is a promising example against ambient moisture and physical damage in the case of AgNW networks.[418] Such TH demonstrated quick thermal responses at low applied voltage (130 °C within 15 s, at 4 V).[418]

5.3. Solar cells

In the last few years, several studies have reported the applications of emerging metallic TEs on solar cells. The rapid growth of CIGS, organic (OPV), dye-sensitized, and perovskite solar cells with the simple solution-based fabrication of active materials has driven the need for low-cost, flexible TEs such as metal-based thin films, metal nanowires, etc.[419] Compared to conventional silicon solar cells, new-generation flexible, (semi)transparent solar cells can be easily fabricated by reducing the thickness of the active layers and using flexible TEs, which

makes them appealing for applications in building-integrated photovoltaics, solar-powered automotive, and wearable electronics.[420] Efficient TEs for solar cells should include several important and unique physical properties.

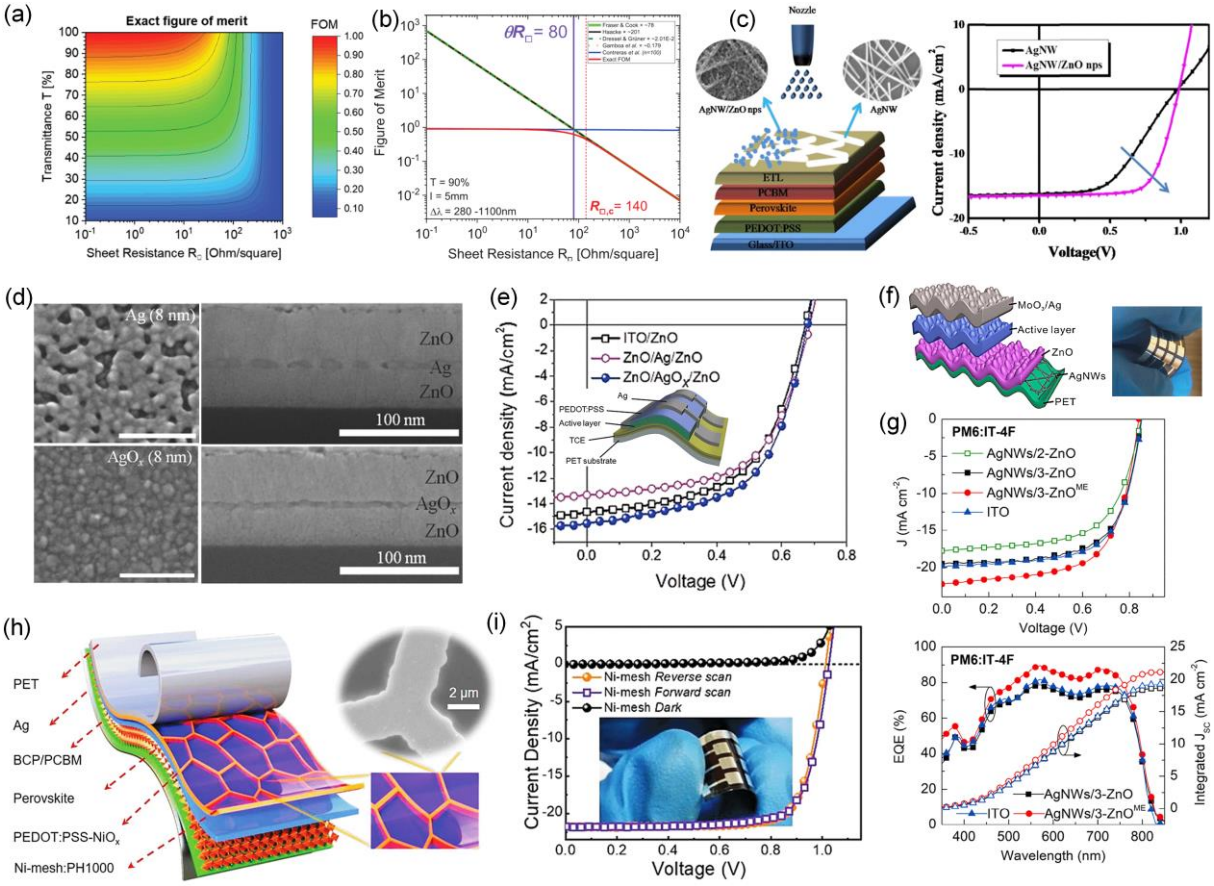

Figure 15: a-b) FoM based on the calculation by Anand et al.[421] with the impact of transmittance and sheet resistance on photovoltaic performance for the spectral range of [280, 1100 nm] and a solar cell length of 5 mm. Reproduced with permission.[421] Copyright 2021, Wiley-VCH. c) Scheme and cells' performances of solution-processed semi-transparent perovskite solar cells with spray-coated AgNWs and AgNWs/ZnO composite top electrode, showing a PCE improvement from 7.31% to 11.13%. Reproduced with permission.[422] Copyright 2018, Elsevier. d) Top-view SEM micrographs of Ag and AgO_x deposited on 50-nm-thick ZnO films, and cross-sectional SEM micrographs of ZnO/Ag/ZnO and ZnO/AgO_x/ZnO TEs using 8-nm-thick Ag and AgO_x layers, respectively, e) J−V characteristics of inverted organic solar cells (IOSCs) using different TEs. The inset represents the device architecture of flexible IOSC fabricated on a PET substrate. Reproduced with permission.[99] Copyright 2013, Wiley-VCH. f) Schematic and photograph of a flexible OSC with moth-eye nanopatterned AgNWs/ZnO TEs on a PET substrate, g) J–V curves and EQE spectra of PM6:IT-4F-based OSCs. Reprinted with permission.[423] Copyright 2019, American Chemical Society. h) Schematic of the perovskite solar cells with Ni mesh/PEDOT:PSS hybrid TE and SEM micrograph of Ni mesh. i) J-V curves of the PET/Ni mesh-based perovskite solar cells. Reproduced with permission.[424] Copyright 2020, Wiley-VCH.

Firstly, they should have a high optical transmittance (> 85%) with as high haziness as possible, which is a typical requirement for solar cells. Indeed, the diffuse photons from TEs have a longer optical pathway in the absorber layer of the solar cells, therefore increase solar cell efficiency by maximizing the light absorption and short-circuit current density. For instance, this has been illustrated in the case of Dye-Sensitized Solar Cells.[34] Zhang *et al.* have also reported similar effects for hazy ZnO-SnO_2:F thin layers with tunable haze factor from 0.4 to 64.2%.[36] Additionally, Choi *et al.* used C_{60} to improve the optical transparency caused by surface plasmonic resonance and destructive interference at the two Ag/C_{60} interfaces of a C_{60}/Ag/C_{60} (CAC) sandwich.[425] They determined the optimal film thicknesses and prepared a semi-transparent perovskite solar cell (PSC) with a 1.08 cm^2 active area and a highly flexible CAC cathode, which showed 5.1% PCE.[425]

The high electrical conductivity of the TEs is the second essential factor towards high-performance solar cells. When optimizing the TEs for solar cells, a critical question is that between transmittance and sheet resistance, which of the two parameters is currently limiting the cell performance. Recently, Anand *et al.* have introduced a new concept of FoM for the assessment of TEs in PVs with taking into account more system-specific parameters such as the bandgap of active materials, the solar cell length (dimension in the current transport direction), and the spectral range ($\Delta\lambda$, usually in the range 280-1100 nm).[421] They have defined a transition sheet resistance that separates two regimes of TE operation in solar cells: transmittance and conductance limited.[421] Figure 15a shows recently developed FoM versus transmittance and sheet resistance. Accordingly, for a given value of transmittance, for instance, 90%, there exists a transition sheet resistance (80 Ω/sq in this example) below which the cell performance is relatively constant, as shown in Figure 15b. The metal-based TEs such as AgNWs, CuNWs, Oxide/Metal/Oxide, TCO/AgNW/TCO could perform excellent FoM (higher than that of ITO) over a spectral range of 350–800 nm and for a solar cell length of 5 mm.[421] At the nanoscale, one should pay particular attention to non-continuous nanostructure-based TEs that a low sheet resistance does not always mean an efficient collection of charges photo-generated from the active layers, but this also depends on the diffusion length of photo-generated charges. For instance, the bare percolating AgNW networks have free space between nanowires, which can be detrimental for photo-generated charge collection, particularly in the case if photo-generated charges have a short diffusion length.[256,422] Figure 15c summarizes the work by Han *et al.*, in which they have found that semi-transparent perovskite solar cells with PCE of 13.27% could be obtained by using ZnO nanoparticles (ZnO NPs) coated AgNWs.[422] Indeed, the ZnO NPs layer can improve the electrical conductivity of the AgNW electrode by filling the voids between AgNWs, resulting in better charge collection and lower series resistance.

Another critical property of TEs used for a solar cell is their work function, which should be adapted with that of the adjacent layers for efficient charge transport. This has also been thoroughly discussed in a recent review by Zhang *et al.*, in which a summary of solution-based TEs for thin-film solar cells is presented.[419] In metallic TEs, one does not have many options to tune the metal's work function, however, using hybrid structures such as oxide/metal/oxide (OMO) or oxide-coated MNW networks have great opportunity in tuning the work function via an appropriate selection of oxide layers. As already mentioned in section 3.1, hole transport layers such as NiO,[94] MoO_3,[97,98] and electron transport layers such as ZnO[99] and TiO_2[100] have been used in the oxide/metal/oxide TEs in organic or dye-sensitized solar cells. The utmost challenge of using OMO structures is the non-continuous nature of metal film when being ultrathin of few nanometers for optical transparency reasons. Wang *et al.* have successfully improved this issue in ZnO/Ag/ZnO TEs by replacing the Ag layer with a continuous AgO_x layer, as observed in Figure 15d.[99] J–V characteristics of inverted organic solar cells (IOSCs) using this kind of OMO TEs exhibits a clearly improved performance compared to cells made with ITO (Figure 15e).

The high surface roughness of TEs is problematic in thin-film solar cells. For instance, metal nanowire networks could have junctions with several nanowires stacked on top of each other, which leads to high surface roughness. For instance in OSCs, the low electron mobility requires organic layers to be relatively thin, i.e. typically < 100-nm thick, therefore, the TEs should have a smooth surface to avoid any short circuit issue. Among recent research, Lee *et al.* have demonstrated an electrodeposition method to develop smooth surface morphology of

the TE and reduce the contact resistance.[426] A gravure printing method has been also investigated for smoother and more uniform AgNW electrodes, leading to a high PCE of 13.61% and a high efficiency of 12.88% for a 1 cm^2 PSC.[427] Seo *et al.* have proposed a top-down approach using electrospun polymeric nanofibers on thin Ag films as a mask to fabricate junction-free metal nanonetworks for (>10%) flexible organic solar cells. This consumes, however, more than 90% of raw materials (Ag, Au) via the etching step. Another efficient approach to fabricate smooth and flexible TEs is to create nanostructures fully embedded in a flexible substrate such as PDMS, or PEN. Figure 15f shows a schematic and photograph of a flexible OSC with > 12% efficiency using AgNWs/ZnO TEs. This work done by Zhang *et al*. showed that the spin-coated ZnO layer allows reducing the surface roughness of AgNWs to only ~ 5 nm. They have also demonstrated that by adopting a soft nanoimprint lithography technique, imprinted light-trapping nanostructures, also called moth-eye nanopatterned AgNWs/ZnO TEs, can enhance the OSC performance via a more efficient light-trapping effect, as shown in Figure 15g. Also, this embedded metal nanostructure-based TEs has been successfully used by Li *et al.* for flexible perovskite solar cells with a PCE of 17.3%, which is the highest efficiency for a PSC based on flexible metal-based TEs to date (Figure 15h-i).[424]

The integrations of metal-mesh flexible TE technology within solar cells have also recently seen remarkable advances. Bellchambers *et al*. elaborated a microcontact printing lithography without the complexity associated with metal mesh transfer and photolithographic or electrochemical deposition steps.[374] They achieved a Cu grid flexible TE with more than 20 times narrower lines, which consequently allows a smaller pitch size and improved charge-collecting interlayer for OPV structures. The obtained power conversion efficiency was 6.0±0.8% on glass and 5.8±0.6% on PET.[374] Sun *et al*. fabricated an ultrathin Ag hexagonal mesh that exhibits high antireflection ability compared to flat Ag film.[428] The fabricated PSC demonstrated an enhanced performance with 17.06% maximum PCE, which is mainly ascribed to the surface plasmon-assisted transmission enhancement and the scattering of incident light.[428]

5.4. Flexible touchscreen panels and displays

Touchscreen panels (TSPs) are integrated within many modern devices of our daily lives including smartphones, tablets and laptops. When TEs are integrated into TSPs, they require specific properties including high optical transparency, low haziness, and mechanical robustness as TSPs undergo mechanical disturbances. It is noted that in most of TSP technologies, sheet resistance of few hundreds Ω/sq is largely acceptable. Among the novel metal materials, metal nanowires (MNWs), hybrids MNWs and oxide/metal/oxide (OMO) have been widely investigated for the development of TE for TSPs and displays.[277,429–431] For instance, Lin *et al* [277] recently presented a stretchable AgNW-patterned TE with high resolution (up to 50 μm) using screen printing and vacuum filtration techniques, obtaining a sheet resistance of 7.3 Ω/sq and optical transmittance of 79.6% (at 550 nm wavelength).

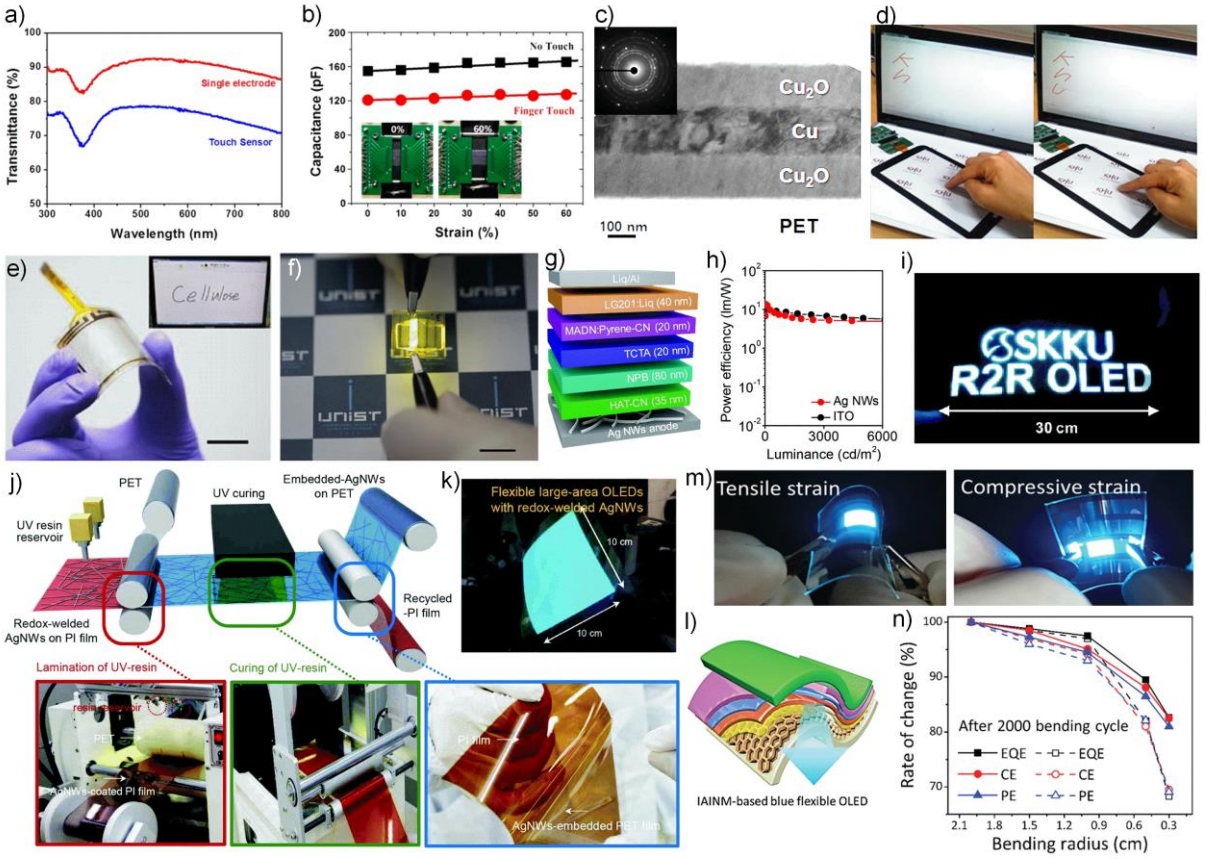

Figure 16: a) Transmittance of stretchable AgNW/reduced graphene oxide (rGO)/polyurethane (PU) electrode and stretchable capacitive touch sensor with two AgNW/rGO/PU electrodes, b) variation of capacitance in the AgNW/rGO/PU capacitive touch sensor under different strains. Reprinted with permission.[431] Copyright 2017, American Chemical Society. c-d) Cross-sectional TEM image of the $Cu_2O/Cu/Cu_2O$ multilayer electrode and photographs of capacitive-type flexible touchscreen panels based on patterned $Cu_2O/Cu/Cu_2O$ mesh electrodes. Reproduced with permission.[429] Copyright 2015, Springer Nature. e-f) photograph of a touchscreen panel based on AgNWs-coated transparent cellulose nanofiber hybrid films, and a photograph of a TOLED emitting light through both directions. Reproduced with permission. Copyright 2016, Springer Nature. g-h-i) schematic illustration of an OLED based on a AgNW anode, power efficiency versus luminance for OLEDs based on the AgNWs and ITO, and a light-emission images of a large-area flexible OLED based on an AgNW anode, fabricated with roll-to-roll process, respectively. Reproduced with permission.[433] Copyright 2018, Royal Society of Chemistry. j-k) schematic illustration of the roll-to-roll embedding process used for the redox-welded AgNWs, and light-emission image of large-area flexible OLEDs under bending. Reproduced with permission.[434] Copyright 2018, Royal Society of Chemistry. l) schematic structure of an IZO/Ag/IZO nanomesh-based blue flexible OLED, also called IAINM OLED, m) photographs of the IAINM OLED under tensile and compressive strains, n) experimentally measured external quantum efficiency (EQE), current efficiency (CE), and power efficiency (PE) of IAINM-OLED (bold) and AgNM-OLED (open) after 2000 times bending cycle at a bending radius of 2.0–0.3 cm. Reproduced with permission.[435] Copyright 2021, Wiley-VCH.

Choi *et al.* developed a stretchable and transparent capacitive touch sensor array based on patterned AgNWs/reduced graphene oxide (AgNWs/rGO) nanocomposites embedded in polyurethane (PU) dielectrics.[431] Their stretchable AgNW/rGO/PU transparent electrode shows a high optical transmittance (> 90%) while the stretchable capacitive touch sensor based on this kind of nanocomposite TE also has a relatively high transmittance (> 75%), as shown in Figure 16a.[431] The AgNW/rGO/PU capacitive touch sensor exhibits good performance for strains of up to 60% (Figure 16b). Besides AgNWs, CuNW have also been studied for TSP applications due to the higher abundancy of copper and its lower cost compared to AgNWs. Chu *et al.* have demonstrated that CuNW TEs (T = 90%, R_{sh} = 52.7 Ω/sq, area > 50 cm^2) prepared by the spray coating method could be assembled as resistive TSPs.[430] Flexible transparent capacitive-force-detection touch sensor based on UV-curable polyurethane acrylate (PUA) resin covered CuNWs electrode was also demonstrated by Kim *et al.* recently.[436] It is worth mentioning that the poor adhesion of MNW networks, their non-uniform topography,

and instability against static electricity is detrimental in most of applications including TSPs. However, as indicated in the above studies, the improved material performance, as well as the enhanced stability and adhesion of the MNW-based TEs with the substrate thanks to PU-based layer enable the possibility to use MNWs as a viable technology for flexible, and even stretchable TSPs. Besides MNWs, OMO structure is also very promising. For instance, Kim *et al.* have demonstrate the fabrication of flexible $Cu_2O/Cu/Cu_2O$ mesh electrodes for flexible TSPs.[429] TEM image of such a structure (T=90%, R=38 Ω/sq) is shown in Figure 16c. The authors have also successfully demonstrated the use of the patterned flexible $Cu_2O/Cu/Cu_2O$ mesh electrodes for capacitive-type flexible TSPs (Figure 16d). The remarkable advantage shown in this study lies on the use of room-temperature scalable techniques, i.e. roll-to-roll (RTR) sputtering and RTR-based wet-patterning to fabricate diamond-type mesh structure of flexible $Cu_2O/Cu/Cu_2O$ on PET substrate. In addition to the cost-effectiveness of materials used, the fabrication techniques are mature and ready to be applied on a large scale.

Cellulose nanofibers (CNFs) can also be used as flexible, transparent films for electronic devices.[437–439] For instance, Ji *et al.* have demonstrated the applications of flexible AgNWs/cellulose nanofiber-based TEs for transparent and flexible touchscreen panel, and transparent OLED (Figure 16e-f). These mentioned studies open new opportunities for high-performance green flexible TSPs and display devices based on biodegradable materials. What remains to improve for CNFs to approach the display market is its relatively high haziness compared to other conventional polymeric substrates. The use of wood-based cellulose nanofibers with ultrahigh transparency (~96%) and haziness (~60%) was even beneficial in solar cells, as demonstrated by Fang *et al.*[440]

A complete touchscreen device is often the assembly of both an input (touchscreen panel) and an output (display device), of which the latter can be an LCD or OLED display. Combining several exciting advantages such as the potential to enable lightweight, flexible and even biodegradable applications, OLEDs is a fascinating technology commonly used now in many daily electronic devices.[441] This explains extensive research devoted to applications of flexible metallic TEs for OLEDs. Requirements of the TEs for OLEDs share many common points such as high optical-electrical conductance, smooth interfaces, and efficient charge injection as in the case of solar cells. In addition, the substrate is also required to be flexible to be compatible with large-scale roll-to-roll production of OLEDs. Contrary to solar cells, OLEDs applications require a narrower wavelength range at which the TEs should have a low residual absorption, and particularly a low haze factor to avoid any blurred effect. Several recent works have reported efficient OLED devices using metallic TEs, which show comparable device performance to ITO-based devices. Bae *et al.* have fabricated an ultra-thin Ag film by using a maskless deposition process. The charge injection and the emission intensity for the flexible OLED fabricated using the ultra-thin Ag electrode were significantly increased compared to those for a conventional ITO-based flexible OLED.[442] Also using AgNW networks, Sim *et al.* have successfully demonstrated the fabrication of a large-area flexible OLED with dimensions of 30 cm×15 cm using a roll-to-roll process. Figure 16g-h illustrate a schematic structure of their flexible OLEDs based on a AgNW networks as anode electrode, and the lighting performance of the devices, respectively. The AgNW-based OLED shows a similar performance, i.e. a luminance of 9389.9 cd m^{-2} compared to 9917.6 cd m^{-2} for ITO-based OLEDs at 6 V bias.[433] Figure 16i displays a photograph of a 30 cm ×15 cm AgNW-based OLED fabricated by the roll-to-roll process, which suggests that AgNW-based TEs are promising alternatives to the brittle ITO for the fabrication of large-area flexible displays.

Towards large-scale production of OLEDs based on metallic TEs, Kim *et al.* have also developed a continuous roll-to-roll redox-welding and embedding method for the fabrication of electrodes of silver nanowire (AgNWs) networks.[434] Figure 16k-j respectively show a scheme of their roll-to-roll embedding process used for the redox-welded AgNWs, and a photograph of large-area flexible OLEDs under bending. The high-performance flexible AgNW-embedded PET film (T >90%, Rsh = 13.5 sq) was achieved owing to the strong fusion and interlocking at the nanowire junction, while the high transparency is maintained. The obtained flat and smooth AgNW-based TEs was successfully applied for flexible OLEDs, showing similar performance compared to the device fabricated with ITO (both required about 5.4-5.7 V to reach a luminance of 10000 cd m^{-2}).

The optical properties of the metal mesh based TE are investigated similarly for the improvement of carrier injecting devices, like OLEDs. Lee *et al*. elaborated IZO/Ag/IZO nanomesh TE that minimize the reflection of emitted light and thus induce the suppression of haze in blue OLEDs.[435] The schematic representation of an IZO/Ag/IZO nanomesh-based blue flexible OLED is shown in Figure 16l. The device showed high external quantum efficiency (≈18.8%) and high mechanical flexibility and durability, as shown in the photos of Figure 16m-n.[435] Concerning other emerging applications, Sun *et al*. have recently developed a large-area transparent red quantum-dot light-emitting diode (QLED) with an external quantum efficiency (EQE) of 11.42% and a transmittance of 72.5%, using a sandwich-structured AgNW/resin/AgNW TE.[443] Additionally, it is worth mentioning a new-generation and exciting devices for lighting and display, namely transparent OLEDs. In this type of devices, light can be emitted through the optically transparent medium in both directions, as these devices use TEs at both ends. A review by Huseynova *et al.* have discussed in details recent advances and challenges for this kind of display devices.[441]

5.5. Energy saving

Metal-based transparent electrodes have recently attracted much attention in the field of energy saving. It is worth mentioning that about 40% of the energy produced in many countries is devoted to cooling and heating of buildings[444]. Therefore, many efforts are devoted to lower this amount of energy consumed thanks to several techniques including, for instance, smart windows and low-emissivity coating. The latter aims at reducing heat transfer between indoor and outdoor environment by blocking IR radiation flow through windows.[381] Three main TE technologies have been mainly investigated to create low-emissivity coatings: silver nanowire networks[389,392], oxide-metal-oxide[381,384] and transparent conductive oxides (TCOs)[377] such as indium tin oxide (ITO), aluminum doped zinc oxide (AZO) or fluorine doped tin oxide (FTO).

The very high electrical conductivity of metal nanowire networks or thin metal film leads to very low infrared emissivity (typically lower than 0.1). For increasing both optical transparency and oxidation/corrosion stability, thin metal films are coated with thin metal oxide layers. These multilayer structures TCO/metal/TCO, such as AZO/Ag/AZO or ITO/Ag/ITO, exhibit very good optical and electrical performances since the optical reflection can be suppressed and the metal is among the most conductive ones (Ag or Cu) in order to consider very thin layers for optimizing transparency. Moreover these multilayers can be deposited at low temperature on low-cost polymeric substrates, to be then compatible with roll-to-roll deposition processes which can significantly reduce the production costs[90]. For instance, Cinali and Coskun reported AZO/Ag/AZO showing promising properties with high visible transmission of 78.7% associated with low-emissivity in far IR with a reflection of 98%[381].

Along a similar route, as depicted in Figure 17a-b, Li *et al*. were able to deposit Ag layer as thin as 6 nm in an AZO/Ag/AZO structure, while the optimized AZO layer thickness was determined thanks to finite-difference time-domain method to search for a compromise between transmittance and reflectance.[382] This results in the fabrication of low-emissivity heaters which exhibit visible transmittance of 93.6% (at 550 nm), an infrared reflectance of 67% (at 1500 nm), as shown by Figure 17c, and a sheet resistance of 5.6 Ω/sq[382].

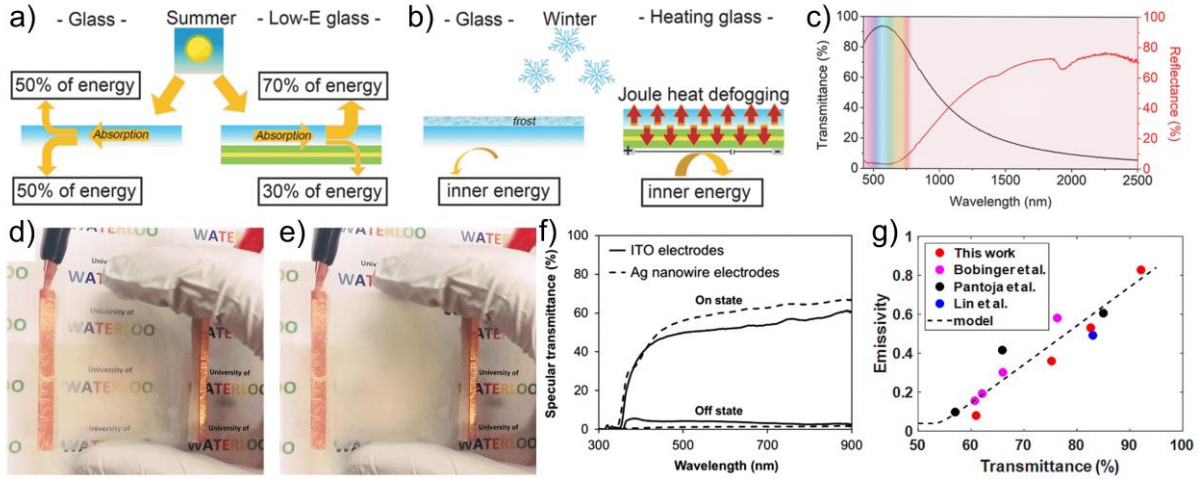

Figure 17: Applications of metal-based TE related to energy saving. a-c) Schematic diagrams comparing: a) the thermal insulation effect of AZO/Ag/AZO based low-emissivity glass and untreated glass in hot weather and b) the defogging effect of AZO/Ag/AZO-based low-emissivity glass in cool weather. c) Transmission and reflectance spectra of an AZO/Ag/AZO-based low-emissivity heater. Reproduced with permission.[382] Copyright 2018, Wiley-VCH. d-f) Integration of AgNW network as TE in a polymer-dispersed liquid-crystal (PDLC) based smart window: d) images obtained with 85 V (on state, associated to an electric-field of 3.4 MV/m and e) without voltage (off state) applied across opposite electrodes. f) Specular transmittance of AgNW network and ITO used as TE in a PDLC smart window in the on and off states. Data shown in d-f) are extracted from the work by Khaligh et al.[390] Reproduced with permission.[390] Copyright 2015, Elsevier. g) Dependency of emissivity in the infrared spectra (5-20 microns) versus optical transmittance (550 nm) of silver nanowire networks. For low-emissivity applications the search area is low-emissivity and high optical transmittance, i.e. in the bottom right area of the graph. Data from Hanauer et al. Reprinted with permission.[392] Copyright 2021, American Chemical Society.

Another significant active domain of research concerning energy saving is smart windows. By definition a smart window is a glass or glazing whose light transmission properties can be altered when external stimuli such as voltage, light, or heat are applied. By modifying the optical transmittance (over a given range of wavelengths) smart windows can for instance create climate adaptive building shells when installed in the envelope of buildings. Dalapati *et al*. recently reviewed the development of energy saving transparent heat regulating (THR) materials and coating for energy saving window applications.[445] The current THR technologies include for instance transparent heat reflecting mirror, transparent solar cells, and thermochromism.[445] The latter, as well the electrochromism, are much used in smart windows technologies.[376] Metal-based TEs have been investigated to integrate them in smart windows. For instance, Li *et al*. reported the fabrication of a large-area flexible TEs based on leaf vein-like hierarchical metal grids (HMG) comprising of mesoscale ‘‘trunk” and microscale ‘‘branches”.[385] Such a metal grid based TEs exhibited an optical transmittance of about 81% and a sheet resistance of 1.36 Ω/sq and was used in a flexible electrochromic devices (ECDs) with very good cyclic performance, which correspond to adequate requirements for integration within smart windows.[385] Another example of integration of metallic TE concerns the investigation of Khaligh *et al*. who replaced ITO by AgNW network for the TE used in polymer-dispersed liquid crystal (PDLC) smart windows.[390] These authors obtained superior electro-optical characteristics for the TE with AgNW networks compared to ITO: indeed the transparency of nanowire PDLC smart windows can be modulated (ΔT_{on-off}) over a larger range

with ΔT_{on-off} value of 57% and 16%, respectively, for AgNW-based and ITO-based devices. Figure 17d-e exhibit the optical images for the off and on states, respectively, while Figure 17f shows the specular transmittance of AgNW network and ITO used as TE in a PDLC smart window in both on and off states. Moreover the required voltage to actuate the AgNW-based smart window appeared 15 V lower compared with ITO based TE[390]. Such results appear very interesting since it also results in a lower cost for the device when using AgNW networks instead of ITO.[390]

Moreover, as shown by Veeramuthu *et al.*, it is also possible to use the interesting properties of AgNW networks for fabricating stretchable transparent heaters with recognized thermochromic properties thanks to the use of thermochromic ink (TM-55-blue) and silver nanowire (AgNW)-coated polydimethylsiloxane (PDMS)[245]. These authors obtained a stretchable heater with desirable credentials such as high transparency, favorable photochromic properties, high stability, and rapid heating rate which are promising assets for an efficient integration into smart windows.[245]

For energy saving, the optimization of the different properties required for any device generally results in a compromise between different parameters. This general trend is illustrated in Figure 17g which reports the dependency of emissivity for AgNW networks in the infrared spectra (averaged in the 5-20 microns wavelength range) versus optical transmittance (measured 550 nm), data from Hanauer *et al*.[392]. For low-emissivity applications the search area is low-emissivity and high optical transmittance, i.e. in the bottom right area of the graph. An efficient and low-emissivity coating based on AgNW, with the dimensions of AgNW used by Hanauer *et al*.[392], can occur only for transmittance of about 70%. The above-mentioned compromise appears here between low-emissivity and optical transmittance, but other compromises are generally considered for many cases in the energy saving domain.

5.6. Other emerging applications

5.6.1. Flexible thin film transistors

Flexible thin film transistor (TFT) is a fundamental component behind flexible electronics, which include various modern devices such as displays, sensors and electronic skin.[38,446] To ensure the long-term mechanical stability of flexible transparent TFT, alternative electrodes to intrinsically brittle ITO have been widely studied, including for instance metal mesh/grid,[447] oxide metal oxide (OMO) structure[448] and metal nanowires.[38] For such flexible and transparent TFTs, the OMO multilayer structure is indeed an ideal choice due to its high electrical, optical, and mechanical properties. Kim *et al.* have successfully fabricated a-IGZO TFT with IZO/Ag/IZO transparent electrodes as source and drain, as schematically shown in Figure 18a. The optimized multilayer electrodes, i.e. IZO/Ag/IZO (40nm/12nm/40nm), exhibit an average visible transmittance of 87.7% and a low sheet resistance of 5.65 Ω/sq, resulting in an enhanced electrical performance in comparison to the TFT with single IZO electrodes.[104] Figure 18b shows outstanding mechanical reliability of the TFT device with IZO/Ag/IZO electrodes during up to 10000 cycles of bending test with 0.08% tensile strain. However, it should be noted that the OMO-based TFTs are not intrinsically stretchable owing to the ceramic layers in OMO structure, thus, not suitable for stretchable electronics.

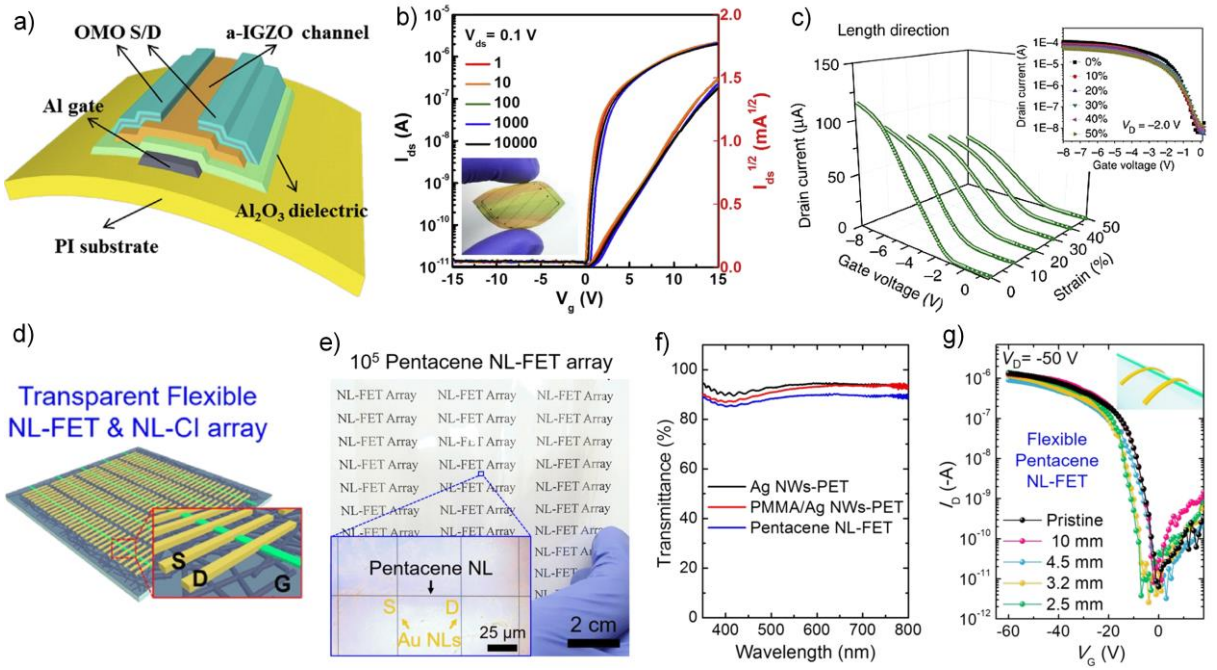

Figure 18: a) Schematic illustration of an amorphous indium-gallium-zinc oxide (a-IGZO) thin-film transistor (TFT) with IZO/Ag/IZO multilayer transparent electrodes on a polyimide substrate, b) I_D-V_G characteristics of the TFT with IZO/Ag/IZO electrodes during 1 to 10000 cycles of bending test with 0.08% tensile strain, showing the high mechanical stability of the devices. Reproduced with permission.[104] Copyright 2016, Elsevier. c) I_D-V_G characteristics (V_D = -2V) under different strains of a TFT device with AgNW-PU acrylate (PUA) composite as the stretchable transparent electrodes, SWCNT network as channel, and a PU-co-polyethylene glycol (PU-co-PEG) as elastomeric dielectric layer. Reproduced with permission.[38] Copyright 2015, Springer Nature. d) Scheme of an array of transparent flexible nanoline field effect transistors (NL-FETs). The semiconductors and the source/drain electrodes are the NLs. The AgNW networks acts as transparent gate electrode and PMMA dielectric are thin layers on a polymer substrate. Reprinted with permission.[447] Copyright 2020, American Chemical Society. e-f-g) photograph of 10^5 pentacene NL-FET array on a PET film, transmittance spectra of the AgNWs-coated PET film, with/without PMMA coating and pentacene NL-FET array, and I_D-V_G characteristics of the pentacene NL-FETs under various bending radius. Reprinted with permission.[447] Copyright 2020, American Chemical Society.

As an option, metal nanowires can also be used in stretchable TFT devices. For instance, Liang *et al.* have fabricated stretchable TFT array based on the screen-printed AgNWs on PET substrate.[449] They demonstrated a stable mobility of one typical TFT in the array during 1000 cycles of continuous wearing on/peeling off a glass vial with radius of 5 mm. Although the obtained electrodes are stretchable, their transparency appears rather low due to a high NW density. Liang *et al.* have reported the fabrication of transparent and stretchable TFTs based on a AgNW-PU acrylate (PUA) composite as the stretchable transparent electrodes. The TFT channel and dielectric layer are made of SWCNT network and a PU-co-polyethylene glycol (PU-co-PEG) elastomer, respectively. The obtained TFT array exhibits excellent optical transparency in the visible range (>90%). Moreover, the authors have demonstrated that the TFTs can be stretched by up to 50% strain and subjected to 500 cycles of repeated stretching to 20% strain without significant loss in electrical property (see Figure 18c).[38] Additionally, the TFT can drive an OLED in a large brightness range. It is noteworthy that the whole fabrication process shown in this work is printable, which is highly preferred for large-scale production. Another recent study by Kim *et al.* demonstrated a pentacene nanoline field-effect transistor (NL-FET) array with high integration (10^5 transistors per 4×4 inch^2).[447] Figure 18d-e show a schematic illustration and photograph of a flexible NL-FET array, in which each transistor consists of semiconductor channel, the source/drain electrodes under the NLs form, AgNW network as transparent gate electrode and PMMA as dielectric layer.[447] Remarkably, the pentacene NL-FET array based on AgNWs-coated PET film exhibits excellent optical transparency (~90%) in the visible range and mechanical robustness, as shown in Figure 18f-g.

As the AgNW network is buried between PET substrate and the PMMA layer, a long-term stability of such structure is also expected. To sum up, the recent advances in flexible metal-based TEs such as AgNWs percolating network or OMO nanostructures have remarkably contributed to the fast growth of flexible displays, sensors, wearable devices. Further studies on device stability under different thermal, electrical and environmental constrains should be carried on to ensure the stable performance and compatibility of the TEs within the devices.

5.6.2. EMI shielding and high frequency antennas

Metals are the most common materials for electromagnetic interference (EMI) shielding to prevent unwanted radiation, owing to their intrinsically high electron density; its performance being characterized by the shielding effectiveness, often mentioned as EMI SE. Some flexible optoelectronic devices such as displays, touch panels and electronic displays require at the same time: efficient EMI SE, excellent optical transmittance, high flexibility, being ultrathin and lightweight, as well as durability. Besides graphene,[450] and transparent conducting oxides (TCOs),[451] metallic nanostructures based on metal nanowires,[452–455] metal mesh/grid,[456,457] and oxide/metal/oxide nanocomposite structures[458] have been investigated to fulfil these requirements for electromagnetic shielding applications.

For instance, Jia *et al.* demonstrated the great potential of AgNW technology as an EMI shielding material for next generation optoelectronic devices. An efficient and reliable transparent EMI shield film made of calcium alginate (CA), silver nanowires (AgNW) and polyurethane (PU) was fabricated using simple and low-cost Mayer-rod coating approach.[459] The obtained CA/AgNW/PU film had high optical transmittance of 92 % and an EMI SE of 20.7 dB. In addition, the transparent film exhibited highly reliable shielding ability with 98% EMI SE retentions even after ultrasound treatment and repeated bending deformations. The combination of metals with thin metal oxides is also an appealing technology for EMI devices. For instance, Wang *et al.* [458] recently reported the production of large-area TE made of ultrathin (8 nm) Cu-Ag alloy thin film on PET substrate by sputtering process and sandwiched by two layers of ITO functioning as effective antireflection layers. This dielectric-metal-dielectric structure leads to an outstanding optical transmittance in the visible range (96.5%) and an average EMI SE of 26 dB. Moreover, the film exhibited excellent mechanical properties with no significant degradation after bending deformations.

Flexible antennas also constitute a component of many electromagnetic devices including wearable devices, Internet of Things (IoT) frameworks, wireless sensor networks, communication devices or radio frequency identification (RFID) systems. Most of the recent studies reported flexible transparent antennas using novel materials such as metal nanowires,[460–463] metal mesh/grid,[464] graphene,[465] CNT,[466] and TCOs.[467] Liu *et al* [464] fabricated a flexible transparent Au nanopatterned antenna on PET substrate. The resulting antenna exhibited optimum flexibility as well as high transparency (94 %). Its efficiency reached up to 29.79 % –36.77 % at high frequency (1800/1900 MHz) in free space, which is about 74.5% – 91.9% of the efficiency of antennas commonly used at present in research and industry. Metal nanowires also appear as a serious candidate material for flexible transparent antennas. It is worth noting that reaching high optical transmittance without changing the electromagnetic performances of the final device is challenging. For instance, Goliya *et al.* [462] produced a transparent antenna composed of AgNW on PET by screen printing approach. The resulting antenna exhibited high radiation efficiency of around 50% with transmittance over 85 % and sheet resistance of 8.5 Ω/sq that enables the antenna to be used as commercial purposes such as transparent RFID tags.

5.6.3. Flexible transparent supercapacitors

The growing demand of transparent, flexible, wearable and self-powered devices has driven the research towards the development of suitable transparent energy storage components. Compared with Li-ion batteries, flexible supercapacitors have attracted greater attention due to their fast charge and discharge rate, large power density, long lifetime, and high safety parameters.[468] Therefore, extensive research has been devoted to the study and fabrication of flexible transparent supercapacitors based on, for instance, metallic nanostructures, including metal grids/meshes,[147,469,470] nanowires,[471] and nanofibers.[307,472]

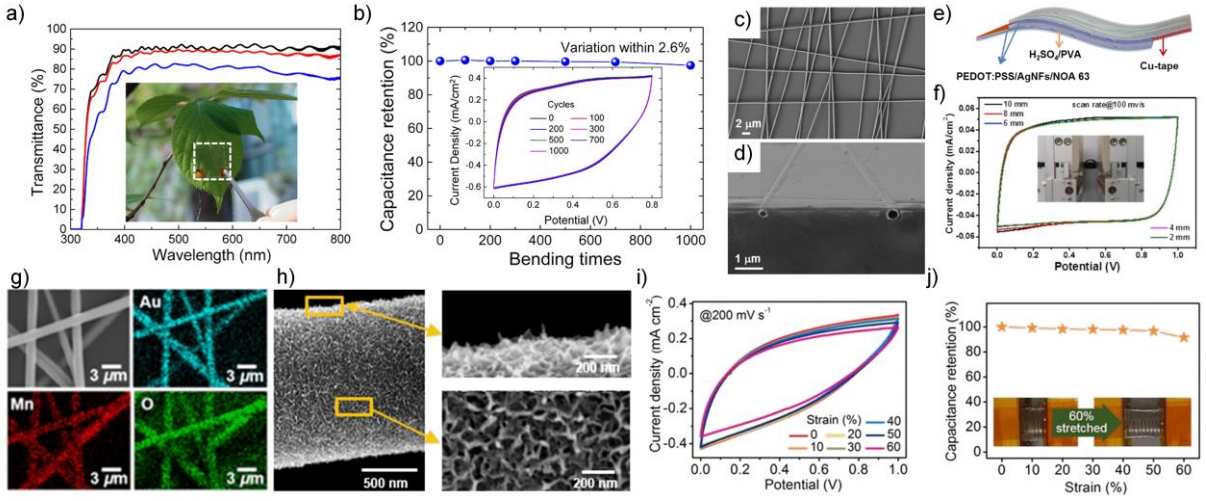

Figure 19: a) Optical transmittance of the embedded Ag grid TE(black), embedded Ag grid/PEDOT:PSS/hybrid TE (red), and the hybrid TE-based flexible transparent supercapacitors (blue),[147] b) Capacitance retention properties of the fabricated supercapacitor fabricated by Xu et al. versus bending times (bending radius of 2 mm). Reprinted with permission.[147] Copyright 2020, American Chemical Society. c-d) SEM micrographs of Ag nanofiber (AgNF) network (top) and embedded PEDOT:PSS/AgNFs/NOA 63 hybrid TE (bottom) fabricated by Singh et al. Reproduced with permission.[307] Copyright 2019, Elsevier. e-f) Schematic representation of a flexible transparent solid-state supercapacitor device, fabricated using two hybrid TE films, and CV characteristics of the obtained supercapacitor device under various bending radius. Reproduced with permission.[307] Copyright 2019, Elsevier. g-h) SEM-EDS mapping images of the MnO_2/Au nanofiber (AuNF) network on PDMS, and a high magnification SEM images of a MnO_2-coated AuNF. MnO_2 was electrodeposited on the electrospun AuNFs via an electrochemical deposition process. Reproduced with permission.[472] Copyright 2020, Elsevier. i-j) CV curves of the obtained supercapacitor with various tensile strains and capacitance retention after different applied strains. Reproduced with permission.[472] Copyright 2020, Elsevier.

Xu *et al.* have demonstrated the use of the embedded Ag grid-based TEs fabricated by UV imprinting lithography combined with the scrap technique, as current collector for flexible transparent supercapacitors.[147] Figure 19a shows the high optical transmittance of Ag grid TEs (~90%) and the obtained supercapacitor device (80%). The TEs also exhibit a low sheet resistance (~2 Ω/sq). The devices exhibit significant mechanical stability (slight capacitance loss of 2.6% after 1000 bending cycles), mainly due to the embedded nature of Ag grid structure, as shown in Figure 19b. Recently, Singh *et al.* have reported the fabrication of embedded PEDOT:PSS/AgNFs/NOA 63 hybrid TE-based supercapacitor by using electrospinning and a peel-off transfer process technique.[307] In addition to high optoelectronic performance (R = 2.12 Ω/sq, T = 84.65%), the hybrid TEs shows a small change (~1%) in resistance after 10000 bending cycles with a bending radius of 2 mm. Figure 19c-d respectively illustrate the top-view and cross-section SEM micrographs of AgNF networks and the embedded AgNFs hybrid TEs, showing the fully embedded nature of AgNWs in the PEDOT:PSS layer on the NOA 63 film. The hybrid TEs were then successfuly used for a flexible transparent solid-state supercapacitor, as shown in Figure 19e-f. The areal capacitance (0.91 mF/cm^2) of the obtained device is,

however, relatively low. Also using the advantages of electrospinning, Lee *et al.* have fabricated MnO_2/AuNF-based supercapacitors with areal capacitance of ~3.68 mF/cm^2, transmittance of ~60%. Figure 19g-h show SEM micrographs of porous MnO_2-coated AuNWs. This porous network structure of the electrochemically deposited MnO_2 is indeed highly desirable for high-performance supercapacitors given the high specific surface area. The typical CV behavior of the supercapacitor device shows negligible degradation in the electrochemical performance up to the strain level of 60%. Moreover, as can be seen in Figure 19j, >97% of the initial areal capacitance value is retained up to 50% tensile strain, showing the promising application of the nanocomposite structure for future bendable and wearable transparent devices.

5.7. Applications related to biological and medical devices

Applications of metal-based TE mainly concern "traditional" applicative domains as described from parts 5.2 to 5.6, while applications related to biological and medical devices correspond to rather recent investigations. This concerns for instance antimicrobial activity, water purification, and artificial actuators. This part 5.7 only briefly reports on some significant progress in these fields where metal-based TEs have been used for. It is worth mentioning that so far only AgNW networks have been used in these applications.

Makvandi *et al.* recently reviewed the integration of metal-based nanomaterials in biomedical applications, at least in antimicrobial activity and cytotoxicity aspects.[473] Integrating materials that exhibit antimicrobial activity is a key societal strategy to combat pathogen-related diseases, and metal-based nanomaterials can be of great help in this regard [473]. Silver is well known to possess efficient antimicrobial activity and is mainly used in nanoparticle form (AgNPs).[474] But AgNPs do not necessarily form a percolating network and therefore a TE. However, metal-based TEs have been lately investigated in this regard. For instance, Kim *et al.* demonstrated lately that when a AgNW network is thermally annealed in air, the fragmentation of AgNWs into small segments due to Rayleigh–Plateau instability and the pre-oxidation process are observed[388]. These two features effectively enhance the antibacterial activity of AgNW network against Staphylococcus aureus and for Escherichia coli (also called S.aureus and E.coli).[388] Such enhancement of the antibacterial activity stems from the morphological and chemical changes which facilitate the dissolution of the AgNW film and hence boost the Ag^+-associated antibacterial actions[388]. Another way to modify the surface morphology and chemical composition of the AgNW network is the use of low-energy electron beam irradiation up to a dose of 1200 kGy, as shown by Kim *et al.*[475] This treatment generates silver oxide (Ag_2O and AgO) over the AgNWs and remarkably improves the antibacterial activity for S.aureus and E.coli. Interestingly, several studies were focused on hybrid materials and promising properties have been found. For instance, Cui *et al.* showed that when AgNW was deposited onto graphene oxide sheets a much potent antibacterial activity was observed, compared to AgNW alone[476]. Moreover, these authors showed that the specimen which decreased bacterial growth the most did not inhibit human skin keratinocyte cell growth compared to the Ag NW, illustrating once more the potential of using hybrid nanomaterials[476]. Along the same vein, Spieser *et al.* reported the fabrication and use of an active ink composed of cellulose nanofibrils and AgNW deposited on flexible and transparent polymer films.[477] These authors demonstrated a good optical transparency (75.6%) and strong reduction of bacterial growth equal to 89.3% and 100% against Gram-negative Escherichia Coli and Gram-positive Staphylococcus Aureus bacteria, respectively, using AATCC contact active standard test.[477] Interestingly, the antibacterial activity was also observed to retain with films produced by a reverse gravure roll-to-roll process, proving the promising capability of this antibacterial

solution to be deployed industrially.[477] Such contributions show that the community aims to better control and improve the AgNW network antibacterial performance thanks to their advantages: easy fabrication, low cost, flexibility and high transparency.

Another interesting application, although far less investigated, concerns water purification which can also be considered as a significant societal problem for many countries. Chen *et al*. reported a very long AgNW-modified composite on a macroporous substrate which can be used as a filter.[478] The use of the electrochemical filtration cell equipped with the composite filter enabled the control of the release of Ag^+ at a μg/L level as well as superior bacterial inactivation performance (>6-log inactivation efficiency) thanks to the use of a low voltage (1 V). Such a device can treat a water flux of 100 $m^3/(h.m^2)$ and requires a very small energy consumption of only ~70 J/m^3.[478] This work appears promising and clearly constitutes an emerging application for metal-based TE. More investigation should be performed to investigate the device lifespan, a potential source of degradation, and ways for improving the bactericidal performance. But this pioneering work paves the way to use metal-based TE for point-of-use drinking water treatment.

A third aspect where metal-based TEs have been used concerns artificial sensors or actuators. A typical example concerns for instance the work of Hwang *et al.* who showed that a nanocomposite based on AgNW and conductive elastomer (PEDOT:PSS) constitutes a sensor able to show high sensitivity to small strains on human skin, stretchability, and optical transparency.[391] This enables to monitor human activities (such as subtle movements of muscles) thanks to invisible stretchable electronics associated with ultra-low-power consumption of the sensor.[391] Another example stems from the work of Seok *et al.* who fabricated a transparent and body-attachable multifunctional sensor capable of simultaneous sensing of temperature and pressure.[394] This sensor consisted of randomly or orderly deposited Ni fibers fabricated by electrospinning and electroplating.[394] These different examples demonstrate that metal-based TEs can also be efficiently integrated into devices for biological or medical applications. One can easily foresee in the future some more applications with the integration of both stable, flexible, and transparent sensors and actuators in this applicative field.

As reported in this review article, metallic based TEs constitute now a very active scientific area with many fundamental and applied aspects associated to these research efforts. The more “natural” applications have mainly concerned transparent heaters, solar cells, touch screen and displays or energy. However, we do believe that many efforts will be devoted towards medical and biological applicative domains into which metallic based TE performances can be further explored and optimized for such purposes.

6. Conclusion and prospects

Metallic transparent electrode (TE) has become a mature technology that can now exhibit promising properties and address efficiently many applicative domains. Indeed metallic TEs have been intensively investigated these last years through different disciplinary approaches (physics, chemistry, modeling, or engineering) to better understand and optimize their overall properties and to improve their stability under thermal, electrical, or chemical stress. Thanks to their diversity, they can offer excellent responses for many applications. Among key examples one can cite metal nanowire (MNW) networks that appear fairly well suited as flexible TEs for touch screens, metal grids with appropriate spacing constitute efficient TE for flexible electronics while dielectric-metal-dielectric structures exhibit excellent optical properties for solar cells. Metallic TEs have been mainly investigated for traditional applications in domains

such as photovoltaic, efficient lighting, or flexible/wearable electronics, however, some more recent and/or niche applications have emerged lately such as low emissivity coating, water purification, or antimicrobial activity, as described in part 5. Without any doubt, some other applications will emerge in the future.

One of the main assets of metallic TEs concerns their fabrication process, for instance, spray coating, slot die, bar-coating, and printing techniques, which generally do not require vacuum chamber nor high-temperature processing. These constitute crucial advantages compared to the usual fabrication route for traditional TCOs. Instead, solution processes used for main metallic TEs can be easily scalable and compatible with roll-to-roll technology; they can therefore be low-cost and environmentally friendly. Such deposition methods have also been shown to be efficient to fabricate, in a fast and reproducible way, nanocomposites that can show improved properties and/or address new challenges[375]. The future paths related to metallic TEs are undoubtedly linked with the fabrication, optimization, and use of nanocomposites where metals can be mixed with other materials such as polymers, carbon-based, or oxides. This aspect has already been well explored to enhance the stability of metallic TEs, as discussed in parts 3.4 and 4. The instability nature being either thermal, electrical, or chemical. Even a thin oxide layer can for instance drastically enhance the electrical and thermal stability of AgNW networks for instance. This appears to be also a clear asset for CuNW based TE whose stability is also much enhanced when coated by a thin oxide layer[31]. This is rather promising since Cu-based materials present a low cost, much lower compared to Ag for instance, however with stronger challenges for integration due to its facile oxidation. Several coating methods have been explored. Among them, an emerging and promising method is the atmospheric pressure spatial atomic layer deposition (AP-SALD), which can deposit conformal thin oxide coating at rather low temperature, and should play a significant role in the future thanks to its cost-effectiveness and compatibility with large upscaling methods such as roll to roll.[121] The obtained MNW coated by a thin and conformal oxide layer constitutes flexible and stable transparent electrodes but can also show improved physical properties since the thin oxide layer can also act as an antireflective coating[239].

Another way of improving metallic TEs could stem from a better design for a realistic figure of merit (FoM) to assess metallic TEs, also in comparison with for instance TCOs. The prevailing two used FoM concern Haacke's FoM by considering the 10^{th} power of the transmittance divided by the sheet resistance[23] and the ratio between the electrical and optical conductivity.[188] However, there is still a clear need to consider more adapted FoM. For instance, metal grids could get the best FoM values considering the two above-mentioned FoM. However, although metal grids would be associated with very large FoM values, their integration could be detrimental for collecting or injecting charge carriers (as in photovoltaics and light emitting diodes, respectively) depending on the mean free path of electrical carriers. While from fundamental approach, this is clearly interesting to consider intrinsic FoM which are not applied for a given application, FoM associated to a given application is still lacking. For instance, a very recent article was devoted to the design of a new FoM of TE for photovoltaics which considers the impact on photovoltaic performance. Anand *et al.* indeed proposed a FoM that is directly proportional to the potential power output of the photovoltaic device[421]. Thanks to this novel approach, a state-of-the-art assessment of semi-transparent electrodes for photovoltaic applications could be performed, providing meaningful guidance for the development of advanced TEs for PVs.

Prospects of metallic TE also concern the pertinent development and/or use of characterization techniques to better investigate the material properties at the appropriate scale. Since most of the metallic TE technologies appear as non-uniform technology (except dielectric-metal-dielectric one), being able to perform mapping at the most appropriate scale appears of high importance. This is more specifically interesting for non-regular spatial arrangement, for instance in the case of geometry based on leaf vein-like hierarchical metal grids which consist of both mesoscale 'trunk' and microscale branches.[385] Being able to map such TE appears crucial to better understand and optimize their properties. Interestingly, there have been several appropriate developments in recent times for mapping metallic TEs. For instance, Balakrishnan *et al.* used scanning dielectric microscopy to map the depth distribution of MNWs within the MNW/polymer-based nanocomposites, in a non-destructive way.[479] This was achieved thanks to a quantitative analysis of sub-surface electrostatic force microscopy measurements with finite-element numerical calculations.[480] Milano *et al.* also demonstrated that the electrical resistance tomography (ERT) method can be used to follow in-situ the evolution of the conductivity of AgNW networks and observe the origin of their degradation.[481] Sannicolo *et al.* used IR imagery to detect the activation of the first percolative paths of sparse AgNW networks[27], as well as the origin of the degradation of AgNW submitted to electrical stress.[170] Chen *et al.* were able to prove that metal grids can constitute efficient microelectrodes that allow high-fidelity co-localized monitoring of heart rhythms during optogenetic pacing and optical mapping[482]. These examples illustrate that these mapping methods can be useful for future studies of metallic based TE, specifically if they are used in combination with numerical simulations since they can shed the light on the influence of key parameters of their physical properties, as well about their potential degradation when submitted to electrical or thermal stress.

On the other side, a significant contribution to better understand and optimize metallic TEs should stem from their modeling. The latter can help to better understand the influence of the prevailing parameters (such as chemical composition, fabrication method and conditions, geometrical aspects, and post-deposition treatment) on their physical properties. This is not only crucial to understand the behavior of the used functional materials in metallic TEs but also to investigate in detail the associated interfaces which play a key role in their integration. A lack of adhesion for instance would be highly detrimental for instance. Modeling is often based on physical approaches of real functional material layers and the main obtained results can be efficiently used as inputs and guide for a better design of metallic TEs.

Finally, metallic TEs can constitute key components for industrial development in many applicative domains. Technologies such as metal nanowire or metal mesh have already appeared in the market for potential large-scale applications. However, their integration into commercial products is not extensively applied yet. Thanks to the current intensive research efforts devoted to metal-based TEs, one should see within the next years still innovations in this domain either associated with new metal-based TEs (for instance by using different materials) or new applicative domain not yet covered by the current TEs. Thanks to its low cost and appealing properties, metallic TE technologies should play a prevailing role in the near future in domains such as flexible photovoltaics, foldable devices, wearable electronics, energy-saving devices, or soft robotics, to cite only a few of them.

Acknowledgments

This work was supported by the European Joint Doctorate FunMat (H2020-MSCA-ITN-2014, Project ID 641640). DMR acknowledges funding through the Marie Curie Actions (FP7/2007-2013, Grant Agreement No. 631111). This work was performed within the framework of the Centre of Excellence of Multifunctional Architectured Materials "CEMAM" n° ANR-10-LABX-44-01, through the Earth project. This research is supported by Vietnam National Foundation for Science and Technology Development (NAFOSTED) under grant number 103.02-2019-341. The authors would like to warmly thank the following colleagues for fruitful discussions: Y. Bréchet, C. Celle, M. Lagrange, D.P. Langley, J.P. Simonato and H.V. Bui.

Received: ((will be filled in by the editorial staff))
Revised: ((will be filled in by the editorial staff))
Published online: ((will be filled in by the editorial staff))

References

[1] D. S. Hecht, L. Hu, G. Irvin, *Advanced Materials* **2011**, *23*, 1482.
[2] K. Ellmer, *Nature Photonics* **2012**, *6*, 809.
[3] T. Sannicolo, M. Lagrange, A. Cabos, C. Celle, J.-P. Simonato, D. Bellet, *Small* **2016**, *12*, 6052.
[4] D. T. Papanastasiou, A. Schultheiss, D. Muñoz-Rojas, C. Celle, A. Carella, J.-P. Simonato, D. Bellet, *Advanced Functional Materials* **2020**, *30*, 1910225.
[5] Harold A. Mcmaster, *Conductive Coating for Glass and Method of Application*, **1947**, US2429420 A.
[6] M. S. Tarnopol, *Indium Oxide Coating on a Silicious Base*, **1954**, US2694649A.
[7] T. M. Barnes, M. O. Reese, J. D. Bergeson, B. A. Larsen, J. L. Blackburn, M. C. Beard, J. Bult, J. van de Lagemaat, *Advanced Energy Materials* **2012**, *2*, 353.
[8] L. He, S. C. Tjong, *Materials Science and Engineering: R: Reports* **2016**, *109*, 1.
[9] F. Mirri, A. W. K. Ma, T. T. Hsu, N. Behabtu, S. L. Eichmann, C. C. Young, D. E. Tsentalovich, M. Pasquali, *ACS Nano* **2012**, *6*, 9737.
[10] Y. Zhou, R. Azumi, *Sci Technol Adv Mater* **2016**, *17*, 493.
[11] L. Yu, C. Shearer, J. Shapter, *Chem. Rev.* **2016**, *116*, 13413.
[12] P. Wang, Z. Peng, M. Li, Y. Wang, *Small* **2018**, *14*, 1802625.
[13] Y. Xu, J. Liu, *Small* **2016**, *12*, 1400.
[14] N. Liu, A. Chortos, T. Lei, L. Jin, T. R. Kim, W.-G. Bae, C. Zhu, S. Wang, R. Pfattner, X. Chen, R. Sinclair, Z. Bao, *Sci. Adv.* **2017**, *3*, e1700159.
[15] C. (John) Zhang, V. Nicolosi, *Energy Storage Materials* **2019**, *16*, 102.
[16] M. V. Fabretto, D. R. Evans, M. Mueller, K. Zuber, P. Hojati-Talemi, R. D. Short, G. G. Wallace, P. J. Murphy, *Chemistry of Materials* **2012**, *24*, 3998.
[17] C. Yeon, S. J. Yun, J. Kim, J. W. Lim, *Advanced Electronic Materials* **2015**, *1*, 1500121.
[18] M. N. Gueye, A. Carella, R. Demadrille, J.-P. Simonato, *ACS Appl. Mater. Interfaces* **2017**, *9*, 27250.
[19] Y. Wang, C. Zhu, R. Pfattner, H. Yan, L. Jin, S. Chen, F. Molina-Lopez, F. Lissel, J. Liu, N. I. Rabiah, Z. Chen, J. W. Chung, C. Linder, M. F. Toney, B. Murmann, Z. Bao, *Science Advances* **2017**, *3*, e1602076.
[20] M. N. Gueye, A. Carella, J. Faure-Vincent, R. Demadrille, J.-P. Simonato, *Progress in Materials Science* **2020**, *108*, 100616.
[21] G. Xu, Y. Li, *Nano Select* **2020**, *1*, 169.
[22] A. W. Wright, *Am J Sci* **1877**, *Series 3 Vol. 13*, 49.
[23] G. Haacke, *Annual Review of Materials Science* **1977**, *7*, 73.
[24] G. H. Heilmeier, L. A. Zanoni, L. A. Barton, *Appl. Phys. Lett.* **1968**, *13*, 46.
[25] D. E. Carlson, C. R. Wronski, *Appl. Phys. Lett.* **1976**, *28*, 671.
[26] D. Langley, G. Giusti, C. Mayousse, C. Celle, D. Bellet, J.-P. Simonato, *Nanotechnology* **2013**, *24*, 452001.
[27] T. Sannicolo, D. Muñoz-Rojas, N. D. Nguyen, S. Moreau, C. Celle, J.-P. Simonato, Y. Bréchet, D. Bellet, *Nano Letters* **2016**, *16*, 7046.
[28] L. He, S. C. Tjong, *Materials Science and Engineering: R: Reports* **2016**, *109*, 1.
[29] A. R. Rathmell, B. J. Wiley, *Advanced Materials* **2011**, *23*, 4798.
[30] A. R. Rathmell, S. M. Bergin, Y.-L. Hua, Z.-Y. Li, B. J. Wiley, *Advanced Materials* **2010**, *22*, 3558.
[31] C. Celle, A. Cabos, T. Fontecave, B. Laguitton, A. Benayad, L. Guettaz, N. Pélissier, V. H. Nguyen, D. Bellet, D. Muñoz-Rojas, J.-P. Simonato, *Nanotechnology* **2018**, *29*, 085701.
[32] I. E. Stewart, A. R. Rathmell, L. Yan, S. Ye, P. F. Flowers, W. You, B. J. Wiley, *Nanoscale* **2014**, *6*, 5980.

[33] A. R. Rathmell, M. Nguyen, M. Chi, B. J. Wiley, *Nano Lett.* **2012**, *12*, 3193.
[34] T. Chih-Hung, H. Sui-Ying, H. Tsung-Wei, T. Yu-Tang, C. Yan-Fang, Y. H. Jhang, L. Hsieh, W. Chung-Chih, C. Yen-Shan, C. Chieh-Wei, L. Chung-Chun, *Organic Electronics* **2011**, *12*, 2003.
[35] G. Giusti, V. Consonni, E. Puyoo, D. Bellet, *ACS Appl. Mater. Interfaces* **2014**, *6*, 14096.
[36] S.-T. Zhang, M. Foldyna, H. Roussel, V. Consonni, E. Pernot, L. Schmidt-Mende, L. Rapenne, C. Jiménez, J.-L. Deschanvres, D. Munoz-Rojas, D. Bellet, *J. Mater. Chem. C* **2017**, *5*, 91.
[37] S. Wang, J. Xu, W. Wang, G.-J. N. Wang, R. Rastak, F. Molina-Lopez, J. W. Chung, S. Niu, V. R. Feig, J. Lopez, T. Lei, S.-K. Kwon, Y. Kim, A. M. Foudeh, A. Ehrlich, A. Gasperini, Y. Yun, B. Murmann, J. B.-H. Tok, Z. Bao, *Nature* **2018**, *555*, 83.
[38] J. Liang, L. Li, D. Chen, T. Hajagos, Z. Ren, S.-Y. Chou, W. Hu, Q. Pei, *Nat Commun* **2015**, *6*, 7647.
[39] P. Won, K. K. Kim, H. Kim, J. J. Park, I. Ha, J. Shin, J. Jung, H. Cho, J. Kwon, H. Lee, S. H. Ko, *Advanced Materials* **2021**, *33*, 2002397.
[40] D. B. Fraser, H. D. Cook, *J. Electrochem. Soc.* **1972**, *119*, 1368.
[41] A. Khan, V. H. Nguyen, D. Muñoz-Rojas, S. Aghazadehchors, C. Jiménez, N. D. Nguyen, D. Bellet, *ACS Applied Materials & Interfaces* **2018**, *10*, 19208.
[42] S. An, H. S. Jo, D.-Y. Kim, H. J. Lee, B.-K. Ju, S. S. Al-Deyab, J.-H. Ahn, Y. Qin, M. T. Swihart, A. L. Yarin, S. S. Yoon, *Advanced Materials* **2016**, *28*, 7149.
[43] H. Wu, D. Kong, Z. Ruan, P.-C. Hsu, S. Wang, Z. Yu, T. J. Carney, L. Hu, S. Fan, Y. Cui, *Nat Nano* **2013**, *8*, 421.
[44] J. van de Groep, P. Spinelli, A. Polman, *Nano Lett.* **2012**, *12*, 3138.
[45] S. Bae, H. Kim, Y. Lee, X. Xu, J.-S. Park, Y. Zheng, J. Balakrishnan, T. Lei, H. Ri Kim, Y. I. Song, Y.-J. Kim, K. S. Kim, B. Özyilmaz, J.-H. Ahn, B. H. Hong, S. Iijima, *Nature Nanotechnology* **2010**, *5*, 574.
[46] D. S. Hecht, A. M. Heintz, R. Lee, L. Hu, B. Moore, C. Cucksey, S. Risser, *Nanotechnology* **2011**, *22*, 075201.
[47] J.-Y. Lee, S. T. Connor, Y. Cui, P. Peumans, *Nano Lett.* **2008**, *8*, 689.
[48] M. Lagrange, D. P. Langley, G. Giusti, C. Jiménez, Y. Bréchet, D. Bellet, *Nanoscale* **2015**, *7*, 17410.
[49] S. De, T. M. Higgins, P. E. Lyons, E. M. Doherty, P. N. Nirmalraj, W. J. Blau, J. J. Boland, J. N. Coleman, *ACS Nano* **2009**, *3*, 1767.
[50] H. Lee, D. Lee, Y. Ahn, E.-W. Lee, L. S. Park, Y. Lee, *Nanoscale* **2014**, *6*, 8565.
[51] B. W. An, B. G. Hyun, S.-Y. Kim, M. Kim, M.-S. Lee, K. Lee, J. B. Koo, H. Y. Chu, B.-S. Bae, J.-U. Park, *Nano Letters* **2014**, *14*, 6322.
[52] B. W. An, E.-J. Gwak, K. Kim, Y.-C. Kim, J. Jang, J.-Y. Kim, J.-U. Park, *Nano Letters* **2016**, *16*, 471.
[53] Y. Jang, J. Kim, D. Byun, *Journal of Physics D: Applied Physics* **2013**, *46*, 155103.
[54] P. B. Catrysse, S. Fan, *Nano Lett.* **2010**, *10*, 2944.
[55] W.-K. Kim, S. Lee, D. Hee Lee, I. Hee Park, J. Seong Bae, T. Woo Lee, J.-Y. Kim, J. Hun Park, Y. Chan Cho, C. Ryong Cho, S.-Y. Jeong, *Sci Rep* **2015**, *5*, 10715.
[56] A. Khan, S. Lee, T. Jang, Z. Xiong, C. Zhang, J. Tang, L. J. Guo, W.-D. Li, *Small* **2016**, *12*, 3021.
[57] K.-N. Chen, C.-F. Yang, C.-C. Wu, Y.-H. Chen, *Materials* **2017**, *10*, 226.
[58] R. A. Maniyara, V. K. Mkhitaryan, T. L. Chen, D. S. Ghosh, V. Pruneri, *Nature Communications* **2016**, *7*, 13771.
[59] Z. Zhao, T. L. Alford, *Solar Energy Materials and Solar Cells* **2016**, *157*, 599.
[60] S. De, J. N. Coleman, *ACS Nano* **2010**, *4*, 2713.
[61] I. R. Cisneros-Contreras, A. L. Muñoz-Rosas, A. Rodríguez-Gómez, *Results in Physics* **2019**, *15*, 102695.

[62] D. S. Ghosh, L. Martinez, S. Giurgola, P. Vergani, V. Pruneri, *Opt Lett* **2009**, *34*, 325.
[63] T. Winkler, H. Schmidt, H. Flügge, F. Nikolayzik, I. Baumann, S. Schmale, T. Weimann, P. Hinze, H.-H. Johannes, T. Rabe, S. Hamwi, T. Riedl, W. Kowalsky, *Organic Electronics* **2011**, *12*, 1612.
[64] J. Ho Kim, J. Hwan Lee, S.-W. Kim, Y.-Z. Yoo, T.-Y. Seong, *Ceramics International* **2015**, *41*, 7146.
[65] B. R. Lee, J. S. Goo, Y. W. Kim, Y.-J. You, H. Kim, S.-K. Lee, J. W. Shim, T. G. Kim, *Journal of Power Sources* **2019**, *417*, 61.
[66] C. Ji, D. Liu, C. Zhang, L. Jay Guo, *Nat Commun* **2020**, *11*, 3367.
[67] N. Kim, S. Kee, S. H. Lee, B. H. Lee, Y. H. Kahng, Y.-R. Jo, B.-J. Kim, K. Lee, *Adv. Mater. Weinheim* **2014**, *26*, 2268.
[68] H.-Z. Geng, K. K. Kim, K. P. So, Y. S. Lee, Y. Chang, Y. H. Lee, *J. Am. Chem. Soc.* **2007**, *129*, 7758.
[69] D. H. Shin, H. C. Shim, J.-W. Song, S. Kim, C.-S. Han, *Scripta Materialia* **2009**, *60*, 607.
[70] P. N. Nirmalraj, P. E. Lyons, S. De, J. N. Coleman, J. J. Boland, *Nano Lett.* **2009**, *9*, 3890.
[71] D.-S. Leem, A. Edwards, M. Faist, J. Nelson, D. D. C. Bradley, J. C. de Mello, *Advanced Materials* **2011**, *23*, 4371.
[72] C. Mayousse, C. Celle, A. Carella, J.-P. Simonato, *Nano Res.* **2014**, *7*, 315.
[73] H.-C. Chu, Y.-C. Chang, Y. Lin, S.-H. Chang, W.-C. Chang, G.-A. Li, H.-Y. Tuan, *ACS Appl. Mater. Interfaces* **2016**, *8*, 13009.
[74] Y. Lee, W.-Y. Jin, K. Y. Cho, J.-W. Kang, J. Kim, *J. Mater. Chem. C* **2016**, *4*, 7577.
[75] Y. Huang, X. Bai, M. Zhou, S. Liao, Z. Yu, Y. Wang, H. Wu, *Nano Lett.* **2016**, *16*, 5846.
[76] S. M. Bergin, Y.-H. Chen, A. R. Rathmell, P. Charbonneau, Z.-Y. Li, B. J. Wiley, *Nanoscale* **2012**, *4*, 1996.
[77] D. Lordan, M. Burke, M. Manning, A. Martin, A. Amann, D. O'Connell, R. Murphy, C. Lyons, A. J. Quinn, *ACS Applied Materials & Interfaces* **2017**, *9*, 4932.
[78] H. B. Lee, W.-Y. Jin, M. M. Ovhal, N. Kumar, J.-W. Kang, *J. Mater. Chem. C* **2019**, *7*, 1087.
[79] J. Atkinson, I. A. Goldthorpe, *Nanotechnology* **2020**, *31*, 365201.
[80] E. Pantoja, R. Bhatt, A. Liu, M. C. Gupta, *Nanotechnology* **2017**, *28*, 505708.
[81] Y. Li, G. Xu, C. Cui, Y. Li, *Adv. Energy Mater.* **2018**, *8*, 1701791.
[82] X. Dong, P. Shi, L. Sun, J. Li, F. Qin, S. Xiong, T. Liu, X. Jiang, Y. Zhou, *J. Mater. Chem. A* **2019**, *7*, 1989.
[83] Y.-G. Bi, J. Feng, J.-H. Ji, Y. Chen, Y.-S. Liu, Y.-F. Li, Y.-F. Liu, X.-L. Zhang, H.-B. Sun, *Nanoscale* **2016**, *8*, 10010.
[84] S. Goetz, M. Bauch, T. Dimopoulos, S. Trassl, *Nanoscale Adv.* **2020**, *2*, 869.
[85] J. Meiss, M. K. Riede, K. Leo, *Journal of Applied Physics* **2009**, *105*, 063108.
[86] N. Formica, D. Sundar Ghosh, T. L. Chen, C. Eickhoff, I. Bruder, V. Pruneri, *Solar Energy Materials and Solar Cells* **2012**, *107*, 63.
[87] S. Liu, W. Liu, J. Yu, W. Zhang, L. Zhang, X. Wen, Y. Yin, W. Xie, *J. Mater. Chem. C* **2014**, *2*, 835.
[88] D. Gu, C. Zhang, Y.-K. Wu, L. J. Guo, *ACS Nano* **2014**, *8*, 10343.
[89] M. D. Groner, S. M. George, R. S. McLean, P. F. Carcia, *Appl. Phys. Lett.* **2006**, *88*, 051907.
[90] C. Guillén, J. Herrero, *Thin Solid Films* **2011**, *520*, 1.
[91] Y. Bi, Y. Liu, X. Zhang, D. Yin, W. Wang, J. Feng, H. Sun, *Advanced Optical Materials* **2019**, *7*, 1800778.
[92] N. Formica, P. Mantilla-Perez, D. S. Ghosh, D. Janner, T. L. Chen, M. Huang, S. Garner, J. Martorell, V. Pruneri, *ACS Appl. Mater. Interfaces* **2015**, *7*, 4541.
[93] R. Jaramillo, S. Ramanathan, *Solar Energy Materials and Solar Cells* **2011**, *95*, 602.

[94] Z. Xue, X. Liu, N. Zhang, H. Chen, X. Zheng, H. Wang, X. Guo, *ACS Appl. Mater. Interfaces* **2014**, *6*, 16403.
[95] S. Y. Ryu, J. H. Noh, B. H. Hwang, C. S. Kim, S. J. Jo, J. T. Kim, H. S. Hwang, H. K. Baik, H. S. Jeong, C. H. Lee, S. Y. Song, S. H. Choi, S. Y. Park, *Appl. Phys. Lett.* **2008**, *92*, 023306.
[96] X. Guo, J. Lin, H. Chen, X. Zhang, Y. Fan, J. Luo, X. Liu, *J. Mater. Chem.* **2012**, *22*, 17176.
[97] N. P. Sergeant, A. Hadipour, B. Niesen, D. Cheyns, P. Heremans, P. Peumans, B. P. Rand, *Adv. Mater.* **2012**, *24*, 728.
[98] S. Schubert, J. Meiss, L. Müller-Meskamp, K. Leo, *Adv. Energy Mater.* **2013**, *3*, 438.
[99] W. Wang, M. Song, T.-S. Bae, Y. H. Park, Y.-C. Kang, S.-G. Lee, S.-Y. Kim, D. H. Kim, S. Lee, G. Min, G.-H. Lee, J.-W. Kang, J. Yun, *Adv. Funct. Mater.* **2014**, *24*, 1551.
[100] B. Yoo, K. Kim, S. H. Lee, W. M. Kim, N.-G. Park, *Solar Energy Materials and Solar Cells* **2008**, *92*, 873.
[101] A. Dhar, T. L. Alford, *Journal of Applied Physics* **2012**, *112*, 103113.
[102] D. Choi, *j nanosci nanotechnol* **2020**, *20*, 379.
[103] D. Miao, S. Jiang, S. Shang, Z. Chen, *Ceramics International* **2014**, *40*, 12847.
[104] Y. C. Kim, S. J. Lee, I.-K. Oh, S. Seo, H. Kim, J.-M. Myoung, *Journal of Alloys and Compounds* **2016**, *688*, 1108.
[105] K.-H. Choi, H.-J. Nam, J.-A. Jeong, S.-W. Cho, H.-K. Kim, J.-W. Kang, D.-G. Kim, W.-J. Cho, *Appl. Phys. Lett.* **2008**, *92*, 223302.
[106] M. Kim, C. Lim, D. Jeong, H.-S. Nam, J. Kim, J. Lee, *Organic Electronics* **2016**, *36*, 61.
[107] V. Sharma, R. Vyas, P. Bazylewski, G. S. Chang, K. Asokan, K. Sachdev, *RSC Adv.* **2016**, *6*, 29135.
[108] H. M. Lee, Y. J. Lee, I. S. Kim, M. S. Kang, S. B. Heo, Y. S. Kim, D. Kim, *Vacuum* **2012**, *86*, 1494.
[109] H. Zhou, J. Xie, M. Mai, J. Wang, X. Shen, S. Wang, L. Zhang, K. Kisslinger, H.-Q. Wang, J. Zhang, Y. Li, J. Deng, S. Ke, X. Zeng, *ACS Appl. Mater. Interfaces* **2018**, *10*, 16160.
[110] J.-A. Jeong, Y.-S. Park, H.-K. Kim, *Journal of Applied Physics* **2010**, *107*, 023111.
[111] A. Dhar, T. L. Alford, *ECS Solid State Letters* **2014**, *3*, N33.
[112] K. Sivaramakrishnan, N. D. Theodore, J. F. Moulder, T. L. Alford, *Journal of Applied Physics* **2009**, *106*, 063510.
[113] H.-J. Seok, H.-W. Jang, D.-Y. Lee, B.-G. Son, H.-K. Kim, *Journal of Alloys and Compounds* **2019**, *775*, 853.
[114] J. Zhao, M. A. Green, *IEEE Transactions on Electron Devices* **1991**, *38*, 1925.
[115] D. Zhang, I. A. Digdaya, R. Santbergen, R. A. C. M. M. van Swaaij, P. Bronsveld, M. Zeman, J. A. M. van Roosmalen, A. W. Weeber, *Solar Energy Materials and Solar Cells* **2013**, *117*, 132.
[116] A. Bou, P. Torchio, S. Vedraine, D. Barakel, B. Lucas, J.-C. Bernède, P.-Y. Thoulon, M. Ricci, *Solar Energy Materials and Solar Cells* **2014**, *125*, 310.
[117] S.-M. Lee, H.-W. Koo, T.-W. Kim, H.-K. Kim, *Surface and Coatings Technology* **2018**, *343*, 115.
[118] D. Muñoz-Rojas, J. MacManus-Driscoll, *Materials Horizons* **2014**, *1*, 314.
[119] D. Muñoz-Rojas, V. H. Nguyen, C. Masse de la Huerta, S. Aghazadehchors, C. Jiménez, D. Bellet, *Comptes Rendus Physique* **2017**, *18*, 391.
[120] V. H. Nguyen, A. Sekkat, C. A. Masse de la Huerta, F. Zoubian, C. Crivello, J. Rubio-Zuazo, M. Jaffal, M. Bonvalot, C. Vallée, O. Aubry, H. Rabat, D. Hong, D. Muñoz-Rojas, *Chem. Mater.* **2020**, *32*, 5153.
[121] V. H. Nguyen, A. Sekkat, C. Jiménez, D. Muñoz, D. Bellet, D. Muñoz-Rojas, *Chemical Engineering Journal* **2021**, *403*, 126234.

[122] J. Schneider, P. Rohner, D. Thureja, M. Schmid, P. Galliker, D. Poulikakos, *Adv. Funct. Mater.* **2016**, *26*, 833.
[123] B. Zhang, H. Lee, D. Byun, *Adv. Eng. Mater.* **2020**, *22*, 1901275.
[124] I. Kim, T. S. Lee, D. S. Jeong, W. S. Lee, W. M. Kim, K.-S. Lee, **2013**, 8.
[125] L. Chang, X. Zhang, Y. Ding, H. Liu, M. Liu, L. Jiang, *ACS Appl. Mater. Interfaces* **2018**, *10*, 29010.
[126] D. Bryant, P. Greenwood, J. Troughton, M. Wijdekop, M. Carnie, M. Davies, K. Wojciechowski, H. J. Snaith, T. Watson, D. Worsley, *Adv. Mater.* **2014**, *26*, 7499.
[127] A. Khan, C. Liang, Y.-T. Huang, C. Zhang, J. Cai, S.-P. Feng, W.-D. Li, *Adv. Eng. Mater.* **2019**, *21*, 1900723.
[128] D. S. Ghosh, T. L. Chen, V. Pruneri, *Applied Physics Letters* **2010**, *96*, 041109.
[129] J. van de Groep, D. Gupta, M. A. Verschuuren, M. M. Wienk, R. A. J. Janssen, A. Polman, *Sci Rep* **2015**, *5*, 11414.
[130] H.-J. Choi, S. Choo, P.-H. Jung, J.-H. Shin, Y.-D. Kim, H. Lee, *Nanotechnology* **2015**, *26*, 055305.
[131] S. Hong, J. Yeo, G. Kim, D. Kim, H. Lee, J. Kwon, H. Lee, P. Lee, S. H. Ko, *ACS Nano* **2013**, *7*, 5024.
[132] Y.-K. Liu, M.-T. Lee, *ACS Appl. Mater. Interfaces* **2014**, *6*, 14576.
[133] W. Zhao, T. Rovere, D. Weerawarne, G. Osterhoudt, N. Kang, P. Joseph, J. Luo, B. Shim, M. Poliks, C.-J. Zhong, *ACS Nano* **2015**, *9*, 6168.
[134] Y.-Y. Zhao, M.-L. Zheng, X.-Z. Dong, F. Jin, J. Liu, X.-L. Ren, X.-M. Duan, Z.-S. Zhao, *Appl. Phys. Lett.* **2016**, *108*, 221104.
[135] W. Shou, B. K. Mahajan, B. Ludwig, X. Yu, J. Staggs, X. Huang, H. Pan, *Adv. Mater.* **2017**, *29*, 1700172.
[136] X. Chen, X. Wu, S. Shao, J. Zhuang, L. Xie, S. Nie, W. Su, Z. Chen, Z. Cui, *Sci Rep* **2017**, *7*, 13239.
[137] S. Feng, S. Cao, Z. Tian, H. Zhu, D. Kong, *ACS Appl. Mater. Interfaces* **2019**, *11*, 45844.
[138] Y. Jang, J. Kim, D. Byun, *J. Phys. D: Appl. Phys.* **2013**, *46*, 155103.
[139] J. S. Park, Y. Song, D. Park, Y.-W. Kim, Y. J. Kim, *Nanotechnology* **2018**, *29*, 255302.
[140] M.-G. Kang, M.-S. Kim, J. Kim, L. J. Guo, *Adv. Mater.* **2008**, *20*, 4408.
[141] L. J. Guo, *Advanced Materials* **2007**, *19*, 495.
[142] M. Song, H.-J. Kim, C. S. Kim, J.-H. Jeong, C. Cho, J.-Y. Lee, S.-H. Jin, D.-G. Choi, D.-H. Kim, *J. Mater. Chem. A* **2015**, *3*, 65.
[143] X. Zhu, M. Liu, X. Qi, H. Li, Y.-F. Zhang, Z. Li, Z. Peng, J. Yang, L. Qian, Q. Xu, N. Gou, J. He, D. Li, H. Lan, *Advanced Materials* **2021**, *33*, 2007772.
[144] J.-S. Yu, G. H. Jung, J. Jo, J. S. Kim, J. W. Kim, S.-W. Kwak, J.-L. Lee, I. Kim, D. Kim, *Solar Energy Materials and Solar Cells* **2013**, *109*, 142.
[145] I. Burgués-Ceballos, N. Kehagias, C. M. Sotomayor-Torres, M. Campoy-Quiles, P. D. Lacharmoise, *Solar Energy Materials and Solar Cells* **2014**, *127*, 50.
[146] J. W. Lim, Y. T. Lee, R. Pandey, T.-H. Yoo, B.-I. Sang, B.-K. Ju, D. K. Hwang, W. K. Choi, *Optics Express* **2014**, *22*, 26891.
[147] J.-L. Xu, Y.-H. Liu, X. Gao, Y. Sun, S. Shen, X. Cai, L. Chen, S.-D. Wang, *ACS Appl. Mater. Interfaces* **2017**, *9*, 27649.
[148] T. Gao, Z. Li, P. Huang, G. J. Shenoy, D. Parobek, S. Tan, J. Lee, H. Liu, P. W. Leu, *ACS Nano* **2015**, *9*, 5440.
[149] K. Neyts, A. Real, M. Marescaux, S. Mladenovski, J. Beeckman, *Journal of Applied Physics* **2008**, *103*, 093113.
[150] K. Bley, J. Semmler, M. Rey, C. Zhao, N. Martic, R. N. K. Taylor, M. Stingl, N. Vogel, *Advanced Functional Materials* **2018**, *28*, 1706965.
[151] M. Layani, M. Gruchko, O. Milo, I. Balberg, D. Azulay, S. Magdassi, *ACS Nano* **2009**, *3*, 3537.

[152] W. Li, H. Zhang, S. Shi, J. Xu, X. Qin, Q. He, K. Yang, W. Dai, G. Liu, Q. Zhou, H. Yu, S. R. P. Silva, M. Fahlman, *J. Mater. Chem. C* **2020**, *8*, 4636.
[153] X. Li, Y. Wang, C. Yin, Z. Yin, *J. Mater. Chem. C* **2020**, *8*, 849.
[154] J. Bang, S. Coskun, K. R. Pyun, D. Doganay, S. Tunca, S. Koylan, D. Kim, H. E. Unalan, S. H. Ko, *Applied Materials Today* **2021**, *22*, 100909.
[155] P. Zhang, I. Wyman, J. Hu, S. Lin, Z. Zhong, Y. Tu, Z. Huang, Y. Wei, *Materials Science and Engineering: B* **2017**, *223*, 1.
[156] K. W. Shah, T. Xiong, *Materials* **2019**, *12*, 1731.
[157] A. Madeira, M. Plissonneau, L. Servant, I. A. Goldthorpe, M. Tréguer-Delapierre, *Nanomaterials* **2019**, *9*, 899.
[158] S.-H. Tseng, L.-M. Lyu, K.-Y. Hsiao, W.-H. Ho, M.-Y. Lu, *Chem. Commun.* **2020**, *56*, 5593.
[159] H. Guo, N. Lin, Y. Chen, Z. Wang, Q. Xie, T. Zheng, N. Gao, S. Li, J. Kang, D. Cai, D.-L. Peng, *Sci Rep* **2013**, *3*, 2323.
[160] C. Mayousse, C. Celle, A. Carella, J.-P. Simonato, *Nano Res.* **2014**, *7*, 315.
[161] H.-C. Chu, Y.-C. Chang, Y. Lin, S.-H. Chang, W.-C. Chang, G.-A. Li, H.-Y. Tuan, *ACS Appl. Mater. Interfaces* **2016**, *8*, 13009.
[162] M. Bobinger, J. Mock, P. La Torraca, M. Becherer, P. Lugli, L. Larcher, *Advanced Materials Interfaces* **2017**, *4*, 1700568.
[163] K. Kim, H.-C. Kwon, S. Ma, E. Lee, S.-C. Yun, G. Jang, H. Yang, J. Moon, *ACS Appl. Mater. Interfaces* **2018**, *10*, 30337.
[164] Y. Ahn, Y. Jeong, D. Lee, Y. Lee, *ACS Nano* **2015**, *9*, 3125.
[165] L. Dou, F. Cui, Y. Yu, G. Khanarian, S. W. Eaton, Q. Yang, J. Resasco, C. Schildknecht, K. Schierle-Arndt, P. Yang, *ACS Nano* **2016**, *10*, 2600.
[166] H. Zhang, S. Wang, Y. Tian, J. Wen, C. Hang, Z. Zheng, Y. Huang, S. Ding, C. Wang, *Nano Materials Science* **2020**, *2*, 164.
[167] S. Polat Genlik, D. Tigan, Y. Kocak, K. E. Ercan, M. O. Cicek, S. Tunca, S. Koylan, S. Coskun, E. Ozensoy, H. E. Unalan, *ACS Appl. Mater. Interfaces* **2020**, *12*, 45136.
[168] M. Azani, A. Hassanpour, T. Torres, *Adv. Energy Mater.* **2020**, 2002536.
[169] H. Wang, Y. Wang, X. Chen, *Colloids and Surfaces A: Physicochemical and Engineering Aspects* **2019**, *565*, 154.
[170] T. Sannicolo, N. Charvin, L. Flandin, S. Kraus, D. T. Papanastasiou, C. Celle, J.-P. Simonato, D. Muñoz-Rojas, C. Jiménez, D. Bellet, *ACS Nano* **2018**, *12*, 4648.
[171] C. Mayousse, C. Celle, A. Fraczkiewicz, J.-P. Simonato, *Nanoscale* **2015**, *7*, 2107.
[172] J. Crêpellière, K. Menguelti, S. Wack, O. Bouton, M. Gérard, P. L. Popa, B. R. Pistillo, R. Leturcq, M. Michel, *ACS Appl. Nano Mater.* **2021**, *4*, 1126.
[173] Y. Jia, C. Chen, D. Jia, S. Li, S. Ji, C. Ye, *ACS Appl. Mater. Interfaces* **2016**, *8*, 9865.
[174] A. Madeira, D. T. Papanastasiou, T. Toupance, L. Servant, M. Tréguer-Delapierre, D. Bellet, I. A. Goldthorpe, *Nanoscale Adv.* **2020**, *2*, 3804.
[175] D.-J. Kim, H.-I. Shin, E.-H. Ko, K.-H. Kim, T.-W. Kim, H.-K. Kim, *Sci Rep* **2016**, *6*, 34322.
[176] H.-J. Seok, J.-K. Kim, H.-K. Kim, *Sci Rep* **2018**, *8*, 1.
[177] X. Xu, G. Han, H. Yu, X. Jin, J. Yang, J. Lin, C. Ma, *J. Phys. D: Appl. Phys.* **2020**, *53*, 05LT02.
[178] Z. Cui, Y. Han, Q. Huang, J. Dong, Y. Zhu, *Nanoscale* **2018**, *10*, 6806.
[179] Q. Huang, K. N. Al-Milaji, H. Zhao, *ACS Appl. Nano Mater.* **2018**, *1*, 4528.
[180] D. J. Finn, M. Lotya, J. N. Coleman, *ACS Appl. Mater. Interfaces* **2015**, *7*, 9254.
[181] W. Zhao, S.-S. Wang, C.-B. Zhao, H.-T. Cao, H. Zhang, A.-Z. Peng, H. Dong, L.-H. Xie, W. Huang, *J. Mater. Chem. C* **2021**, *9*, 1874.
[182] S. Hemmati, M. T. Harris, D. P. Barkey, *Journal of Nanomaterials* **2020**, *2020*, 1.
[183] J.-L. Wang, Z.-H. Wang, J.-W. Liu, S.-H. Yu, *Sci. China Mater.* **2016**, *59*, 538.

[184] B. Yoo, Y. Kim, C. J. Han, M. S. Oh, J.-W. Kim, *Applied Surface Science* **2018**, *429*, 151.
[185] S. Han, S. Hong, J. Yeo, D. Kim, B. Kang, M.-Y. Yang, S. H. Ko, *Adv. Mater.* **2015**, *27*, 6397.
[186] B. Omaña-Sanz, D. Toybou, L. Lesven, V. Gaucher, A. Fadel, A. Addad, P. Recourt, D. Yeghicheyan, D. Arndt, C. Celle, J.-P. Simonato, C. Vulpe, L. Charlet, S. Sobanska, B. Gilbert, A. Hofmann, *NanoImpact* **2020**, *18*, 100217.
[187] D. Bellet, M. Lagrange, T. Sannicolo, S. Aghazadehchors, V. H. Nguyen, D. P. Langley, D. Muñoz-Rojas, C. Jiménez, Y. Bréchet, N. D. Nguyen, *Materials* **2017**, *10*, 570.
[188] S. De, T. M. Higgins, P. E. Lyons, E. M. Doherty, P. N. Nirmalraj, W. J. Blau, J. J. Boland, J. N. Coleman, *ACS Nano* **2009**, *3*, 1767.
[189] S. De, P. J. King, P. E. Lyons, U. Khan, J. N. Coleman, *ACS Nano* **2010**, *4*, 7064.
[190] S. Sorel, D. Bellet, J. N. Coleman, *ACS Nano* **2014**, *8*, 4805.
[191] D. T. Papanastasiou, N. Charvin, J. Resende, V. H. Nguyen, A. Sekkat, D. Muñoz-Rojas, C. Jiménez, L. Flandin, D. Bellet, *Nanotechnology* **2021**, *32*, 445702.
[192] H. Hu, S. Wang, X. Feng, M. Pauly, G. Decher, Y. Long, *Chem. Soc. Rev.* **2020**, *49*, 509.
[193] P. T. Probst, S. Sekar, T. A. F. König, P. Formanek, G. Decher, A. Fery, M. Pauly, *ACS Appl. Mater. Interfaces* **2018**, *10*, 3046.
[194] D. Xiao, R. Navik, Y. Gai, H. Tan, Y. Zhao, *Ind. Eng. Chem. Res.* **2020**, *59*, 13572.
[195] M. Azani, A. Hassanpour, *ChemistrySelect* **2019**, *4*, 2716.
[196] Z. Niu, F. Cui, E. Kuttner, C. Xie, H. Chen, Y. Sun, A. Dehestani, K. Schierle-Arndt, P. Yang, *Nano Lett.* **2018**, *18*, 5329.
[197] M. M. Menamparambath, K. Yang, H. H. Kim, O. S. Bae, M. S. Jeong, J.-Y. Choi, S. Baik, *Nanotechnology* **2016**, *27*, 465706.
[198] A. Bid, A. Bora, A. K. Raychaudhuri, *Phys. Rev. B* **2006**, *74*, 035426.
[199] Q. Huang, C. M. Lilley, M. Bode, *Applied Physics Letters* **2009**, *95*, 103112.
[200] D. P. Langley, M. Lagrange, N. D. Nguyen, D. Bellet, *Nanoscale Horizons* **2018**, *3*, 545.
[201] Y. Mao, H. Yang, C. Hu, J. Guo, X. Meng, Y. Yang, *J Mater Sci: Mater Electron* **2017**, *28*, 5308.
[202] H. Moon, P. Won, J. Lee, S. H. Ko, *Nanotechnology* **2016**, *27*, 295201.
[203] C. Hwang, J. An, B. D. Choi, K. Kim, S.-W. Jung, K.-J. Baeg, M.-G. Kim, K. M. Ok, J. Hong, *J. Mater. Chem. C* **2016**, *4*, 1441.
[204] L. Zhang, F. Jiang, B. Wu, C. Lv, M. Wu, *Nanotechnology* **2021**, *32*, 105710.
[205] D. Toybou, C. Celle, C. Aude-Garcia, T. Rabilloud, J.-P. Simonato, *Environmental Science: Nano* **2019**, *6*, 684.
[206] T. Araki, J. Jiu, M. Nogi, H. Koga, S. Nagao, T. Sugahara, K. Suganuma, *Nano Res.* **2014**, *7*, 236.
[207] T. Kim, A. Canlier, G. H. Kim, J. Choi, M. Park, S. M. Han, *ACS Appl. Mater. Interfaces* **2013**, *5*, 788.
[208] G. Haacke, *Journal of Applied Physics* **1976**, *47*, 4086.
[209] D. P. Langley, M. Lagrange, G. Giusti, C. Jiménez, Y. Bréchet, N. D. Nguyen, D. Bellet, *Nanoscale* **2014**, *6*, 13535.
[210] T. C. Hauger, S. M. I. Al-Rafia, J. M. Buriak, *ACS Appl. Mater. Interfaces* **2013**, *5*, 12663.
[211] Y. Wang, L. Zhang, D. Wang, *Adv. Mater. Technol.* **2019**, *4*, 1900721.
[212] K. Zhang, J. Li, Y. Fang, B. Luo, Y. Zhang, Y. Li, J. Zhou, B. Hu, *Nanoscale* **2018**, *10*, 12981.
[213] Y. Liu, J. Zhang, H. Gao, Y. Wang, Q. Liu, S. Huang, C. F. Guo, Z. Ren, *Nano Letters* **2017**, *17*, 1090.
[214] R. Wang, H. Zhai, T. Wang, X. Wang, Y. Cheng, L. Shi, J. Sun, *Nano Res.* **2016**, *9*, 2138.
[215] W.-H. Chung, S.-H. Kim, H.-S. Kim, *Sci Rep* **2016**, *6*, 32086.

[216] S. Dai, Q. Li, G. Liu, H. Yang, Y. Yang, D. Zhao, W. Wang, M. Qiu, *Applied Physics Letters* **2016**, *108*, 121103.
[217] S. Han, S. Hong, J. Ham, J. Yeo, J. Lee, B. Kang, P. Lee, J. Kwon, S. S. Lee, M.-Y. Yang, S. H. Ko, *Adv. Mater.* **2014**, *26*, 5808.
[218] Y. Huang, Y. Tian, C. Hang, Y. Liu, S. Wang, M. Qi, H. Zhang, J. Zhao, *ACS Applied Materials & Interfaces* **2019**, *11*, 21850.
[219] Y. Ding, Y. Cui, X. Liu, G. Liu, F. Shan, *Applied Materials Today* **2020**, *20*, 100634.
[220] A. T. Bellew, H. G. Manning, C. Gomes da Rocha, M. S. Ferreira, J. J. Boland, *ACS Nano* **2015**, *9*, 11422.
[221] Q. Nian, M. Saei, Y. Xu, G. Sabyasachi, B. Deng, Y. P. Chen, G. J. Cheng, *ACS Nano* **2015**, *9*, 10018.
[222] D. Kumar, V. Stoichkov, E. Brousseau, G. C. Smith, J. Kettle, *Nanoscale* **2019**, *11*, 5760.
[223] N. Charvin, J. Resende, D. T. Papanastasiou, D. Muñoz-Rojas, C. Jiménez, A. Nourdine, D. Bellet, L. Flandin, *Nanoscale Adv.* **2021**, *3*, 675.
[224] H. Kang, S.-J. Song, Y. E. Sul, B.-S. An, Z. Yin, Y. Choi, L. Pu, C.-W. Yang, Y. S. Kim, S. M. Cho, J.-G. Kim, J. H. Cho, *ACS Nano* **2018**, *12*, 4894.
[225] D. Fantanas, A. Brunton, S. J. Henley, R. A. Dorey, *Nanotechnology* **2018**, *29*, 465705.
[226] H. H. Khaligh, L. Xu, A. Khosropour, A. Madeira, M. Romano, C. Pradére, M. Tréguer-Delapierre, L. Servant, M. A. Pope, I. A. Goldthorpe, *Nanotechnology* **2017**, *28*, 425703.
[227] D. Chen, F. Zhao, K. Tong, G. Saldanha, C. Liu, Q. Pei, *Advanced Electronic Materials* **2016**, *2*, 1600167.
[228] J. J. Patil, W. H. Chae, A. Trebach, K. Carter, E. Lee, T. Sannicolo, J. C. Grossman, *Adv. Mater.* **2020**, 2004356.
[229] N. M. Batra, A. Syed, P. M. F. J. Costa, *Nanoscale* **2019**, *11*, 3606.
[230] M. Lagrange, T. Sannicolo, D. Muñoz-Rojas, B. G. Lohan, A. Khan, M. Anikin, C. Jiménez, F. Bruckert, Y. Bréchet, D Bellet, *Nanotechnology* **2017**, *28*, 055709.
[231] F. N. Kholid, H. Huang, Y. Zhang, H. J. Fan, *Nanotechnology* **2016**, *27*, 025703.
[232] K. Maize, S. R. Das, S. Sadeque, A. M. S. Mohammed, A. Shakouri, D. B. Janes, M. A. Alam, *Applied Physics Letters* **2015**, *106*, 143104.
[233] Y. Zhu, T. Wan, P. Guan, Y. Wang, T. Wu, Z. Han, G. Tang, D. Chu, *Journal of Colloid and Interface Science* **2020**, *566*, 375.
[234] J. Wang, J. Jiu, S. Zhang, T. Sugahara, S. Nagao, K. Suganuma, P. He, *Nanotechnology* **2018**, *29*, 435701.
[235] A.-T. Pham, X.-Q. Nguyen, D.-H. Tran, V. Ngoc Phan, T.-T. Duong, D.-C. Nguyen, *Nanotechnology* **2016**, *27*, 335202.
[236] M. Go, B. Hwang, S. Lim, *Materials and Manufacturing Processes* **2019**, *34*, 1605.
[237] B. Hwang, Y. An, H. Lee, E. Lee, S. Becker, Y.-H. Kim, H. Kim, *Sci Rep* **2017**, *7*, 41336.
[238] J.-M. Lee, Y.-H. Kim, H.-K. Kim, H.-J. Kim, C.-H. Hong, *Sci Rep* **2020**, *10*, 4592.
[239] S. Aghazadehchors, V. H. Nguyen, D. Muñoz-Rojas, C. Jiménez, L. Rapenne, N. D. Nguyen, D. Bellet, *Nanoscale* **2019**, *11*, 19969.
[240] S. Zhang, S. Li, Z. Xia, K. Cai, *J. Mater. Chem. B* **2020**, *8*, 852.
[241] J. Wang, H. Lou, J. Meng, Z. Peng, B. Wang, J. Wan, *Sensors and Actuators B: Chemical* **2020**, *305*, 127529.
[242] Q. Han, Y. Chen, W. Song, M. Zhang, S. Wang, P. Ren, L. Hao, A. Wang, S. Bai, J. Yin, *Bio-des. Manuf.* **2019**, *2*, 269.
[243] T. Araki, T. Uemura, S. Yoshimoto, A. Takemoto, Y. Noda, S. Izumi, T. Sekitani, *Adv. Mater.* **2020**, *32*, 1902684.
[244] M. Zhao, D. Li, J. Huang, D. Wang, A. Mensah, Q. Wei, *J. Mater. Chem. C* **2019**, *7*, 13468.
[245] L. Veeramuthu, B.-Y. Chen, C.-Y. Tsai, F.-C. Liang, M. Venkatesan, D.-H. Jiang, C.-W. Chen, X. Cai, C.-C. Kuo, *RSC Advances* **2019**, *9*, 35786.

[246] M. Jo, S. Bae, I. Oh, J. Jeong, B. Kang, S. J. Hwang, S. S. Lee, H. J. Son, B.-M. Moon, M. J. Ko, P. Lee, *ACS Nano* **2019**, *13*, 12500.
[247] H. S. Jo, S. An, C.-W. Park, D.-Y. Woo, A. L. Yarin, S. S. Yoon, *ACS Appl. Mater. Interfaces* **2019**, *11*, 40232.
[248] S. Yao, J. Yang, F. R. Poblete, X. Hu, Y. Zhu, *ACS Appl. Mater. Interfaces* **2019**, *11*, 31028.
[249] W. A. D. M. Jayathilaka, K. Qi, Y. Qin, A. Chinnappan, W. Serrano-García, C. Baskar, H. Wang, J. He, S. Cui, S. W. Thomas, S. Ramakrishna, *Adv. Mater.* **2019**, *31*, 1805921.
[250] S. Huang, Y. Liu, Y. Zhao, Z. Ren, C. F. Guo, *Advanced Functional Materials* **2019**, *29*, 1805924.
[251] Z. H. Chen, R. Fang, W. Li, J. Guan, *Adv. Mater.* **2019**, *31*, 1900756.
[252] Q. Huang, Y. Zhu, *Advanced Materials Technologies* **2019**, *4*, 1800546.
[253] J. Kwon, Y. D. Suh, J. Lee, P. Lee, S. Han, S. Hong, J. Yeo, H. Lee, S. H. Ko, *Journal of Materials Chemistry C* **2018**, *6*, 7445.
[254] H. Sohn, C. Park, J.-M. Oh, S. W. Kang, M.-J. Kim, *Materials* **2019**, *12*, 2526.
[255] J. Jung, H. Cho, R. Yuksel, D. Kim, H. Lee, J. Kwon, P. Lee, J. Yeo, S. Hong, H. E. Unalan, S. Han, S. H. Ko, *Nanoscale* **2019**, *11*, 20356.
[256] V. H. Nguyen, J. Resende, D. T. Papanastasiou, N. Fontanals, C. Jiménez, D. Muñoz-Rojas, D. Bellet, *Nanoscale* **2019**, *11*, 12097.
[257] M. Park, W. Kim, B. Hwang, S. M. Han, *Scripta Materialia* **2019**, *161*, 70.
[258] J. Kim, J. Park, U. Jeong, J.-W. Park, *J. Appl. Polym. Sci.* **2016**, *133*, n/a.
[259] G.-W. Huang, H.-M. Xiao, S.-Y. Fu, *Scientific Reports* **2015**, *5*, 13971.
[260] F. Xu, Y. Zhu, *Advanced Materials* **2012**, *24*, 5117.
[261] S. Hong, H. Lee, J. Lee, J. Kwon, S. Han, Y. D. Suh, H. Cho, J. Shin, J. Yeo, S. H. Ko, *Adv. Mater.* **2015**, *27*, 4744.
[262] H.-S. Liu, B.-C. Pan, G.-S. Liou, *Nanoscale* **2017**, *9*, 2633.
[263] H. Jeong, Y. Noh, S. H. Ko, D. Lee, *Composites Science and Technology* **2019**, *174*, 50.
[264] G.-H. Lim, K. Ahn, S. Bok, J. Nam, B. Lim, *Nanoscale* **2017**, *9*, 8938.
[265] X. Ho, C. K. Cheng, J. N. Tey, J. Wei, *Nanotechnology* **2015**, *26*, 195504.
[266] Y. Seo, B. S. Kim, W. C. Ballance, N. Aw, B. Sutton, H. Kong, *ACS Appl. Mater. Interfaces* **2020**, *12*, 13040.
[267] H.-J. Lee, S. Oh, K.-Y. Cho, W.-L. Jeong, D.-S. Lee, S.-J. Park, *ACS Appl. Mater. Interfaces* **2018**, *10*, 14124.
[268] Y. Chen, R. S. Carmichael, T. B. Carmichael, *ACS Appl. Mater. Interfaces* **2019**, *11*, 31210.
[269] C. Weng, Z. Dai, G. Wang, L. Liu, Z. Zhang, *ACS Appl. Mater. Interfaces* **2019**, *11*, 6541.
[270] X. He, R. He, Q. Lan, W. Wu, F. Duan, J. Xiao, M. Zhang, Q. Zeng, J. Wu, J. Liu, *Materials* **2017**, *10*, 220.
[271] S. Bok, K. Ahn, H. Oh, N. Kwon, J. H. Lee, J. Nam, B. Lim, *Adv. Electron. Mater.* **2020**, 1901440.
[272] L. Zhang, Y. Ji, Y. Qiu, C. Xu, Z. Liu, Q. Guo, *J. Mater. Chem. C* **2018**, *6*, 4887.
[273] C. Celle, C. Mayousse, E. Moreau, H. Basti, A. Carella, J.-P. Simonato, *Nano Res.* **2012**, *5*, 427.
[274] R. Gupta, K. D. M. Rao, S. Kiruthika, G. U. Kulkarni, *ACS Appl. Mater. Interfaces* **2016**, *8*, 12559.
[275] D. T. Papanastasiou, A. Schultheiss, D. Muñoz-Rojas, C. Celle, A. Carella, J.-P. Simonato, D. Bellet, *Adv. Funct. Mater.* **2020**, 1910225.
[276] H. Hosseinzadeh Khaligh, K. Liew, Y. Han, N. M. Abukhdeir, I. A. Goldthorpe, *Solar Energy Materials and Solar Cells* **2015**, *132*, 337.

[277] Y. Lin, W. Yuan, C. Ding, S. Chen, W. Su, H. Hu, Z. Cui, F. Li, *ACS Appl. Mater. Interfaces* **2020**, *12*, 24074.
[278] R. Yuksel, S. Coskun, G. Gunbas, A. Cirpan, L. Toppare, H. E. Unalan, *J. Electrochem. Soc.* **2017**, *164*, A721.
[279] F. Guo, N. Li, V. V. Radmilović, V. R. Radmilović, M. Turbiez, E. Spiecker, K. Forberich, C. J. Brabec, *Energy Environ. Sci.* **2015**, *8*, 1690.
[280] D. P. Langley, G. Giusti, M. Lagrange, R. Collins, C. Jiménez, Y. Bréchet, D. Bellet, *Solar Energy Materials and Solar Cells* **2014**, *125*, 318.
[281] P. Aurang, D. Doganay, A. Bek, R. Turan, H. E. Unalan, *Solar Energy* **2017**, *141*, 110.
[282] S. Lee, J. Jang, T. Park, Y. M. Park, J. S. Park, Y.-K. Kim, H.-K. Lee, E.-C. Jeon, D.-K. Lee, B. Ahn, C.-H. Chung, *ACS Appl. Mater. Interfaces* **2020**, *12*, 6169.
[283] L. J. Andrés, M. F. Menéndez, D. Gómez, A. L. Martínez, N. Bristow, J. P. Kettle, A. Menéndez, B. Ruiz, *Nanotechnology* **2015**, *26*, 265201.
[284] J. Turan, M. Kesik, S. Soylemez, S. Goker, S. Coskun, H. E. Unalan, L. Toppare, *Sensors and Actuators B: Chemical* **2016**, *228*, 278.
[285] H. Kim, H. Lee, I. Ha, J. Jung, P. Won, H. Cho, J. Yeo, S. Hong, S. Han, J. Kwon, K.-J. Cho, S. H. Ko, *Advanced Functional Materials* **2018**, *28*, 1801847.
[286] A. Elsayes, V. Sharma, K. Yiannacou, A. Koivikko, A. Rasheed, V. Sariola, *Adv. Sustainable Syst.* **2020**, 2000056.
[287] J. Liu, D. Jia, J. M. Gardner, E. M. J. Johansson, X. Zhang, *Materials Today Energy* **2019**, *13*, 152.
[288] L. Zhang, Y. Chen, C. Xu, Z. Liu, Y. Qiu, *RSC Advances* **2018**, *8*, 14532.
[289] J. Wang, Z. Zhang, S. Wang, R. Zhang, Y. Guo, G. Cheng, Y. Gu, K. Liu, K. Chen, *Nano Energy* **2020**, *71*, 104638.
[290] Y. Fang, Y. Li, Y. Li, M. Ding, J. Xie, B. Hu, *ACS Appl. Mater. Interfaces* **2020**, acsami.0c04134.
[291] C.-C. Lin, D.-X. Lin, S.-H. Lin, *Nanotechnology* **2020**, *31*, 215705.
[292] J. Li, S.-L. Zhang, *Phys. Rev. E* **2009**, *80*, 040104.
[293] H. Fong, I. Chun, D. H. Reneker, *Polymer* **1999**, *40*, 4585.
[294] D. Li, Y. Xia, *Nano Lett.* **2003**, *3*, 555.
[295] H. Wu, W. Pan, D. Lin, H. Li, *J Adv Ceram* **2012**, *1*, 2.
[296] M. Inagaki, Y. Yang, F. Kang, *Adv. Mater.* **2012**, *24*, 2547.
[297] C. Wang, J. Wang, L. Zeng, Z. Qiao, X. Liu, H. Liu, J. Zhang, J. Ding, *Molecules* **2019**, *24*, 834.
[298] K. Azuma, K. Sakajiri, H. Matsumoto, S. Kang, J. Watanabe, M. Tokita, *Materials Letters* **2014**, *115*, 187.
[299] J. Choi, Y. S. Shim, C. H. Park, H. Hwang, J. H. Kwack, D. J. Lee, Y. W. Park, B.-K. Ju, *Small* **2018**, *14*, 1702567.
[300] H. Wu, L. Hu, M. W. Rowell, D. Kong, J. J. Cha, J. R. McDonough, J. Zhu, Y. Yang, M. D. McGehee, Y. Cui, *Nano Lett.* **2010**, *10*, 4242.
[301] J. Jang, B. G. Hyun, S. Ji, E. Cho, B. W. An, W. H. Cheong, J.-U. Park, *NPG Asia Materials* **2017**, *9*, e432.
[302] H. S. Jo, S. An, J.-G. Lee, H. G. Park, S. S. Al-Deyab, A. L. Yarin, S. S. Yoon, *NPG Asia Materials* **2017**, *9*, e347.
[303] P.-C. Hsu, D. Kong, S. Wang, H. Wang, A. J. Welch, H. Wu, Y. Cui, *J. Am. Chem. Soc.* **2014**, *136*, 10593.
[304] G. H. Kim, J. H. Shin, T. An, G. Lim, *Sci Rep* **2018**, *8*, 13581.
[305] S. B. Singh, Y. Hu, T. Kshetri, N. H. Kim, J. H. Lee, *Journal of Materials Chemistry C* **2017**, *5*, 4198.
[306] S. Ji, J. Park, Y. Jo, Y.-B. Kim, J. Jang, S.-K. Kim, S. Jeong, J.-U. Park, *Applied Surface Science* **2019**, *483*, 1101.

[307] S. B. Singh, T. Kshetri, T. I. Singh, N. H. Kim, J. H. Lee, *Chemical Engineering Journal* **2019**, *359*, 197.
[308] J. Lee, S. Varagnolo, M. Walker, R. A. Hatton, *Adv. Funct. Mater.* **2020**, *30*, 2005959.
[309] S. Varagnolo, J. Lee, H. Amari, R. A. Hatton, *Mater. Horiz.* **2020**, *7*, 143.
[310] W. P. Lee, A. F. Routh, *Langmuir* **2004**, *20*, 9885.
[311] S. Mani, T. M. Saif, *Appl. Phys. Lett.* **2005**, *86*, 201903.
[312] K. B. Singh, M. S. Tirumkudulu, *Phys. Rev. Lett.* **2007**, *98*, 218302.
[313] P. Xu, A. S. Mujumdar, B. Yu, *Drying Technology* **2009**, *27*, 636.
[314] K. D. M. Rao, C. Hunger, R. Gupta, G. U. Kulkarni, M. Thelakkat, *Phys. Chem. Chem. Phys.* **2014**, *16*, 15107.
[315] B. Han, K. Pei, Y. Huang, X. Zhang, Q. Rong, Q. Lin, Y. Guo, T. Sun, C. Guo, D. Carnahan, M. Giersig, Y. Wang, J. Gao, Z. Ren, K. Kempa, *Adv. Mater.* **2014**, *26*, 873.
[316] K. D. M. Rao, G. U. Kulkarni, *Nanoscale* **2014**, *6*, 5645.
[317] C. P. Muzzillo, E. Wong, L. M. Mansfield, J. Simon, A. J. Ptak, *ACS Appl. Mater. Interfaces* **2020**, *12*, 41471.
[318] Y. D. Suh, J. Kwon, J. Lee, H. Lee, S. Jeong, D. Kim, H. Cho, J. Yeo, S. H. Ko, *Advanced Electronic Materials* **2016**, *2*, 1600277.
[319] X. Huang, F. Zhang, Y. Liu, J. Leng, *ACS Appl. Mater. Interfaces* **2020**, *12*, 23236.
[320] R. Khan, B. Shong, B. G. Ko, J. K. Lee, H. Lee, J. Y. Park, I.-K. Oh, S. S. Raya, H. M. Hong, K.-B. Chung, E. J. Luber, Y.-S. Kim, C.-H. Lee, W.-H. Kim, H.-B.-R. Lee, *Chem. Mater.* **2018**, *30*, 7603.
[321] J. Erlebacher, M. J. Aziz, A. Karma, N. Dimitrov, K. Sieradzki, *Nature* **2001**, *410*, 35068529.
[322] I. McCue, E. Benn, B. Gaskey, J. Erlebacher, *Annu. Rev. Mater. Res.* **2016**, *46*, 263.
[323] J. Erlebacher, Y. Ding, *Method of Forming Nanoporous Membranes*, **2004**.
[324] A. Chauvin, W. Txia Cha Heu, J. Buh, P.-Y. Tessier, A.-A. El Mel, *npj Flex Electron* **2019**, *3*, 5.
[325] N. Bouts, A.-A. El Mel, B. Angleraud, P.-Y. Tessier, *Carbon* **2015**, *83*, 250.
[326] H.-G. Im, B. W. An, J. Jin, J. Jang, Y.-G. Park, J.-U. Park, B.-S. Bae, *Nanoscale* **2016**, *8*, 3916.
[327] J.-Y. Moon, D.-Y. Youn, C. Kim, J.-H. Lee, Z. Luo, I.-D. Kim, *Nanoscale* **2018**, *10*, 7927.
[328] K.-H. Choi, J. Kim, Y.-J. Noh, S.-I. Na, H.-K. Kim, *Solar Energy Materials and Solar Cells* **2013**, *110*, 147.
[329] E. Lee, J. Ahn, H.-C. Kwon, S. Ma, K. Kim, S. Yun, J. Moon, *Adv. Energy Mater.* **2018**, *8*, 1702182.
[330] J. Park, Z. Ouyang, C. Yan, K. Sun, H. Sun, F. Liu, M. Green, X. Hao, *J. Phys. Chem. C* **2017**, *121*, 20597.
[331] A.-T. Pham, X.-Q. Nguyen, D.-H. Tran, V. Ngoc Phan, T.-T. Duong, D.-C. Nguyen, *Nanotechnology* **2016**, *27*, 335202.
[332] F. S. F. Morgenstern, D. Kabra, S. Massip, T. J. K. Brenner, P. E. Lyons, J. N. Coleman, R. H. Friend, *Applied Physics Letters* **2011**, *99*, 183307.
[333] D. Tigan, S. P. Genlik, B. Imer, H. E. Unalan, *Nanotechnology* **2019**, *30*, 325202.
[334] T.-B. Song, Y. S. Rim, F. Liu, B. Bob, S. Ye, Y.-T. Hsieh, Y. Yang, *ACS Applied Materials & Interfaces* **2015**, *7*, 24601.
[335] H. Van Bui, F. Grillo, J. R. van Ommen, *Chemical Communications* **2017**, *53*, 45.
[336] D. Muñoz-Rojas, T. Maindron, A. Esteve, F. Piallat, J. C. S. Kools, J.-M. Decams, *Materials Today Chemistry* **2019**, *12*, 96.
[337] M. Göbelt, R. Keding, S. W. Schmitt, B. Hoffmann, S. Jäckle, M. Latzel, V. V. Radmilović, V. R. Radmilović, E. Spiecker, S. Christiansen, *Nano Energy* **2015**, *16*, 196.

[338] R. Liu, M. Tan, X. Zhang, L. Xu, J. Chen, Y. Chen, X. Tang, L. Wan, *Solar Energy Materials and Solar Cells* **2018**, *174*, 584.
[339] S. Jon, G. Sin, G. Kim, G. Jong, J. Ri, *Synthetic Metals* **2020**, *262*, 116286.
[340] J. Resende, A. Sekkat, V. H. Nguyen, T. Chatin, C. Jiménez, M. Burriel, D. Bellet, D. Muñoz-Rojas, *Small* **2021**, *17*, 2007344.
[341] R. Chen, S. R. Das, C. Jeong, M. R. Khan, D. B. Janes, M. A. Alam, *Adv. Funct. Mater.* **2013**, *23*, 5150.
[342] D. Lee, H. Lee, Y. Ahn, Y. Jeong, D.-Y. Lee, Y. Lee, *Nanoscale* **2013**, *5*, 7750.
[343] J. Liang, L. Li, K. Tong, Z. Ren, W. Hu, X. Niu, Y. Chen, Q. Pei, *ACS Nano* **2014**, *8*, 1590.
[344] B.-T. Liu, H.-L. Kuo, *Carbon* **2013**, *63*, 390.
[345] H.-W. Tien, S.-T. Hsiao, W.-H. Liao, Y.-H. Yu, F.-C. Lin, Y.-S. Wang, S.-M. Li, C.-C. M. Ma, *Carbon* **2013**, *58*, 198.
[346] Y. Ahn, Y. Jeong, Y. Lee, *ACS Applied Materials & Interfaces* **2012**, *4*, 6410.
[347] I. N. Kholmanov, M. D. Stoller, J. Edgeworth, W. H. Lee, H. Li, J. Lee, C. Barnhart, J. R. Potts, R. Piner, D. Akinwande, J. E. Barrick, R. S. Ruoff, *ACS Nano* **2012**, *6*, 5157.
[348] R. Arat, G. Jia, J. Dellith, A. Dellith, J. Plentz, *Materials Today Communications* **2021**, *26*, 102162.
[349] Y. Liu, J. Feng, X.-L. Ou, H. Cui, M. Xu, H.-B. Sun, *Organic Electronics* **2016**, *31*, 247.
[350] N. M. Nair, J. K. Pakkathillam, K. Kumar, K. Arunachalam, D. Ray, P. Swaminathan, *ACS Appl. Electron. Mater.* **2020**, *2*, 1000.
[351] S. Kim, S. Jeong Lee, S. Cho, S. Shin, U. Jeong, J.-M. Myoung, *Chemical Communications* **2017**, *53*, 8292.
[352] D. Shin, T. Kim, B. T. Ahn, S. M. Han, *ACS Appl. Mater. Interfaces* **2015**, *7*, 13557.
[353] X.-Y. Zeng, Q.-K. Zhang, R.-M. Yu, C.-Z. Lu, *Advanced Materials* **2010**, *22*, 4484.
[354] H. Koga, M. Nogi, N. Komoda, T. T. Nge, T. Sugahara, K. Suganuma, *NPG Asia Mater* **2014**, *6*, e93.
[355] J. Sun, X. Li, Z. Chen, S. Yan, L. Qin, J. Zeng, S. Wang, J. Xu, L. Zhao, W. Zhou, Q. Wang, H. Gong, A. Lu, J. Yu, *Organic Electronics* **2018**, *63*, 392.
[356] R. Zhu, C.-H. Chung, K. C. Cha, W. Yang, Y. B. Zheng, H. Zhou, T.-B. Song, C.-C. Chen, P. S. Weiss, G. Li, Y. Yang, *ACS Nano* **2011**, *5*, 9877.
[357] N. M. Abbasi, H. Yu, L. Wang, Zain-ul-Abdin, W. A. Amer, M. Akram, H. Khalid, Y. Chen, M. Saleem, R. Sun, J. Shan, *Materials Chemistry and Physics* **2015**, *166*, 1.
[358] F.-C. Liang, Y.-W. Chang, C.-C. Kuo, C.-J. Cho, D.-H. Jiang, F.-C. Jhuang, S.-P. Rwei, R. Borsali, *Nanoscale* **2019**, *11*, 1520.
[359] R. Li, K. Zhang, G. Chen, *Materials* **2019**, *12*, 322.
[360] P.-C. Lin, C.-T. Hsieh, X. Liu, F.-C. Chang, W.-C. Chen, J. Yu, C.-C. Chueh, *Chemical Engineering Journal* **2021**, *405*, 126996.
[361] F. Hoeng, A. Denneulin, N. Reverdy-Bruas, G. Krosnicki, J. Bras, *Applied Surface Science* **2017**, *394*, 160.
[362] R. J. B. Pinto, M. A. Martins, J. M. F. Lucas, C. Vilela, A. J. M. Sales, L. C. Costa, P. A. A. P. Marques, C. S. R. Freire, *ACS Appl. Mater. Interfaces* **2020**, *12*, 34208.
[363] J. Xiong, S. Li, Y. Ye, J. Wang, K. Qian, P. Cui, D. Gao, M.-F. Lin, T. Chen, P. S. Lee, *Advanced Materials* **2018**, *30*, 1802803.
[364] S. Choi, S. I. Han, D. Kim, T. Hyeon, D.-H. Kim, *Chem. Soc. Rev.* **2019**, *48*, 1566.
[365] H. Eom, J. Lee, A. Pichitpajongkit, M. Amjadi, J.-H. Jeong, E. Lee, J.-Y. Lee, I. Park, *Small* **2014**, *10*, 4171.
[366] T. Gao, S. Haghanifar, M. G. Lindsay, P. Lu, M. I. Kayes, B. D. Pafchek, Z. Zhou, P. R. Ohodnicki, P. W. Leu, *Advanced Optical Materials* **2018**, *6*, 1700829.
[367] B.-Y. Wang, T.-H. Yoo, J. W. Lim, B.-I. Sang, D.-S. Lim, W. K. Choi, D. K. Hwang, Y.-J. Oh, *Small* **2015**, *11*, 1905.

[368] J. Han, S. Yuan, L. Liu, X. Qiu, H. Gong, X. Yang, C. Li, Y. Hao, B. Cao, *J. Mater. Chem. A* **2015**, *3*, 5375.
[369] C. G. Granqvist, *Solar Energy Materials and Solar Cells* **2007**, *91*, 1529.
[370] B. Li, S. Ye, I. E. Stewart, S. Alvarez, B. J. Wiley, *Nano Lett.* **2015**, *15*, 6722.
[371] European Commission, "Critical raw materials," can be found under https://ec.europa.eu/docsroom/documents/42849, **2020**.
[372] T. Sannicolo, M. Lagrange, A. Cabos, C. Celle, J.-P. Simonato, D. Bellet, *Small* **2016**, *12*, 6052.
[373] D. Tan, C. Jiang, Q. Li, S. Bi, J. Song, *J Mater Sci: Mater Electron* **2020**, *31*, 15669.
[374] P. Bellchambers, S. Varagnolo, C. Maltby, R. A. Hatton, *ACS Appl. Energy Mater.* **2021**, acsaem.1c00469.
[375] W. Cheong, Y. Kim, J. Lee, C. Hong, H. Choi, Y. Kwak, Y. J. Kim, Y. S. Kim, *Advanced Materials Technologies* **2019**, *4*, 1800550.
[376] C. G. Granqvist, *Thin Solid Films* **2014**, *564*, 1.
[377] F. Giovannetti, S. Föste, N. Ehrmann, G. Rockendorf, *Solar Energy* **2014**, *104*, 52.
[378] S. Duzyer, S. Sinha-Ray, S. Sinha-Ray, A. L. Yarin, *Macromolecular Materials and Engineering* **2017**, *302*, 1700188.
[379] S. Kim, J.-S. Oh, M.-G. Kim, W. Jang, M. Wang, Y. Kim, H. W. Seo, Y. C. Kim, J.-H. Lee, Y. Lee, J.-D. Nam, *ACS Appl. Mater. Interfaces* **2014**, *6*, 17647.
[380] J. Jang, J.-W. Choi, *J. Mater. Chem. C* **2021**, *9*, 4670.
[381] M. B. Cinali, Ö. D. Coşkun, *Journal of Alloys and Compounds* **2021**, *853*, 157073.
[382] P. Li, H. Li, J. Ma, Y. Zhou, W. Zhang, L. Cong, H. Xu, Y. Liu, *Adv. Mater. Interfaces* **2018**, *5*, 1801287.
[383] V. B. Nam, J. Shin, Y. Yoon, T. T. Giang, J. Kwon, Y. D. Suh, J. Yeo, S. Hong, S. H. Ko, D. Lee, *Advanced Functional Materials* **2019**, *29*, 1806895.
[384] D. Li, W.-Y. Lai, Y.-Z. Zhang, W. Huang, *Adv. Mater.* **2018**, *30*, 1704738.
[385] T. Li, S. Li, X. Li, Z. Xu, J. Zhao, Y. Shi, Y. Wang, R. Yu, X. Liu, Q. Xu, W. Guo, *Science Bulletin* **2020**, *65*, 225.
[386] C. Celle, C. Mayousse, E. Moreau, H. Basti, A. Carella, J.-P. Simonato, *Nano Research* **2012**, *5*, 427.
[387] T. Kim, Y. W. Kim, H. S. Lee, H. Kim, W. S. Yang, K. S. Suh, *Advanced Functional Materials* **2013**, *23*, 1250.
[388] J.-H. Kim, J. Ma, S. Jo, S. Lee, C. S. Kim, *Nanomaterials* **2020**, *10*, 938.
[389] S. Lin, H. Wang, X. Zhang, D. Wang, D. Zu, J. Song, Z. Liu, Y. Huang, K. Huang, N. Tao, Z. Li, X. Bai, B. Li, M. Lei, Z. Yu, H. Wu, *Nano Energy* **2019**, *62*, 111.
[390] H. Hosseinzadeh Khaligh, K. Liew, Y. Han, N. M. Abukhdeir, I. A. Goldthorpe, *Solar Energy Materials and Solar Cells* **2015**, *132*, 337.
[391] B.-U. Hwang, J.-H. Lee, T. Q. Trung, E. Roh, D.-I. Kim, S.-W. Kim, N.-E. Lee, *ACS Nano* **2015**, *9*, 8801.
[392] S. Hanauer, C. Celle, C. Crivello, H. Szambolics, D. Muñoz-Rojas, D. Bellet, J.-P. Simonato, *ACS Appl. Mater. Interfaces* **2021**, *13*, 21971.
[393] D. Tigan, S. P. Genlik, B. Imer, H. E. Unalan, *Nanotechnology* **2019**, *30*, 325202.
[394] H. Seok Jo, S. An, H.-J. Kwon, A. L. Yarin, S. S. Yoon, *Sci Rep* **2020**, *10*, 2701.
[395] R. Hu, Y. Liu, S. Shin, S. Huang, X. Ren, W. Shu, J. Cheng, G. Tao, W. Xu, R. Chen, X. Luo, *Adv. Energy Mater.* **2020**, *10*, 1903921.
[396] H. Zhai, R. Wang, X. Wang, Y. Cheng, L. Shi, J. Sun, *Nano Res.* **2016**, *9*, 3924.
[397] H. S. Jo, H.-J. Kwon, T.-G. Kim, C.-W. Park, S. An, A. L. Yarin, S. S. Yoon, *Nanoscale* **2018**, *10*, 19825.
[398] H. Wang, S. Lin, D. Zu, J. Song, Z. Liu, L. Li, C. Jia, X. Bai, J. Liu, Z. Li, D. Wang, Y. Huang, M. Fang, M. Lei, B. Li, H. Wu, *Advanced Materials Technologies* **2019**, 1900045.
[399] S. Kiruthika, R. Gupta, G. U. Kulkarni, *RSC Adv.* **2014**, *4*, 49745.

[400] H.-J. Kim, Y. Kim, J.-H. Jeong, J.-H. Choi, J. Lee, D.-G. Choi, *Journal of Materials Chemistry A* **2015**, *3*, 16621.
[401] J. Jang, N. S. Parmar, W.-K. Choi, J.-W. Choi, *ACS Appl. Mater. Interfaces* **2020**, *12*, 38406.
[402] K. Wang, Y. Jin, B. Qian, J. Wang, F. Xiao, *J. Mater. Chem. C* **2020**, *8*, 4372.
[403] T. Kang, S. H. Kim, M. Kim, E. Cho, S. Lee, *Plasma Process Polym* **2020**, *17*, 1900188.
[404] V. Sharma, A. Koivikko, K. Yiannacou, K. Lahtonen, V. Sariola, *npj Flex Electron* **2020**, *4*, 27.
[405] S. Y. Lee, J. Y. Hwang, *Sci Rep* **2020**, *10*, 9697.
[406] D. Lee, G. Bang, M. Byun, D. Choi, *Thin Solid Films* **2020**, *697*, 137835.
[407] X. He, Q. Cao, J. Pan, L. Yang, S. He, *RSC Adv.* **2021**, *11*, 11481.
[408] B. Stahlmecke, F.-J. M. zu Heringdorf, L. I. Chelaru, M. H. Hoegen, G. Dumpich, K. R. Roos, *Applied Physics Letters* **2006**, *88*, 053122.
[409] Q. Huang, C. M. Lilley, R. Divan, *Nanotechnology* **2009**, *20*, 075706.
[410] D. Kim, J. Bang, W. Lee, I. Ha, J. Lee, H. Eom, M. Kim, J. Park, J. Choi, J. Kwon, S. Han, H. Park, D. Lee, S. H. Ko, *J. Mater. Chem. A* **2020**, *8*, 8281.
[411] J. Park, S. Lee, D.-I. Kim, Y.-Y. Kim, S. Kim, H.-J. Kim, Y. Kim, *Sensors* **2019**, *19*, 4918.
[412] H.-J. Kim, J. Kim, Y. Kim, *ACS Appl. Nano Mater.* **2020**, acsanm.0c01404.
[413] J.-E. Lee, H.-K. Kim, *Sci Rep* **2019**, *9*, 16723.
[414] Z. Wang, J. Li, J. Xu, J. Huang, Y. Yang, R. Tan, G. Chen, X. Fang, Y. Zhao, W. Song, *Journal of Materials Science & Technology* **2020**, *48*, 156.
[415] S.-H. Lim, H.-K. Kim, *Sci Rep* **2020**, *10*, 8357.
[416] J. C. Goak, T. Y. Kim, D. U. Kim, K. S. Chang, C. S. Lee, N. Lee, *Applied Surface Science* **2020**, *510*, 145445.
[417] Z. Ma, S. Kang, J. Ma, L. Shao, A. Wei, C. Liang, J. Gu, B. Yang, D. Dong, L. Wei, Z. Ji, *ACS Nano* **2019**, *13*, 7578.
[418] I. S. Jin, J. Choi, J. W. Jung, *Adv. Electron. Mater.* **2021**, *7*, 2000698.
[419] Y. Zhang, S.-W. Ng, X. Lu, Z. Zheng, *Chem. Rev.* **2020**, *120*, 2049.
[420] Q. Tai, F. Yan, *Advanced Materials* **2017**, *29*, 1700192.
[421] A. Anand, M. M. Islam, R. Meitzner, U. S. Schubert, H. Hoppe, *Advanced Energy Materials* **n.d.**, *n/a*, 2100875.
[422] K. Han, M. Xie, L. Zhang, L. Yan, J. Wei, G. Ji, Q. Luo, J. Lin, Y. Hao, C.-Q. Ma, *Solar Energy Materials and Solar Cells* **2018**, *185*, 399.
[423] Y.-X. Zhang, J. Fang, W. Li, Y. Shen, J.-D. Chen, Y. Li, H. Gu, S. Pelivani, M. Zhang, Y. Li, J.-X. Tang, *ACS Nano* **2019**, *13*, 4686.
[424] M. Li, W.-W. Zuo, A. G. Ricciardulli, Y.-G. Yang, Y.-H. Liu, Q. Wang, K.-L. Wang, G.-X. Li, M. Saliba, D. D. Girolamo, A. Abate, Z.-K. Wang, *Advanced Materials* **2020**, *32*, 2003422.
[425] D.-H. Choi, H.-J. Seok, D.-H. Kim, S.-K. Kim, H.-K. Kim, *Science and Technology of Advanced Materials* **2020**, *21*, 435.
[426] S. Lee, J. Jang, T. Park, Y. M. Park, J. S. Park, Y.-K. Kim, H.-K. Lee, E.-C. Jeon, D.-K. Lee, B. Ahn, C.-H. Chung, *ACS Appl. Mater. Interfaces* **2020**, *12*, 6169.
[427] Z. Wang, Y. Han, L. Yan, C. Gong, J. Kang, H. Zhang, X. Sun, L. Zhang, J. Lin, Q. Luo, C. Ma, *Adv. Funct. Mater.* **2021**, *31*, 2007276.
[428] Q. Sun, J. Chen, J. Zheng, T. Qu, T. Jin, Y. Li, J. Tang, *Adv. Optical Mater.* **2019**, *7*, 1900847.
[429] D.-J. Kim, H.-J. Kim, K.-W. Seo, K.-H. Kim, T.-W. Kim, H.-K. Kim, *Sci Rep* **2015**, *5*, 16838.
[430] H.-C. Chu, Y.-C. Chang, Y. Lin, S.-H. Chang, W.-C. Chang, G.-A. Li, H.-Y. Tuan, *ACS Appl. Mater. Interfaces* **2016**, *8*, 13009.

[431] T. Y. Choi, B.-U. Hwang, B.-Y. Kim, T. Q. Trung, Y. H. Nam, D.-N. Kim, K. Eom, N.-E. Lee, *ACS Appl. Mater. Interfaces* **2017**, *9*, 18022.
[432] S. Ji, B. G. Hyun, K. Kim, S. Y. Lee, S.-H. Kim, J.-Y. Kim, M. H. Song, J.-U. Park, *NPG Asia Mater* **2016**, *8*, e299.
[433] H. Sim, C. Kim, S. Bok, M. Ki Kim, H. Oh, G.-H. Lim, S. Min Cho, B. Lim, *Nanoscale* **2018**, *10*, 12087.
[434] Y. Kim, Y. E. Sul, H. Kang, Y. Choi, H. S. Lim, S. Lee, L. Pu, G.-R. Yi, S. M. Cho, J. H. Cho, *Nanoscale* **2018**, *10*, 18627.
[435] Ho Jin Lee, B.-H. Kim, A. V. Takaloo, K. R. Son, T. D. Dongale, K. M. Lim, T. G. Kim, *Advanced Optical Materials* **2021**, 2002010.
[436] D. Kim, J. Kwon, J. Jung, K. Kim, H. Lee, J. Yeo, S. Hong, S. Han, S. H. Ko, *Small Methods* **2018**, *2*, 1800077.
[437] W. Kang, C. Yan, C. Y. Foo, P. S. Lee, *Advanced Functional Materials* **2015**, *25*, 4203.
[438] Y. H. Jung, T.-H. Chang, H. Zhang, C. Yao, Q. Zheng, V. W. Yang, H. Mi, M. Kim, S. J. Cho, D.-W. Park, H. Jiang, J. Lee, Y. Qiu, W. Zhou, Z. Cai, S. Gong, Z. Ma, *Nat Commun* **2015**, *6*, 7170.
[439] V. R. Voggu, J. Sham, S. Pfeffer, J. Pate, L. Fillip, T. B. Harvey, R. M. Brown, B. A. Korgel, *ACS Energy Lett.* **2017**, *2*, 574.
[440] Z. Fang, H. Zhu, Y. Yuan, D. Ha, S. Zhu, C. Preston, Q. Chen, Y. Li, X. Han, S. Lee, G. Chen, T. Li, J. Munday, J. Huang, L. Hu, *Nano Lett.* **2014**, *14*, 765.
[441] G. Huseynova, J.-H. Lee, Y. H. Kim, J. Lee, *Advanced Optical Materials* **n.d.**, *n/a*, 2002040.
[442] S. K. Bae, D. C. Choo, H. S. Kang, K. H. Yoo, T. W. Kim, *Nano Energy* **2020**, *71*, 104649.
[443] J. Sun, H. Wang, H. Shi, S. Wang, J. Xu, J. Ma, B. Ma, M. Wen, J. Li, J. Zhao, H. Liu, Y. Wang, L. Jiang, *ACS Appl. Mater. Interfaces* **2020**, *12*, 48820.
[444] R.-T. Wen, M. A. Arvizu, G. A. Niklasson, C. G. Granqvist, *Surface and Coatings Technology* **2015**, *278*, 121.
[445] G. K. Dalapati, A. K. Kushwaha, M. Sharma, V. Suresh, S. Shannigrahi, S. Zhuk, S. Masudy-Panah, *Progress in Materials Science* **2018**, *95*, 42.
[446] K. Xu, Y. Lu, K. Takei, *Advanced Materials Technologies* **2019**, *4*, 1800628.
[447] D. W. Kim, S.-Y. Min, Y. Lee, U. Jeong, *ACS Nano* **2020**, *14*, 907.
[448] Y. C. Kim, S. J. Lee, I.-K. Oh, S. Seo, H. Kim, J.-M. Myoung, *Journal of Alloys and Compounds* **2016**, *688*, 1108.
[449] J. Liang, K. Tong, Q. Pei, *Adv. Mater.* **2016**, *28*, 5986.
[450] L. Ma, Z. Lu, J. Tan, J. Liu, X. Ding, N. Black, T. Li, J. Gallop, L. Hao, *ACS Appl. Mater. Interfaces* **2017**, *9*, 34221.
[451] J. L. Huang, B. S. Yau, C. Y. Chen, W. T. Lo, D. F. Lii, *Ceramics International* **2001**, *27*, 363.
[452] W. Chen, L.-X. Liu, H.-B. Zhang, Z.-Z. Yu, *ACS Nano* **2020**, *14*, 16643.
[453] D. G. Kim, J. H. Choi, D.-K. Choi, S. W. Kim, *ACS Appl. Mater. Interfaces* **2018**, *10*, 29730.
[454] S. Yang, Y.-Y. Wang, Y.-N. Song, L.-C. Jia, G.-J. Zhong, L. Xu, D.-X. Yan, J. Lei, Z.-M. Li, *J. Mater. Chem. C* **2021**, *9*, 3307.
[455] R. Ravindren, S. Mondal, K. Nath, N. C. Das, *Composites Part B: Engineering* **2019**, *164*, 559.
[456] Y. Han, J. Lin, Y. Liu, H. Fu, Y. Ma, P. Jin, J. Tan, *Sci Rep* **2016**, *6*, 25601.
[457] H. Wang, Z. Lu, Y. Liu, J. Tan, L. Ma, S. Lin, *Opt. Lett.* **2017**, *42*, 1620.
[458] H. Wang, C. Ji, C. Zhang, Y. Zhang, Z. Zhang, Z. Lu, J. Tan, L. J. Guo, *ACS Appl. Mater. Interfaces* **2019**, *11*, 11782.

[459] L.-C. Jia, D.-X. Yan, X. Liu, R. Ma, H.-Y. Wu, Z.-M. Li, *ACS Appl. Mater. Interfaces* **2018**, *10*, 11941.
[460] L. Song, A. C. Myers, J. J. Adams, Y. Zhu, *ACS Appl. Mater. Interfaces* **2014**, *6*, 4248.
[461] B. S. Kim, K.-Y. Shin, J. B. Pyo, J. Lee, J. G. Son, S.-S. Lee, J. H. Park, *ACS Appl. Mater. Interfaces* **2016**, *8*, 2582.
[462] Y. Goliya, A. Rivadeneyra, J. F. Salmeron, A. Albrecht, J. Mock, M. Haider, J. Russer, B. Cruz, P. Eschlwech, E. Biebl, M. Becherer, M. R. Bobinger, *Adv. Optical Mater.* **2019**, *7*, 1900995.
[463] W. Li, A. Meredov, A. Shamim, *npj Flex Electron* **2019**, *3*, 19.
[464] D. Liu, J. Niu, H. Zhu, J. Zhang, *Nanotechnology* **2018**, *29*, 06LT01.
[465] Y. K. Kim, Y. Lee, K.-Y. Shin, J. Jang, *J. Mater. Chem. C* **2019**, *7*, 7915.
[466] S. Park, M. Vosguerichian, Z. Bao, *Nanoscale* **2013**, *5*, 1727.
[467] S. Sheikh, M. Shokooh-Saremi, M.-M. Bagheri-Mohagheghi, *Journal of Electromagnetic Waves and Applications* **2015**, *29*, 1557.
[468] J. Liang, C. Jiang, W. Wu, *Nanoscale* **2019**, *11*, 7041.
[469] S. Kiruthika, C. Sow, G. U. Kulkarni, *Small* **2017**, *13*, 1701906.
[470] S. Kiruthika, G. U. Kulkarni, *Energy Technol.* **2020**, *8*, 1901364.
[471] J. Liu, G. Shen, S. Zhao, X. He, C. Zhang, T. Jiang, J. Jiang, B. Chen, *J. Mater. Chem. A* **2019**, *7*, 8184.
[472] Y. Lee, S. Chae, H. Park, J. Kim, S.-H. Jeong, *Chemical Engineering Journal* **2020**, *382*, 122798.
[473] P. Makvandi, C. Wang, E. N. Zare, A. Borzacchiello, L. Niu, F. R. Tay, *Adv. Funct. Mater.* **2020**, 1910021.
[474] K. Zheng, M. I. Setyawati, D. T. Leong, J. Xie, *Coordination Chemistry Reviews* **2018**, *357*, 1.
[475] J.-H. Kim, J. Ma, S. Jo, S. Lee, C. S. Kim, *ACS Appl. Bio Mater.* **2020**, *3*, 2117.
[476] J. Cui, Y. Liu, *RSC Adv.* **2015**, *5*, 85748.
[477] H. Spieser, A. Denneulin, D. Deganello, D. Gethin, R. Koppolu, J. Bras, *Carbohydrate Polymers* **2020**, *240*, 116305.
[478] W. Chen, J. Jiang, W. Zhang, T. Wang, J. Zhou, C.-H. Huang, X. Xie, *Environ. Sci. Technol.* **2019**, *53*, 7504.
[479] H. Balakrishnan, R. Millan-Solsona, M. Checa, R. Fabregas, L. Fumagalli, G. Gomila, *Nanoscale* **2021**, *13*, 10116.
[480] H. Balakrishnan, R. Millan-Solsona, M. Checa, R. Fabregas, L. Fumagalli, G. Gomila, *Nanoscale* **2021**, 10.1039.D1NR01058A.
[481] G. Milano, A. Cultrera, K. Bejtka, N. De Leo, L. Callegaro, C. Ricciardi, L. Boarino, *ACS Appl. Nano Mater.* **2020**, *3*, 11987.
[482] Z. Chen, N. Boyajian, Z. Lin, R. T. Yin, S. N. Obaid, J. Tian, J. A. Brennan, S. W. Chen, A. N. Miniovich, L. Lin, Y. Qi, X. Liu, I. R. Efimov, L. Lu, *Adv. Mater. Technol.* **2021**, 2100225.

Biographies

Viet Huong Nguyen completed a B.S in Materials Science at National Institute of Applied Science of Lyon, France in 2013, and a Ph.D in Materials Science & Engineering from University Grenoble Alpes, France in 2018. Then, he worked as a postdoctoral fellow in the Laboratory of Materials Science and Physical Engineering (LMGP, Grenoble, France). Since August 2019, he is an assistant professor at Faculty of Materials Science and Engineering, Phenikaa University. His current research interests include the synthesis, surface engineering, and processing of nanostructured materials using Atomic Layer Deposition for applications in flexible electronics, energy conversion & storage.

David Muñoz-Rojas obtained his degree in Organic Chemistry at the Instituto Químico de Sarrià (IQS, Barcelona, 1999) and his PhD in Materials Science (2004) at the Instituto de Ciencia de Materiales de Barcelona. Thereafter, he worked as a postdoc at the Laboratoire de Réactivité et Chimie des Solides in Amiens, the Research Centre for Nanoscience and Nanotechnology in Barcelona and at the University of Cambridge. He is currently a CNRS researcher at Laboratoire des Matériaux et du Génie Physique in Grenoble. His research focuses on using and developing cheap and scalable chemical approaches for the fabrication of novel functional materials for electronic and optoelectronic applications

Daniel Bellet is a physicist and has worked in different fields such as single-crystal superalloys, porous silicon, liquid metal embrittlement, sintering of metallic powders, and synchrotron microtomography. His main research now concerns transparent conductive materials. He has been a full professor at Grenoble Institute of Technology since 1998. He was a junior member at IUF from 1999 to 2004 and director of the Academic Research Community “Energies” between 2011 and 2017. He is now the academic scientific director of the Carnot of Future Energies.